

UCD-02-18  
SCIPP 02/37  
IUHEX-202  
December, 2002  
hep-ph/0301023

## Higgs Physics at the Linear Collider

John F. Gunion\*, Howard E. Haber† and Rick Van Kooten‡

\* *Davis Institute for High Energy Physics*  
*University of California, Davis, CA 95616, U.S.A.*

† *Santa Cruz Institute for Particle Physics*  
*University of California, Santa Cruz, CA 95064, U.S.A.*

‡ *Department of Physics*  
*Indiana University, Bloomington, IN 47405, U.S.A.*

### Abstract

We review the theory of Higgs bosons, with emphasis on the Higgs scalars of the Standard Model and its non-supersymmetric and supersymmetric extensions. After surveying the expected knowledge of Higgs boson physics after the Tevatron and LHC experimental programs, we examine in detail expectations for precision Higgs measurements at a future  $e^+e^-$  linear collider (LC). A comprehensive phenomenological profile can be assembled from LC Higgs studies (both in  $e^+e^-$  and  $\gamma\gamma$  collisions). The Giga- $Z$  option can provide important constraints and consistency checks for the theory of electroweak symmetry breaking.

To appear in *Linear Collider Physics in the New Millennium*,  
edited by K. Fujii, D. Miller and A. Soni (World Scientific)

## CHAPTER 1

### HIGGS PHYSICS AT THE LINEAR COLLIDER

John F. Gunion

*Davis Institute for High Energy Physics  
University of California, Davis, CA 95616, U.S.A.  
E-mail: jfgucd@higgs.ucdavis.edu*

Howard E. Haber

*Santa Cruz Institute for Particle Physics  
University of California, Santa Cruz, CA 95064, U.S.A.  
E-mail: haber@scipp.ucsc.edu*

Rick Van Kooten

*Department of Physics  
Indiana University, Bloomington, IN 47405, U.S.A.  
E-mail: rickv@paoli.physics.indiana.edu*

We review the theory of Higgs bosons, with emphasis on the Higgs scalars of the Standard Model and its non-supersymmetric and supersymmetric extensions. After surveying the expected knowledge of Higgs boson physics after the Tevatron and LHC experimental programs, we examine in detail expectations for precision Higgs measurements at a future  $e^+e^-$  linear collider (LC). A comprehensive phenomenological profile can be assembled from LC Higgs studies (both in  $e^+e^-$  and  $\gamma\gamma$  collisions). The Giga- $Z$  option can provide important constraints and consistency checks for the theory of electroweak symmetry breaking.

**Contents**

1	Introduction . . . . .	3
2	Expectations for electroweak symmetry breaking . . . . .	6
3	The Standard Model Higgs boson—theory . . . . .	11
3.1	Standard Model Higgs boson decay modes . . . . .	12
3.2	Standard Model Higgs boson production at the LC . . . . .	13
4	SM Higgs searches before the linear collider . . . . .	16
4.1	Direct search limits from LEP . . . . .	16
4.2	Implications of precision electroweak measurements . . . . .	16
4.3	Expectations for Tevatron searches . . . . .	17
4.4	Expectations for LHC searches . . . . .	19
5	Higgs bosons in low-energy supersymmetry . . . . .	22
5.1	MSSM Higgs sector at tree level . . . . .	24
5.2	The radiatively corrected MSSM Higgs sector . . . . .	26
5.3	MSSM Higgs boson decay modes . . . . .	33
5.4	MSSM Higgs boson production at the LC . . . . .	35
6	MSSM Higgs boson searches before the LC . . . . .	36
6.1	Direct search limits from LEP . . . . .	36
6.2	MSSM Higgs searches at the Tevatron . . . . .	37
6.3	MSSM Higgs searches at the LHC . . . . .	39
7	Non-exotic extended Higgs sectors . . . . .	41
7.1	The decoupling limit . . . . .	43
7.2	Constraints from precision electroweak data and LC implications . . . . .	43
7.3	Constraints on Higgs bosons with $VV$ coupling . . . . .	45
7.4	Detection of non-exotic extended Higgs sector scalars at the Tevatron and LHC . . . . .	46
7.5	LC production mechanisms for non-exotic extended Higgs sector scalars . . . . .	47
8	Exotic Higgs sectors and other possibilities . . . . .	51
8.1	A triplet Higgs sector . . . . .	51
8.2	Pseudo Nambu Goldstone bosons . . . . .	53
9	LC Measurements of Higgs Boson Properties . . . . .	53
9.1	Mass . . . . .	54
9.2	Coupling Determinations – Light Higgs Boson . . . . .	56
9.2.1	Cross Sections . . . . .	56
9.2.2	Branching Ratios . . . . .	57
9.2.3	Radiative Production, $t\bar{t}h$ . . . . .	61
9.2.4	Self-Coupling . . . . .	61
9.2.5	Implications for the MSSM Higgs Sector . . . . .	63
9.3	Coupling Determinations – Intermediate Mass Higgs Boson . . . . .	65
9.3.1	Cross Sections . . . . .	65

9.3.2	Branching Ratios . . . . .	66
9.4	Coupling Determinations – Heavy Higgs Boson . . . . .	66
9.4.1	Cross Sections . . . . .	66
9.4.2	Branching Ratios . . . . .	67
9.5	Summary of Couplings . . . . .	67
9.6	Total Width . . . . .	68
9.7	Quantum Numbers . . . . .	69
9.8	Precision studies of non-SM-like Higgs bosons . . . . .	72
10	The Giga- $Z$ option—implications for Higgs physics . . . . .	74
10.1	Giga- $Z$ and the MSSM . . . . .	75
10.2	Giga- $Z$ and non-exotic extended Higgs sectors . . . . .	76
11	The $\gamma\gamma$ collider option . . . . .	77
12	Concluding Remarks . . . . .	83
	Acknowledgments . . . . .	83
	References . . . . .	84

## 1. Introduction

This chapter shows how an  $e^+e^-$  linear collider (LC) can contribute to our understanding of the Higgs sector through detailed studies of the physical Higgs boson state(s). Although this subject has been reviewed several times in the past [1–6], there are at least two reasons to revisit the subject. First, the completion of the LEP Higgs search, together with precise measurements from SLC, LEP, and the Tevatron, provides a clearer idea of what to expect. The simplest interpretation of these results point to a light Higgs boson with (nearly) standard couplings to  $W$  and  $Z$ . The key properties of such a particle can be investigated with a LC with a center-of-mass energy of  $\sqrt{s} = 500$  GeV. Second, the luminosity expected from the LC is now higher: 200–300  $\text{fb}^{-1}\text{yr}^{-1}$  at  $\sqrt{s} = 500$  GeV, and 300–500  $\text{fb}^{-1}\text{yr}^{-1}$  at  $\sqrt{s} = 800$  GeV. In particular, detailed designs have been developed for the LC by the American/Asian collaboration (the NLC/JLC design [7, 8]) and by the DESY-based European collaboration (the TESLA design [9]). At  $\sqrt{s} = 500$  GeV, the nominal  $10^7$  sec year integrated luminosities are 220  $\text{fb}^{-1}\text{yr}^{-1}$  and 340  $\text{fb}^{-1}\text{yr}^{-1}$  for the NLC/JLC and TESLA designs, respectively [10]. Consequently, several tens of thousands of Higgs bosons should be produced in each year of operation. With such samples, numerous precision Higgs measurements become feasible, and will provide fundamental insights into the properties of the Higgs boson(s) and the underlying dynamics of electroweak symmetry breaking.

The  $e^+e^-$  LC with center-of-mass energy  $\sqrt{s}$  can also be designed to operate as a photon-photon collider. This is achieved by using Compton

backscattered photons in the scattering of intense laser photons on the initial polarized  $e^+e^-$  beams [11, 12]. The resulting  $\gamma\gamma$  center of mass energy is peaked at about  $0.8\sqrt{s}$  for the appropriate choices of machine parameters. The luminosity achievable as a function of the photon beam energy depends strongly on the machine parameters (in particular, the choice of laser polarizations). The photon collider provides additional opportunities for Higgs physics [13–19].

Finally, we note that substantial improvements are possible for precision measurements of  $m_W$ ,  $m_t$  and electroweak mixing angle measurements at the LC [20]. But, the most significant improvements can be achieved at the Giga- $Z$  [21], where the LC operates at  $\sqrt{s} = m_Z$  and  $\sqrt{s} \simeq 2m_W$ . With an integrated luminosity of  $50 \text{ fb}^{-1}$ , one can collect  $1.5 \times 10^9$   $Z$  events and about  $10^6$   $W^+W^-$  pairs in the threshold region. Employing a global fit to the precision electroweak data in the Standard Model, the anticipated fractional Higgs mass uncertainty achievable would be about 8%. This would provide a stringent test for the theory of the Higgs boson, as well as very strong constraints on any new physics beyond the Standard Model that couples to the  $W$  and  $Z$  gauge bosons.

There is an enormous literature on the Higgs boson and, more generally, on possible mechanisms of electroweak symmetry breaking. It is impossible to review all theoretical approaches here. To provide a manageable, but nevertheless illustrative, survey of the LC capabilities, we focus mostly on the Higgs boson of the Standard Model (SM), and on the Higgs bosons of the minimal supersymmetric extension of the Standard Model (MSSM). Although this choice is partly motivated by simplicity, a stronger impetus comes from the precision data collected over the past few years, and some other related considerations.

The SM, which adds to the observed particles a single complex doublet of scalar fields, is economical. It provides a good fit to the precision electroweak data. Many extended models of electroweak symmetry breaking possess a limit, called the decoupling limit [22], that is experimentally almost indistinguishable from the SM at low energies. These models agree with the data equally well, and even away from the decoupling limit they usually predict a weakly coupled Higgs boson whose mass is at most several hundred GeV. Thus, the SM serves as a basis for discussing the Higgs phenomenology of a wide range of models, all of which are compatible with present experimental constraints.

However, the SM suffers from several theoretical problems, which are either absent or less severe with weak-scale supersymmetry. The Higgs sector

of the minimal supersymmetric extension of the Standard Model (MSSM) is a constrained two-Higgs-doublet model (2HDM), consisting of two CP-even Higgs bosons,  $h^0$  and  $H^0$ , a CP-odd Higgs boson,  $A^0$ , and a charged Higgs pair,  $H^\pm$ . The MSSM is especially attractive because the superpartners modify the running of the strong, weak, and electromagnetic gauge couplings in just the right way as to yield unification at about  $10^{16}$  GeV [23]. For this reason, the MSSM is arguably the most compelling extension of the SM. This is directly relevant to Higgs phenomenology, because a theoretical bound requires the mass of the lightest CP-even Higgs boson  $h^0$  of the MSSM to be less than about 135 GeV (in most non-minimal supersymmetric models,  $m_{h^0} \lesssim 200$  GeV), as discussed in Section 5.2. Furthermore, the MSSM offers, in some regions of parameter space, very non-standard Higgs phenomenology, so the full range of possibilities in the MSSM can be used to indicate how well the LC performs in non-standard scenarios. Thus, we use the SM to show how the LC fares when there is only one observable Higgs boson, and the MSSM to illustrate how extra fields can complicate the phenomenology. We also use various other models to illustrate important exceptions to conclusions that would be drawn from the SM and MSSM alone.

The rest of this chapter is organized as follows. Section 2 presents, in some detail, the argument that one should expect a weakly coupled Higgs boson with a mass that is probably below about 200 GeV. In Section 3, we summarize the theory of the SM Higgs boson. In Section 4, we review the expectations for Higgs discovery and the determination of Higgs boson properties at the Tevatron and LHC. In Section 5, we introduce the Higgs sector of the MSSM and discuss its theoretical properties. The present direct search limits are reviewed, and expectations for discovery at the Tevatron and LHC are described in Section 6. In Section 7, we treat the theory of the non-minimal Higgs sector more generally. In particular, we focus on the decoupling limit, in which the properties of the lightest Higgs scalar are nearly identical to those of the Standard Model Higgs boson, and discuss how to distinguish the two. We also discuss some non-decoupling exceptions to the usual decoupling scenario. In Section 8, we briefly discuss the case of a Higgs sector containing triplet Higgs representations and also consider the Higgs-like particles that can arise if the underlying assumption of a weakly coupled elementary Higgs sector is *not* realized in Nature.

Finally, we turn to the program of Higgs measurements that can be carried out at the LC, focusing on  $e^+e^-$  collisions at higher energy, but also addressing the impact of the Giga-Z operation and  $\gamma\gamma$  collisions. This

material summarizes and updates the results of the American Linear Collider Working Group that were presented in [10]. The measurement of Higgs boson properties in  $e^+e^-$  collisions is outlined in Section 9, and includes a survey of the measurements that can be made for a SM-like Higgs boson for all masses up to 500 GeV. We also discuss measurements of the extra Higgs bosons that appear in the MSSM. Because the phenomenology of the decoupling limit mimics that of the SM Higgs boson, we emphasize how the precision that stems from high luminosity helps to diagnose the underlying dynamics. In Section 10, we outline the impact of the Giga- $Z$  operation on constraining and exploring various scenarios. In Section 11, the most important gains from a photon-photon collider are reviewed. We end this chapter with some brief conclusions in Section 12.

## 2. Expectations for electroweak symmetry breaking

With the recent completion of experimentation at the LEP collider, the Standard Model of particle physics appears close to final experimental verification. After more than ten years of precision measurements of electroweak observables at LEP, SLC and the Tevatron, no definitive departures from Standard Model predictions have been found [24]. In some cases, theoretical predictions have been checked with an accuracy of one part in a thousand or better. However, the dynamics responsible for electroweak symmetry breaking have not yet been directly identified. Nevertheless, these dynamics affect predictions for currently observed electroweak processes at the one-loop quantum level. Consequently, the analysis of precision electroweak data can already provide some useful constraints on the nature of electroweak symmetry breaking dynamics.

In the Standard Model, electroweak symmetry breaking dynamics arise via a self-interacting complex doublet of scalar fields, which consists of four real degrees of freedom. Renormalizable interactions are arranged in such a way that the neutral component of the scalar doublet acquires a vacuum expectation value,  $v = 246$  GeV, which sets the scale of electroweak symmetry breaking. Hence, three massless Goldstone bosons are generated that are absorbed by the  $W^\pm$  and  $Z$ , thereby providing the resulting massive gauge bosons with longitudinal components. The fourth scalar degree of freedom remains in the physical spectrum, and it is the CP-even neutral Higgs boson of the Standard Model. It is further assumed in the Standard Model that the scalar doublet also couples to fermions through Yukawa interactions. After electroweak symmetry breaking, these interactions are

responsible for the generation of quark and charged lepton masses.

The global analysis of electroweak observables provides a good fit to the Standard Model predictions. Such analyses take the Higgs mass as a free parameter. The electroweak observables depend logarithmically on the Higgs mass through its one-loop effects. The accuracy of the current data (and the reliability of the corresponding theoretical computations) already provides a significant constraint on the value of the Higgs mass. In [24], the constraints of the global precision electroweak analysis yield a one-sided 95% CL upper limit of  $m_{h_{\text{SM}}} \leq 193$  GeV at 95% CL. Meanwhile, direct searches for the Higgs mass at LEP achieved a 95% CL limit of  $m_{h_{\text{SM}}} > 114.4$  GeV [25].

One can question the significance of these results. After all, the self-interacting scalar field is only one model of electroweak symmetry breaking; other approaches, based on different dynamics, are also possible. For example, one can introduce new fermions and new forces, in which the Goldstone bosons are a consequence of the strong binding of the new fermion fields [26]. Present experimental data does not sufficiently constrain the nature of the dynamics responsible for electroweak symmetry breaking. Nevertheless, one can attempt to classify alternative scenarios and study the constraints of the global precision electroweak fits and the implications for phenomenology at future colliders. Since electroweak symmetry dynamics must affect the one-loop corrections to electroweak observables, constraints on alternative approaches can be obtained by generalizing the global precision electroweak fits to allow for new contributions at one-loop. These enter primarily through corrections to the self-energies of the gauge bosons (the so-called ‘‘oblique’’ corrections). Under the assumption that new physics is characterized by a mass scale  $M \gg m_Z$ , one can parameterize the leading oblique corrections by three constants,  $S$ ,  $T$ , and  $U$ , first introduced by Peskin and Takeuchi [27]. In almost all theories of electroweak symmetry breaking dynamics,  $U \ll S, T$ , so it is sufficient to consider a global electroweak fit in which  $m_{h_{\text{SM}}}$ ,  $S$  and  $T$  are free parameters. (The zero of the  $S$ - $T$  plane must be defined relative to some fixed value of the Higgs mass, usually taken to be 100 GeV.) New electroweak symmetry breaking dynamics could generate non-zero values of  $S$  and  $T$ , while allowing for a much heavier Higgs mass (or equivalent). Various possibilities have been classified by Peskin and Wells [28], who found that all models in the literature allowing a significantly heavier Higgs boson also generate experimental signatures of new physics at the TeV scale. At the LC, such new physics could be studied either directly by producing new particles or indirectly by



improving precision measurements of electroweak observables.

In this chapter, we mainly consider the case of a light weakly coupled Higgs boson, corresponding to the simplest interpretation of the precision electroweak data. Nevertheless, this still does not fix the theory of electroweak symmetry breaking. It is easy to construct extensions of the scalar boson dynamics and generate non-minimal Higgs sectors. Such theories can contain charged Higgs bosons and neutral Higgs bosons of opposite (or indefinite) CP-quantum numbers. Although some theoretical constraints exist, there is still considerable freedom in constructing models which satisfy all known experimental constraints. Moreover, in most extensions of the Standard Model, there exists a large range of parameter space in which the properties of the lightest Higgs scalar are virtually indistinguishable from those of the Standard Model Higgs boson. Once the Higgs boson is discovered, one of the challenges for experiments at future colliders is to detect deviations from the properties expected for the Standard Model Higgs boson, in order to better constrain the underlying scalar dynamics.

Although the Standard Model provides a remarkably successful description of the properties of the quarks, leptons and spin-1 gauge bosons at energy scales of  $\mathcal{O}(100)$  GeV and below, the Standard Model is not the ultimate theory of the fundamental particles and their interactions. At an energy scale above the Planck scale,  $M_{\text{PL}} \simeq 10^{19}$  GeV, quantum gravitational effects become significant and the Standard Model must be replaced by a more fundamental theory that incorporates gravity. Furthermore, on theoretical grounds it is very likely that the Standard Model breaks down at some energy scale,  $\Lambda$ . In this case, the Standard Model degrees of freedom are no longer adequate for describing the physics above  $\Lambda$  and new physics must enter. Thus, the Standard Model is not a *fundamental* theory; at best, it is an *effective field theory* [29]. At energies below the scale  $\Lambda$ , the Standard Model (with higher-dimension operators to parameterize the new physics at the scale  $\Lambda$ ) provides an extremely good description of all observable phenomena.

To assess the potential of future experiments, it is essential to ask how large  $\Lambda$  can be. After all, if  $\Lambda$  is as large as  $M_{\text{PL}}$ , it does not matter much whether the Standard Model is a fundamental or an effective field theory. The energy scale  $\Lambda$  arises when analyzing the scale dependence of the Higgs self-coupling and the Higgs-top quark Yukawa coupling, so the value of  $\Lambda$  depends on the Higgs mass  $m_{h_{\text{SM}}}$  and the top quark mass  $m_t$ . (Recall that  $m_{h_{\text{SM}}}^2 = \frac{1}{2}\lambda v^2$  and  $m_t = h_t v/\sqrt{2}$ , where  $\lambda$  is the Higgs quartic self-coupling and  $h_t$  is the Higgs-top quark Yukawa coupling.) If  $m_{h_{\text{SM}}}$  is too large, then

the perturbatively evolved Higgs self-coupling  $\lambda$  blows up at some scale  $\Lambda$  [30,31]. If  $m_{h_{\text{SM}}}$  is too small (compared to  $m_t$ ), then the (perturbative) Higgs potential develops a second (global) minimum at a large value of the scalar field of order  $\Lambda$  [32]. Thus, new physics must enter at or below  $\Lambda$ , in order that the true minimum of the theory correspond to the observed  $\text{SU}(2)\times\text{U}(1)$  broken vacuum with  $v = 246$  GeV for scales above  $\Lambda$ .

The arguments just given are based on perturbation theory so, taken on their own, are not completely persuasive. Once the couplings become strong, it is *a priori* conceivable that a novel, non-perturbative scaling behavior would rescue the theory. This possibility has been checked, mostly in an approximation neglecting the gauge couplings [30]. Let us consider first the case of large Higgs mass (large  $\lambda$ ), so the Yukawa coupling can be neglected. By a number of methods, particularly numerical lattice methods [33,34] and strong coupling expansions [35], one finds that non-perturbative renormalization effects rapidly bring the self-coupling back into the perturbative regime. This is the so-called triviality phenomenon: if one starts with finite  $\Lambda$  and tries to take the limit  $\Lambda \rightarrow \infty$ , one ends up with a renormalized self-coupling  $\lambda \rightarrow 0$ . A similar phenomenon occurs for large Yukawa couplings. In these studies [36], the vacuum is never unstable (non-perturbatively). Instead, strong renormalization effects drive the Yukawa coupling back into the perturbative regime.

The non-perturbative studies very much favor a finite  $\Lambda$ , despite exhaustive attempts [34] to find non-trivial behavior for  $\Lambda \rightarrow \infty$ . They also justify the use of perturbation theory, because the renormalized self- and Yukawa couplings end up being small enough at scales below  $\Lambda$ . Thus, with the perturbative analysis and a given value of  $\Lambda$ , one can compute the minimum and maximum Higgs mass allowed. The results of such an analysis (with shaded bands indicating the theoretical uncertainty of the result) are illustrated in fig. 1 [31,37]. From the upper bound one sees that if  $\Lambda \sim 10^3$  GeV = 1 TeV, then  $m_{h_{\text{SM}}} \lesssim 800$  GeV. If  $\Lambda$  is more remote, say  $\Lambda \gtrsim 10^6$  GeV, then  $m_{h_{\text{SM}}} \lesssim 300$  GeV.

In the Higgs mass range  $130$  GeV  $\lesssim m_{h_{\text{SM}}} \lesssim 180$  GeV, it seems that an effective Standard Model could survive all the way to the Planck scale.<sup>1</sup> However, such a possibility seems unlikely, based on the following “naturalness” argument [39]. In an effective field theory, masses and dimensionless

---

<sup>1</sup>The constraint on  $\Lambda$  due to vacuum stability in fig. 1 can be relaxed somewhat if one allows for the electroweak vacuum to be metastable, with a lifetime greater than the age of the universe. The analysis of [38] finds that for a sufficiently long-lived electroweak vacuum, the Higgs mass lower limit of 130 GeV just quoted is reduced to about 115 GeV.

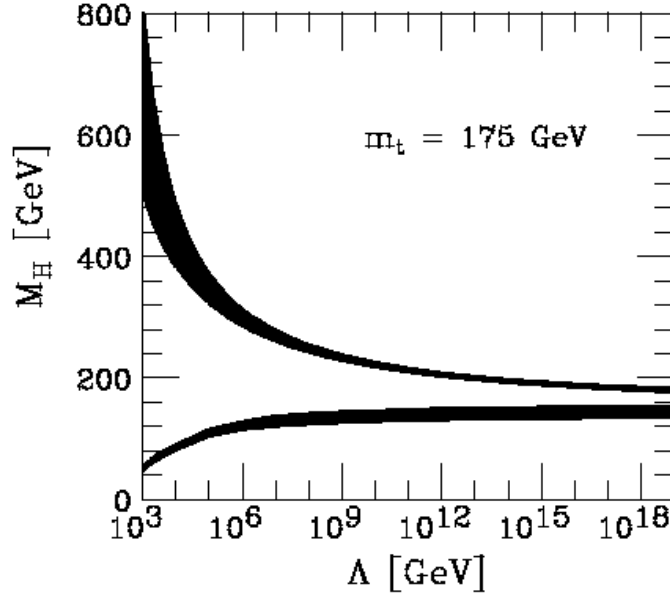


Fig. 1: The upper [30,31] and the lower [32] Higgs mass bounds as a function of the energy scale  $\Lambda$  at which the Standard Model breaks down, assuming  $m_t = 175$  GeV and  $\alpha_s(m_Z) = 0.118$ . The shaded areas above reflect the theoretical uncertainties in the calculations of the Higgs mass bounds From [37].

couplings are calculable in terms of parameters of a more fundamental theory that describes physics at the energy scale  $\Lambda$ . All low-energy couplings and fermion masses are logarithmically sensitive to  $\Lambda$ . In contrast, scalar squared-masses are *quadratically* sensitive to  $\Lambda$ . The Higgs mass (at one-loop) has the following heuristic form:

$$m_h^2 = (m_h^2)_0 + \frac{cg^2}{16\pi^2}\Lambda^2, \quad (1)$$

where  $(m_h^2)_0$  is a parameter of the fundamental theory and  $c$  is a constant, presumably of  $\mathcal{O}(1)$ , that depends on the physics near the scale  $\Lambda$ . The “natural” value for the scalar squared-mass is  $g^2\Lambda^2/16\pi^2$ . Thus, the expectation for  $\Lambda$  is

$$\Lambda \simeq \frac{4\pi m_h}{g} \sim \mathcal{O}(1 \text{ TeV}). \quad (2)$$

If  $\Lambda$  is significantly larger than 1 TeV then the only way for the Higgs mass to be of order the scale of electroweak symmetry breaking is to have

an “unnatural” cancellation between the two terms of eq. (1). This seems highly unlikely given that the two terms of eq. (1) have completely different origins.

An attractive theoretical framework that incorporates weakly coupled Higgs bosons and satisfies the constraint of eq. (2) is that of “low-energy” or “weak-scale” supersymmetry [40,41]. In this framework, supersymmetry is used to relate fermion and boson masses and interaction strengths. Since fermion masses are only logarithmically sensitive to  $\Lambda$ , boson masses will exhibit the same logarithmic sensitivity if supersymmetry is exact. Since no supersymmetric partners of Standard Model particles have yet been found, supersymmetry cannot be an exact symmetry of nature. Thus,  $\Lambda$  should be identified with the supersymmetry breaking scale. The naturalness constraint of eq. (2) is still relevant. It implies that the scale of supersymmetry breaking should not be much larger than 1 TeV, to preserve the naturalness of scalar masses. The supersymmetric extension of the Standard Model would then replace the Standard Model as the effective field theory of the TeV scale.

One advantage of the supersymmetric approach is that the effective low-energy supersymmetric theory *can* be valid all the way up to the Planck scale, while still being natural. The unification of the three gauge couplings at an energy scale close to the Planck scale, which does not occur in the Standard Model, is seen to occur in the minimal supersymmetric extension of the Standard Model [23], and provides an additional motivation for seriously considering the low-energy supersymmetric framework. However, the fundamental origin of supersymmetry breaking is not known at present. Without a fundamental theory of supersymmetry breaking, one ends up with an effective low-energy theory characterized by over 100 unknown parameters that in principle would have to be measured by experiment. This remains one of the main stumbling blocks for creating a truly predictive supersymmetric model of fundamental particles and their interactions. Nevertheless, the Higgs sectors of the simplest supersymmetric models are quite strongly constrained and exhibit very specific phenomenological profiles.

### 3. The Standard Model Higgs boson—theory

In the Standard Model, the Higgs mass,  $m_{h_{\text{SM}}}^2 = \frac{1}{2}\lambda v^2$ , depends on the Higgs self-coupling  $\lambda$ . Since  $\lambda$  is unknown at present, the value of the SM Higgs mass is not predicted, although other theoretical considerations (discussed in Section 2) place constraints on the Higgs mass, as exhibited

in fig. 1. The Higgs couplings to fermions [gauge bosons] are proportional to the corresponding particle masses [squared-masses]. As a result, Higgs phenomenology is governed primarily by the couplings of the Higgs boson to the  $W^\pm$  and  $Z$  and the third-generation quarks and leptons. Two-loop-induced Higgs couplings are also phenomenologically important: the  $h_{\text{SM}}gg$  coupling ( $g$  is the gluon), which is induced by the one-loop graph in which the Higgs boson couples to a virtual  $t\bar{t}$  pair, and the  $h_{\text{SM}}\gamma\gamma$  coupling, for which the  $W^+W^-$  loop contribution is dominant. Further details of the SM Higgs boson properties are given in [1].

### 3.1. Standard Model Higgs boson decay modes

The Higgs boson mass is the only unknown parameter in the Standard Model. Thus, one can compute Higgs boson branching ratios and production cross sections as a function of  $m_{h_{\text{SM}}}$ . The branching ratios for the dominant decay modes of a Standard Model Higgs boson are shown as a function of Higgs boson mass in fig. 2. Note that subdominant channels are important to establish a complete phenomenological profile of the Higgs boson, and to check consistency (or look for departures from) Standard Model predictions. For  $115 \text{ GeV} \sim m_{h_{\text{SM}}} \lesssim 2m_W$  many decays modes are large enough to measure, as discussed in Section 9.

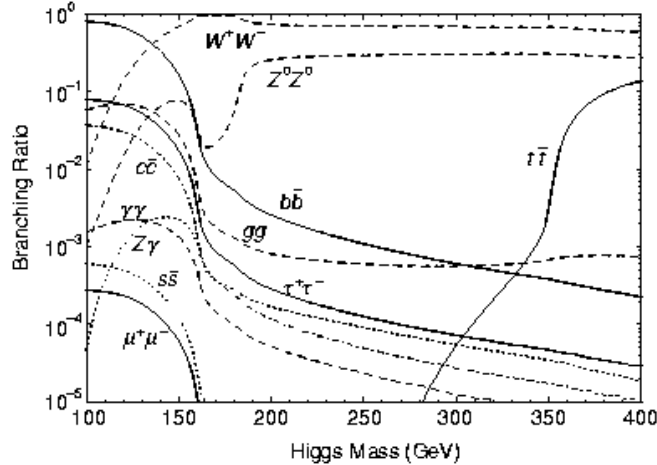


Fig. 2: Branching ratios of the dominant decay modes of the Standard Model Higgs boson. These results have been obtained with the program HDECAY [42], and include QCD corrections beyond the leading order.

For  $m_{h_{\text{SM}}} \lesssim 135$  GeV, the main Higgs decay mode is  $h_{\text{SM}} \rightarrow b\bar{b}$ , while the decays  $h_{\text{SM}} \rightarrow \tau^+\tau^-$  and  $c\bar{c}$  can also be phenomenologically relevant. In addition, although one-loop suppressed, the decay  $h_{\text{SM}} \rightarrow gg$  is competitive with other decays for  $m_{h_{\text{SM}}} \lesssim 2m_W$  because of the large top Yukawa coupling and the color factor. As the Higgs mass increases above 135 GeV, the branching ratio to vector boson pairs becomes dominant. In particular, the main Higgs decay mode is  $h_{\text{SM}} \rightarrow WW^{(*)}$ , where one of the  $W$ 's must be off-shell (indicated by the star superscript) if  $m_{h_{\text{SM}}} < 2m_W$ . For Higgs bosons with  $m_{h_{\text{SM}}} \gtrsim 2m_t$ , the decay  $h_{\text{SM}} \rightarrow t\bar{t}$  begins to increase until it reaches its maximal value of about 20%.

Rare Higgs decay modes can also play an important role. The one-loop decay  $h_{\text{SM}} \rightarrow \gamma\gamma$  is a suppressed mode. For  $m_W \lesssim m_{h_{\text{SM}}} \lesssim 2m_W$ ,  $\text{BR}(h_{\text{SM}} \rightarrow \gamma\gamma)$  is above  $10^{-3}$ . This decay channel provides an important Higgs discovery mode at the LHC for  $100 \text{ GeV} \lesssim m_{h_{\text{SM}}} \lesssim 150 \text{ GeV}$ . At the LC, the direct observation of  $h_{\text{SM}} \rightarrow \gamma\gamma$  is also possible in  $Zh_{\text{SM}}$  production despite its suppressed branching ratio. The partial width  $\Gamma(h^0 \rightarrow \gamma\gamma)$  is also significant in that it governs the Higgs production rate at a  $\gamma\gamma$  collider.

### 3.2. Standard Model Higgs boson production at the LC

In the Standard Model there are two main processes to produce the Higgs boson in  $e^+e^-$  annihilation. These processes are also relevant in many extensions of the Standard Model, particularly near the decoupling limit, in which the lightest CP-even Higgs boson possesses properties nearly identical to those of the SM Higgs boson. In the ‘‘Higgsstrahlung’’ process, a virtual  $Z$  boson decays to an on-shell  $Z$  and the  $h_{\text{SM}}$ , as depicted in fig. 3(a).

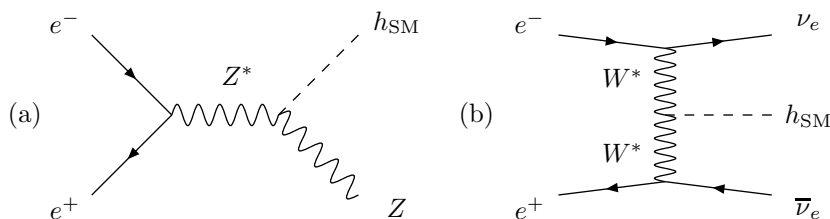


Fig. 3: Main production processes for Higgs production in  $e^+e^-$  annihilation. (a) Higgsstrahlung. (b)  $WW$  fusion.

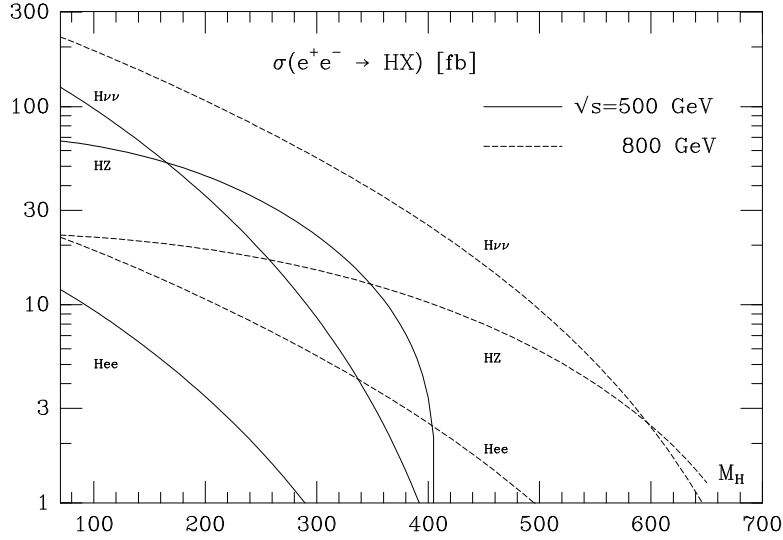


Fig. 4: Cross sections for Higgsstrahlung ( $e^+e^- \rightarrow Zh_{\text{SM}}$ ) and Higgs production via  $W^+W^-$  fusion ( $e^+e^- \rightarrow \nu\bar{\nu}h_{\text{SM}}$ ) and  $ZZ$  fusion ( $e^+e^- \rightarrow e^+e^-h_{\text{SM}}$ ) as a function of  $m_{h_{\text{SM}}}$  for two center-of-mass energies,  $\sqrt{s} = 500$  and  $800$  GeV [5].

The cross section for Higgsstrahlung rises sharply at threshold to a maximum a few tens of GeV above  $m_h + m_Z$ , and then falls off as  $s^{-1}$ , as shown in fig. 4. The associated production of the  $Z$  provides an important trigger for Higgsstrahlung events. In particular, in some theories beyond the Standard Model, the Higgs boson decays into invisible modes, in which case the ability to reconstruct the Higgs boson mass peak in the spectrum of the missing mass recoiling against the  $Z$  will be crucial. The other production process is called “vector boson fusion”, where the incoming  $e^+$  and  $e^-$  each emit a virtual vector boson, followed by vector boson fusion to the  $h_{\text{SM}}$ . Fig. 3(b) depicts the  $W^+W^-$  fusion process. Similarly, the  $ZZ$  fusion process corresponds to  $e^+e^- \rightarrow e^+e^-h_{\text{SM}}$ . In contrast to Higgsstrahlung, the vector boson fusion cross section grows as  $\ln s$ , and thus is the dominant Higgs production mechanism for  $\sqrt{s} \gg m_{h_{\text{SM}}}$ . The cross section for  $WW$  fusion is about ten times larger than that for  $ZZ$  fusion. Nevertheless, the latter provides complementary information on the  $ZZh_{\text{SM}}$  vertex. Note that at an  $e^-e^-$  collider, the Higgsstrahlung and  $W^+W^-$  fusion processes are absent, so that  $ZZ$  fusion is the dominant Higgs production process [43].

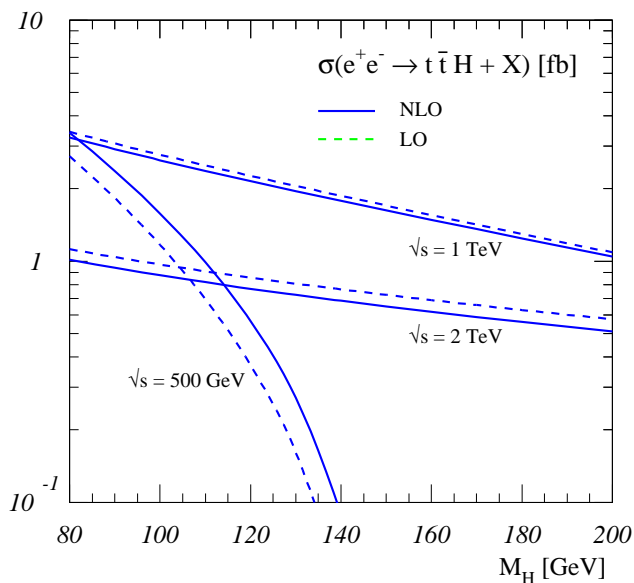


Fig. 5: Cross-sections for  $e^+e^- \rightarrow t\bar{t}h_{\text{SM}}$  in fb for three choices of center-of-mass energy. The dashed lines correspond to the tree-level result [44], and the solid lines include the next-to-leading order QCD corrections [45].

Other relevant processes for producing Higgs bosons are associated production with a fermion-antifermion pair, and multi-Higgs production. Among production mechanisms of the former class, only  $e^+e^- \rightarrow t\bar{t}h_{\text{SM}}$  has a significant cross section, around the femtobarn level in the Standard Model, as depicted in fig. 5. As a result, if  $m_{h_{\text{SM}}}$  is small enough (or  $\sqrt{s}$  is large enough), this process can be used for determining the Higgs-top quark Yukawa coupling. The cross section for double Higgs production ( $e^+e^- \rightarrow Zh_{\text{SM}}h_{\text{SM}}$ ) is even smaller, of order 0.1 fb for  $100 \text{ GeV} \lesssim m_{h_{\text{SM}}} \lesssim 150 \text{ GeV}$  and  $\sqrt{s}$  ranging between 500 GeV and 1 TeV. With sufficient luminosity, the latter can be used for extracting the triple Higgs self-coupling.

At the  $\gamma\gamma$  collider, a Higgs boson is produced as an  $s$ -channel resonance via the one-loop triangle diagram. Every charged particle whose mass is generated by the Higgs boson contributes to this process. In the Standard Model, the main contributors are the  $W^\pm$  and the  $t$ -quark loops. See Section 11 for further discussion.



## 4. SM Higgs searches before the linear collider

### 4.1. Direct search limits from LEP

The LEP collider completed its final run in 2000, and presented tantalizing hints for the possible observation of the Higgs boson. The combined data from all four LEP collaborations exhibits a slight preference for the signal plus background hypothesis for a Standard Model Higgs boson mass in the vicinity of 116 GeV, as compared to the background only hypothesis [25]. However, the excess over the expected background was not sufficiently significant to support a claim of discovery or even an “observation” of evidence for the Higgs boson. A more conservative interpretation of the data yields a 95% CL lower limit of  $m_{h_{\text{SM}}} > 114.4$  GeV.

### 4.2. Implications of precision electroweak measurements

Indirect constraints on the Higgs boson mass within the SM can be obtained from confronting the SM predictions with results of electroweak precision measurements. In the case of the top quark mass, the indirect determination turned out to be in remarkable agreement with the actual experimental value [24]. In comparison, to obtain constraints on  $m_{h_{\text{SM}}}$  of similar precision, much higher accuracy is required for both the experimental results and the theory predictions. This is due to the fact that the leading dependence of the precision observables on  $m_{h_{\text{SM}}}$  is only logarithmic, while the dominant effects of the top-quark mass enter quadratically.

Fig. 6(a) shows the currently most precise result for  $m_W$  as function of  $m_{h_{\text{SM}}}$  in the SM, and compares it with the present experimental value of  $m_W$ . The calculation incorporates the complete electroweak fermion-loop contributions at  $\mathcal{O}(\alpha^2)$  [46]. Based on this result, the remaining theoretical uncertainty from unknown higher-order corrections has been estimated to be about 6 MeV [46]. This is about a factor five smaller than the uncertainty induced by the current experimental error on the top-quark mass,  $\Delta m_t^{\text{exp}} = \pm 5.1$  GeV, which presently dominates the theoretical uncertainty. Fig. 6(b) shows the prospective situation at a future  $e^+e^-$  linear collider after the Giga- $Z$  operation and a threshold measurement of the  $W$  mass (keeping the present experimental central values for simplicity), which are expected to reduce the experimental errors to  $\Delta m_W^{\text{exp}} = 6$  MeV and  $\Delta m_t^{\text{exp}} = 200$  MeV. The plot clearly shows a considerable improvement in the sensitivity to  $m_{h_{\text{SM}}}$  achievable at the LC via very precise measurements of  $m_W$  and  $m_t$ . Since furthermore the experimental error of  $\sin^2 \theta_{\text{eff}}$

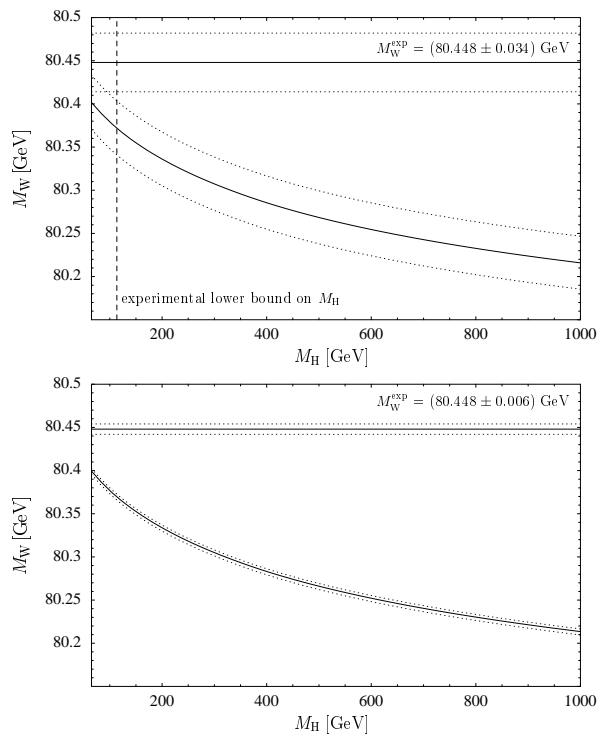


Fig. 6: The prediction for  $m_W$  as a function of  $m_{h_{\text{SM}}}$  is compared with the experimental value of  $m_W$  (a) for the current experimental accuracies of  $m_W$  and  $m_t$ , and (b) for the prospective future accuracies at the LC with the Giga- $Z$  option and a precise  $W$  threshold scan, assuming the present experimental central values [46]. The present experimental 95% CL lower bound on the Higgs-boson mass,  $m_{h_{\text{SM}}} = 114.4$  GeV, is indicated in (a) by the vertical dashed line.

is expected to be reduced by almost a factor of 20 at Giga- $Z$ , the accuracy in the indirect determination of the Higgs-boson mass from all data will improve by about a factor of 10 compared to the present situation [21].

### 4.3. Expectations for Tevatron searches

The upgraded Tevatron began taking data in the spring of 2001. This is the only collider at which the Higgs boson can be produced until the LHC begins operation in 2007. The Tevatron Higgs Working Group [47] presented a detailed analysis of the Higgs discovery reach at the upgraded Tevatron. Here, we summarize the main results. Two Higgs mass

ranges were considered separately: (i)  $100 \text{ GeV} \lesssim m_{h_{\text{SM}}} \lesssim 135 \text{ GeV}$  and (ii)  $135 \text{ GeV} \lesssim m_{h_{\text{SM}}} \lesssim 190 \text{ GeV}$ , corresponding to the two different dominant Higgs decay modes:  $h_{\text{SM}} \rightarrow b\bar{b}$  for the lighter mass range and  $h_{\text{SM}} \rightarrow WW^{(*)}$  for the heavier mass range.

In mass range (i), the relevant production mechanisms are  $q_i\bar{q}_j \rightarrow Vh_{\text{SM}}$ , where  $V = W$  or  $Z$ . In all cases, the dominant  $h_{\text{SM}} \rightarrow b\bar{b}$  decay was employed. The most relevant final-state signatures correspond to events in which the vector boson decays leptonically ( $W \rightarrow \ell\nu$ ,  $Z \rightarrow \ell^+\ell^-$  and  $Z \rightarrow \nu\bar{\nu}$ , where  $\ell = e$  or  $\mu$ ), resulting in  $\ell\nu b\bar{b}$ ,  $\nu\bar{\nu} b\bar{b}$  and  $\ell^+\ell^- b\bar{b}$  final states. In mass range (ii), the relevant production mechanisms include  $gg \rightarrow h_{\text{SM}}$ ,  $V^*V^* \rightarrow h_{\text{SM}}$  and  $q_i\bar{q}_j \rightarrow Vh_{\text{SM}}$ , with decays  $h_{\text{SM}} \rightarrow WW^{(*)}$ ,  $ZZ^{(*)}$ . The most relevant phenomenological signals are those in which two of the final-state vector bosons decay leptonically, resulting in  $\ell^+\ell^-\nu\bar{\nu}$  or  $\ell^\pm\ell^\pm jjX$ , where  $j$  is a hadronic jet and  $X$  consists of two additional leptons (either charged or neutral). For example, the latter can arise from  $Wh_{\text{SM}}$  production followed by  $h_{\text{SM}} \rightarrow WW^{(*)}$ , where the two like-sign  $W$  bosons decay leptonically, and the third  $W$  decays into hadronic jets. In this case  $X$  is a pair of neutrinos.

Fig. 7 summarizes the Higgs discovery reach versus the total integrated luminosity delivered to the Tevatron (and by assumption, delivered to each detector). As the plot shows, the required integrated luminosity increases rapidly with Higgs mass to 140 GeV, beyond which the high-mass channels play the dominant role. With  $2 \text{ fb}^{-1}$  per detector, the 95% CL limits will barely extend the expected LEP limits, but with  $10 \text{ fb}^{-1}$ , the SM Higgs boson can be excluded up to 180 GeV if the Higgs boson does not exist in that mass range.

With further machine improvements, the Tevatron may provide a total integrated luminosity as high as  $15 \text{ fb}^{-1}$  before the LHC starts to yield significant results. If such an integrated luminosity could be reached and if  $m_{h_{\text{SM}}} \simeq 115 \text{ GeV}$ , then the Tevatron experiments will be able to achieve a  $5\sigma$  discovery of the Higgs boson. If no Higgs events are detected, the LEP limits will be significantly extended, with a 95% CL exclusion possible up to about  $m_{h_{\text{SM}}} \simeq 185 \text{ GeV}$ .<sup>2</sup> Moreover, evidence for a Higgs boson at the  $3\sigma$  level could be achieved up to about  $m_{h_{\text{SM}}} \simeq 175 \text{ GeV}$ .

Evidence for or discovery of a Higgs boson at the Tevatron would be a landmark in high energy physics. However, even if a Higgs boson is seen, the

<sup>2</sup>The Higgs mass region around 140 GeV might require more luminosity, depending on the magnitude of systematic errors due to uncertainties in  $b$ -tagging efficiency, background rate, the  $b\bar{b}$  mass resolution, etc.

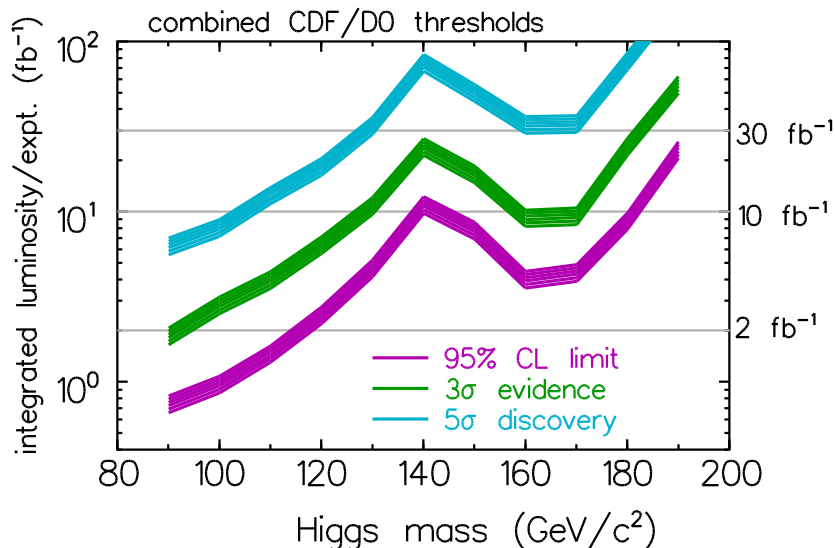


Fig. 7: The integrated luminosity required per experiment, to either exclude a SM Higgs boson at 95% CL or discover it at the  $3\sigma$  or  $5\sigma$  level, as a function of the Higgs mass. These results are based on the combined statistical power of both experiments. The curves shown are obtained by combining the  $\ell\nu b\bar{b}$ ,  $\nu\bar{\nu} b\bar{b}$  and  $\ell^+\ell^- b\bar{b}$  channels using the neural network selection in the low-mass Higgs region ( $90 \text{ GeV} \lesssim m_{h_{\text{SM}}} \lesssim 135 \text{ GeV}$ ), and the  $\ell^\pm\ell^\pm jjX$  and  $\ell^+\ell^-\nu\bar{\nu}$  channels in the high-mass Higgs region ( $135 \text{ GeV} \lesssim m_{h_{\text{SM}}} \lesssim 190 \text{ GeV}$ ). The lower edge of the bands is the calculated threshold; the bands extend upward from these nominal thresholds by 30% as an indication of the uncertainties in  $b$ -tagging efficiency, background rate, mass resolution, and other effects. Taken from [47].

Tevatron data would only provide a very rough phenomenological profile of the Higgs boson. In contrast, the LHC and the LC (the latter with greater precision) could measure enough of its properties to verify that the interactions of the Higgs boson provide the dynamics responsible for the generation of mass for the vector bosons, quarks and charged leptons.

#### 4.4. Expectations for LHC searches

At the LHC, the ATLAS and CMS detectors have been specifically designed to guarantee observation of a SM Higgs boson, regardless of its mass (below about 1 TeV). The most important production processes for the  $h_{\text{SM}}$  are the gluon fusion process,  $gg \rightarrow h_{\text{SM}}$ , and the vector boson fusion

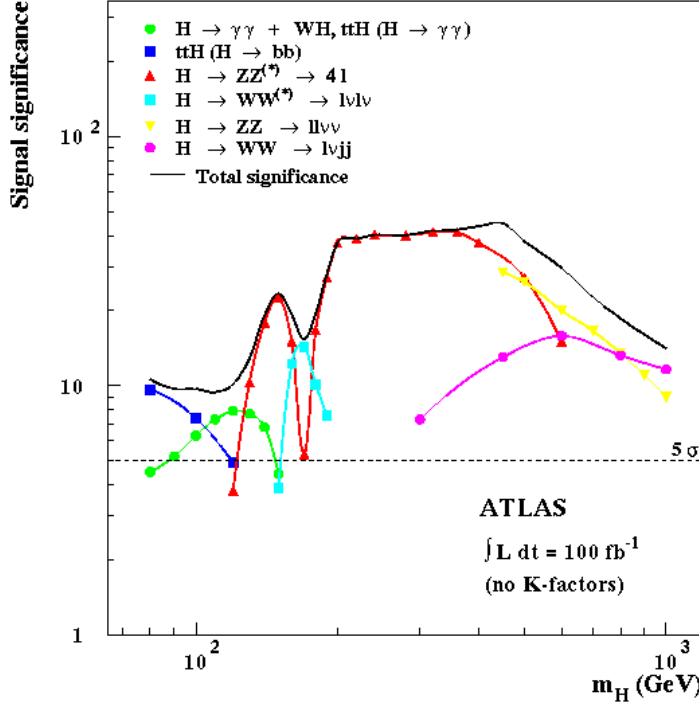


Fig. 8: Statistical significance levels as a function of the Higgs mass for the ATLAS experiment at the LHC, assuming an integrated luminosity of  $100 \text{ fb}^{-1}$ . Taken from [48].

process,  $WW \rightarrow h_{\text{SM}}$ . In particular, for  $m_{h_{\text{SM}}} \lesssim 130 \text{ GeV}$  the important discovery modes are  $gg, WW \rightarrow h_{\text{SM}} \rightarrow \gamma\gamma, \tau^+\tau^-$ . At high luminosity,  $q_i\bar{q}_j \rightarrow W^\pm h_{\text{SM}}$  and  $gg \rightarrow t\bar{t}h_{\text{SM}}$  with  $h_{\text{SM}} \rightarrow \gamma\gamma$  and  $h_{\text{SM}} \rightarrow b\bar{b}$  should also be visible. For  $m_{h_{\text{SM}}} > 130 \text{ GeV}$ ,  $gg \rightarrow h_{\text{SM}} \rightarrow ZZ^{(*)} \rightarrow 4\ell$  is extremely robust except for the small mass region with  $m_{h_{\text{SM}}}$  just above  $2m_W$  in which  $h_{\text{SM}} \rightarrow WW$  is allowed and  $\text{BR}(h_{\text{SM}} \rightarrow ZZ^*)$  drops sharply. In this region,  $gg, WW \rightarrow h_{\text{SM}} \rightarrow WW \rightarrow \ell\nu\ell\nu$  provides a strong Higgs signal. For  $m_{h_{\text{SM}}} > 300\text{--}400 \text{ GeV}$ , the final states  $h_{\text{SM}} \rightarrow WW \rightarrow \ell\nu jj$  and  $h_{\text{SM}} \rightarrow ZZ \rightarrow \ell\nu\nu$ , where the  $h_{\text{SM}}$  is produced by a combination of  $gg$  and  $WW$  fusion, provide excellent discovery channels for Higgs masses up to about 1 TeV (*i.e.*, well beyond the  $m_{h_{\text{SM}}} \sim 800 \text{ GeV}$  limit of viability for the  $h_{\text{SM}} \rightarrow 4\ell$  mode). These results are summarized in fig. 8, from which we observe that the net statistical significance for the  $h_{\text{SM}}$ , after combin-

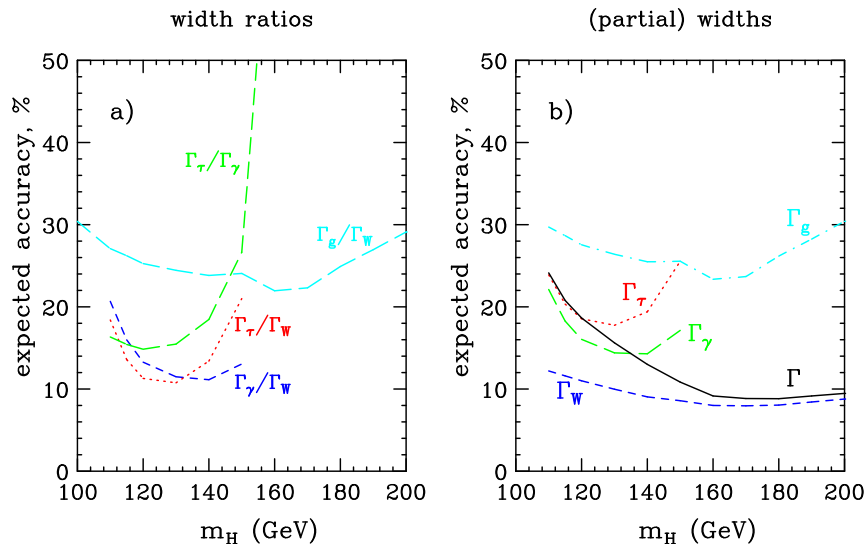


Fig. 9: Relative accuracy expected at the LHC with  $200 \text{ fb}^{-1}$  of data for (a) various ratios of Higgs boson partial widths and (b) the indirect determination of partial and total widths. Expectations for width ratios assume  $W, Z$  universality; indirect width measurements also assume  $b, \tau$  universality and a small branching ratio for unobserved modes. Taken from the parton-level analysis of [53].

ing channels, exceeds  $10\sigma$  for all  $m_{h_{\text{SM}}} > 80 \text{ GeV}$ , assuming accumulated luminosity of  $L = 100 \text{ fb}^{-1}$  at the ATLAS detector [48]. Similar results are obtained by the CMS collaboration [49, 50], with the  $h_{\text{SM}}\gamma\gamma$  discovery mode even more prominent for  $m_{h_{\text{SM}}} \lesssim 150 \text{ GeV}$ .

Precision measurements for a certain number of quantities will be possible, depending upon the exact value of  $m_{h_{\text{SM}}}$ . For example, in [51] it is estimated that  $m_{h_{\text{SM}}}$  can be measured to  $< 0.1\%$  for  $m_{h_{\text{SM}}} < 400 \text{ GeV}$  and to  $0.1\text{--}1\%$  for  $400 < m_{h_{\text{SM}}} < 700 \text{ GeV}$ . Using the  $4\ell$  final state,  $\Gamma_{h_{\text{SM}}}^T$  can be determined for  $m_{h_{\text{SM}}} \gtrsim 250 \text{ GeV}$  from the shape of the  $4\ell$  mass peak. Various ratios of branching ratios and a selection of cross sections times branching ratios can be measured in any given mass region. Some early estimates of possibilities and achievable accuracies appear in [2]. A more recent, but rather optimistic parton-level theoretical study [52, 53] (see fig. 9) finds that if  $m_{h_{\text{SM}}} \lesssim 200 \text{ GeV}$  then good accuracies can be achieved for many absolute partial widths and for the total width provided: (a)  $WW$  fusion production can be reliably separated from  $gg$  fusion; (b) the  $WW/ZZ$

coupling ratio is as expected in the SM from the  $SU(2)\times U(1)$  symmetry; (c) the  $WW^*$  final state can be observed in both  $gg$  and  $WW$  fusion; and (d) there are no unexpected decays of the  $h_{\text{SM}}$ . Errors estimated in this way for  $L = 200 \text{ fb}^{-1}$  of accumulated data are given in fig. 9. However, errors found in recent ATLAS studies of a few of these channels are substantially larger [54]. For example, for  $L = 300 \text{ fb}^{-1}$  ATLAS finds that the smallest error on  $\Gamma_\tau/\Gamma_W$  is achieved for  $m_{h_{\text{SM}}} \sim 130 \text{ GeV}$  and is of order  $\pm 27\%$  (as compared to the  $\pm 11\%$  of fig. 9) and that the error rises rapidly for  $m_{h_{\text{SM}}}$  away from 130 GeV, reaching  $\pm 60\%$  for  $m_{h_{\text{SM}}} = 150 \text{ GeV}$ . Invisible Higgs decays have also been addressed in the theoretical work [55]; CMS simulations show some promise for this channel.

## 5. Higgs bosons in low-energy supersymmetry

The Higgs sector of the MSSM, the simplest realistic model of low-energy supersymmetry, consists of the two-Higgs-doublet extension of the Standard Model plus the corresponding superpartners. Two Higgs doublets, one with  $Y = +1$  and one with  $Y = -1$ , are needed in order that gauge anomalies due to the higgsino superpartners are exactly canceled. In particular, the Higgs sector contains eight scalar degrees of freedom: one complex  $Y = -1$  doublet,  $\Phi_d = (\Phi_d^0, \Phi_d^-)$  and one complex  $Y = +1$  doublet,  $\Phi_u = (\Phi_u^+, \Phi_u^0)$ . This notation reflects the fact that in the MSSM, the interaction Lagrangian that describes the Higgs couplings to fermions is constrained by supersymmetry and obeys the following property:  $\Phi_d^0$  couples exclusively to down-type fermion pairs and  $\Phi_u^0$  couples exclusively to up-type fermion pairs. This pattern of Higgs-fermion couplings defines the Type-II two-Higgs-doublet model [56, 57].

When the Higgs potential is minimized, the neutral components of the Higgs fields acquire vacuum expectation values<sup>3</sup>  $\langle \Phi_d^0 \rangle = v_d/\sqrt{2}$  and  $\langle \Phi_u^0 \rangle = v_u/\sqrt{2}$ , where the normalization has been chosen such that  $v^2 \equiv v_d^2 + v_u^2 = (246 \text{ GeV})^2$ . The ratio of vacuum expectation values is denoted by

$$\tan \beta \equiv v_u/v_d. \quad (3)$$

The physical Higgs spectrum consists of a charged Higgs pair

$$H^\pm = \Phi_d^\pm \sin \beta + \Phi_u^\pm \cos \beta, \quad (4)$$

<sup>3</sup>The phases of the Higgs fields can be chosen such that the vacuum expectation values are real and positive. That is, the tree-level MSSM Higgs sector conserves CP, which implies that the neutral Higgs mass eigenstates possess definite CP quantum numbers.

one CP-odd scalar

$$A^0 = \sqrt{2} (\text{Im } \Phi_d^0 \sin \beta + \text{Im } \Phi_u^0 \cos \beta) , \quad (5)$$

and two CP-even scalars:

$$\begin{aligned} h^0 &= -(\sqrt{2} \text{Re } \Phi_d^0 - v_d) \sin \alpha + (\sqrt{2} \text{Re } \Phi_u^0 - v_u) \cos \alpha , \\ H^0 &= (\sqrt{2} \text{Re } \Phi_d^0 - v_d) \cos \alpha + (\sqrt{2} \text{Re } \Phi_u^0 - v_u) \sin \alpha , \end{aligned} \quad (6)$$

(with  $m_{h^0} \leq m_{H^0}$ ). The angle  $\alpha$  arises when the CP-even Higgs squared-mass matrix (in the  $\Phi_d^0$ – $\Phi_u^0$  basis) is diagonalized to obtain the physical CP-even Higgs states. The Goldstone bosons,  $G^\pm$  and  $G^0$ , which are orthogonal to  $H^\pm$  and  $A^0$  respectively, provide the longitudinal components of the massive  $W^\pm$  and  $Z$  via the Higgs mechanism.

In two-Higgs-doublet models with Type-II Higgs-fermion couplings, the  $Y = -1$  Higgs doublet generates mass for “up”-type quarks and the  $Y = +1$  Higgs doublet generates mass for “down”-type quarks (and charged leptons) [58, 59]. The tree-level relations between the quark masses and the Higgs-fermion Yukawa couplings (using 3rd family notation) are given by:

$$h_b = \frac{\sqrt{2} m_b}{v_d} = \frac{\sqrt{2} m_b}{v \cos \beta} , \quad (7)$$

$$h_t = \frac{\sqrt{2} m_t}{v_u} = \frac{\sqrt{2} m_t}{v \sin \beta} . \quad (8)$$

Radiative corrections to these relations will be examined in Section 5.2.

At this stage,  $\tan \beta$  is a free parameter of the model. However, theoretical considerations suggest that  $\tan \beta$  cannot be too small or too large. The crudest bounds arise from unitarity constraints. If  $\tan \beta$  becomes too small, then the Higgs coupling to top quarks becomes strong and the tree-unitarity of processes involving the Higgs-top quark Yukawa coupling is violated. A rough lower bound advocated by [60],  $\tan \beta \gtrsim 0.3$ , corresponds to a value of  $h_t$  in the perturbative region. A similar argument involving  $h_b$  would yield  $\tan \beta \lesssim 120$ . A more restrictive theoretical constraint is based on the requirement that Higgs-fermion Yukawa couplings,  $h_t$  and  $h_b$ , remain finite when running from the electroweak scale to some large energy scale  $\Lambda$ , above which new physics enters. The limits on  $\tan \beta$  depend on the choice of  $\Lambda$ . Integrating the Yukawa coupling renormalization group equations from the electroweak scale to  $\Lambda$  (allowing for the possible existence of a supersymmetry-breaking scale,  $m_Z \leq M_{\text{SUSY}} \leq \Lambda$ ), one can determine the range of  $\tan \beta$  for which  $h_t$  and  $h_b$  remain finite. This exercise has been carried out at two-loops in [61]. Suppose that the low-energy



theory at the electroweak scale is the MSSM, and that there is no additional new physics below the grand unification scale of  $\Lambda = 2 \times 10^{16}$  GeV. Then, for  $m_t = 175$  GeV, the Higgs-fermion Yukawa couplings remain finite at all energy scales below  $\Lambda$  if  $1.5 \lesssim \tan \beta \lesssim 65$ . Note that this result is consistent with the scenario of radiative electroweak symmetry breaking in low-energy supersymmetry based on supergravity, which requires that  $1 \lesssim \tan \beta \lesssim m_t/m_b$ .<sup>4</sup> Thus, we expect  $\tan \beta$  to lie in the range  $1 \lesssim \tan \beta \lesssim 55$ .<sup>5</sup>

### 5.1. MSSM Higgs sector at tree level

The supersymmetric structure of the theory imposes constraints on the Higgs sector of the model. As a result, all Higgs sector parameters at tree level are determined by two free parameters:  $\tan \beta$  and one Higgs mass, conveniently chosen to be  $m_{A^0}$ . In particular,

$$m_{H^\pm}^2 = m_{A^0}^2 + m_W^2, \quad (9)$$

and the CP-even Higgs bosons  $h^0$  and  $H^0$  are eigenstates of the following squared-mass matrix (with respect to the  $\text{Re } \Phi_d^0$ - $\text{Re } \Phi_u^0$  basis):

$$\mathcal{M}_0^2 = \begin{pmatrix} m_{A^0}^2 \sin^2 \beta + m_Z^2 \cos^2 \beta & -(m_{A^0}^2 + m_Z^2) \sin \beta \cos \beta \\ -(m_{A^0}^2 + m_Z^2) \sin \beta \cos \beta & m_{A^0}^2 \cos^2 \beta + m_Z^2 \sin^2 \beta \end{pmatrix}. \quad (10)$$

The eigenvalues of  $\mathcal{M}_0^2$  are the tree-level squared-masses of the two CP-even Higgs scalars

$$m_{H^0, h^0}^2 = \frac{1}{2} \left( m_{A^0}^2 + m_Z^2 \pm \sqrt{(m_{A^0}^2 + m_Z^2)^2 - 4m_Z^2 m_{A^0}^2 \cos^2 2\beta} \right), \quad (11)$$

Note that eq. (11) yields an upper bound to the tree-level mass of the light CP-even Higgs boson:  $m_{h^0}^2 \leq m_Z^2 |\cos 2\beta| \leq m_Z^2$ . Radiative corrections can significantly increase this upper bound by as much as 50% as described in Section 5.2. Nevertheless, it is already apparent that the MSSM favors a CP-even Higgs boson whose mass is not much larger than  $m_Z$ , a result that is consistent with the inferred Higgs mass limit from precision electroweak measurements discussed in Section 2.

From the above results, one also obtains:

$$\cos^2(\beta - \alpha) = \frac{m_{h^0}^2(m_Z^2 - m_{h^0}^2)}{m_{A^0}^2(m_{H^0}^2 - m_{h^0}^2)}, \quad (12)$$

<sup>4</sup>Here, the quark masses are evaluated at  $m_Z$ . We take  $m_t(m_Z) \simeq 165$  GeV and  $m_b(m_Z) \simeq 3$  GeV.

<sup>5</sup>The lower bound on  $\tan \beta$  can be taken to be  $\tan \beta \gtrsim 2.4$ , based on the LEP MSSM Higgs search discussed in Section 6.1.

where  $\alpha$  is the angle that diagonalizes the CP-even Higgs squared-mass matrix [see eq. (6)]. In the convention where  $\tan \beta$  is positive (*i.e.*,  $0 \leq \beta \leq \pi/2$ ), the angle  $\alpha$  lies in the range  $-\pi/2 \leq \alpha \leq 0$ .

The limit of  $m_{A^0} \gg m_Z$  is of particular interest. The expressions for the Higgs masses and mixing angle simplify in this limit and one finds

$$m_{h^0}^2 \simeq m_Z^2 \cos^2 2\beta, \quad (13)$$

$$m_{H^0}^2 \simeq m_{A^0}^2 + m_Z^2 \sin^2 2\beta, \quad (14)$$

$$m_{H^\pm}^2 = m_{A^0}^2 + m_W^2, \quad (15)$$

$$\cos^2(\beta - \alpha) \simeq \frac{m_Z^4 \sin^2 4\beta}{4m_{A^0}^4}. \quad (16)$$

Two consequences are immediately apparent. First,  $m_{A^0} \simeq m_{H^0} \simeq m_{H^\pm}$ , up to corrections of  $\mathcal{O}(m_Z^2/m_{A^0})$ . Second,  $\cos(\beta - \alpha) = 0$  up to corrections of  $\mathcal{O}(m_Z^2/m_{A^0}^2)$ . This is the *decoupling* limit [22, 62] because when  $m_{A^0}$  is large, the effective low-energy theory below the scale of  $m_{A^0}$  contains a single CP-even Higgs boson,  $h^0$ , whose properties are nearly identical to those of the Standard Model Higgs boson,  $h_{\text{SM}}$ .

The phenomenology of the Higgs sector is determined by the various couplings of the Higgs bosons to gauge bosons, Higgs bosons and fermions. The couplings of the two CP-even Higgs bosons to  $W$  and  $Z$  pairs are given in terms of the angles  $\alpha$  and  $\beta$  by

$$g_{h^0 VV} = g_V m_V \sin(\beta - \alpha), \quad g_{H^0 VV} = g_V m_V \cos(\beta - \alpha), \quad (17)$$

where  $g_V \equiv 2m_V/v$  for  $V = W$  or  $Z$ . There are no tree-level couplings of  $A^0$  or  $H^\pm$  to  $VV$ . The couplings of one gauge boson to two neutral Higgs bosons are given by:

$$g_{h^0 A^0 Z} = \frac{g \cos(\beta - \alpha)}{2 \cos \theta_W}, \quad g_{H^0 A^0 Z} = \frac{-g \sin(\beta - \alpha)}{2 \cos \theta_W}. \quad (18)$$

As noted earlier, the pattern of Higgs-fermion couplings in the MSSM are those of the Type-II two-Higgs-doublet model [56, 57]. The couplings of the neutral Higgs bosons to  $f\bar{f}$  relative to the Standard Model value,

$gm_f/2m_W$ , are given by

$$\begin{aligned}
h^0 b\bar{b} \quad (\text{or } h^0 \tau^+ \tau^-) : & \quad -\frac{\sin \alpha}{\cos \beta} = \sin(\beta - \alpha) - \tan \beta \cos(\beta - \alpha), \\
h^0 t\bar{t} : & \quad \frac{\cos \alpha}{\sin \beta} = \sin(\beta - \alpha) + \cot \beta \cos(\beta - \alpha), \\
H^0 b\bar{b} \quad (\text{or } H^0 \tau^+ \tau^-) : & \quad \frac{\cos \alpha}{\cos \beta} = \cos(\beta - \alpha) + \tan \beta \sin(\beta - \alpha), \\
H^0 t\bar{t} : & \quad \frac{\sin \alpha}{\sin \beta} = \cos(\beta - \alpha) - \cot \beta \sin(\beta - \alpha), \\
A^0 b\bar{b} \quad (\text{or } A^0 \tau^+ \tau^-) : & \quad \gamma_5 \tan \beta, \\
A^0 t\bar{t} : & \quad \gamma_5 \cot \beta,
\end{aligned} \tag{19}$$

(the  $\gamma_5$  indicates a pseudoscalar coupling), and the charged Higgs boson couplings to fermion pairs (with all particles pointing into the vertex) are given by

$$\begin{aligned}
g_{H^- t\bar{b}} &= \frac{g}{\sqrt{2}m_W} \left[ m_t \cot \beta P_R + m_b \tan \beta P_L \right], \\
g_{H^- \tau^+ \nu} &= \frac{g}{\sqrt{2}m_W} \left[ m_\tau \tan \beta P_L \right],
\end{aligned} \tag{20}$$

where  $P_{R,L} \equiv \frac{1}{2}(1 \pm \gamma_5)$  are the right and left-handed projection operators, respectively.

The neutral Higgs couplings to fermion pairs [eq. (19)] have been written in such a way that their behavior can be immediately ascertained in the decoupling limit ( $m_{A^0} \gg m_Z$ ) by setting  $\cos(\beta - \alpha) = 0$ . In particular, in the decoupling limit, the couplings of  $h^0$  to vector bosons and fermion pairs are equal to the corresponding couplings of the SM Higgs boson.

The region of MSSM Higgs sector parameter space in which the decoupling limit applies is large, because  $\cos(\beta - \alpha)$  approaches zero quite rapidly once  $m_{A^0}$  is larger than about 200 GeV, as shown in fig. 10. As a result, over a significant region of the MSSM parameter space, the search for the lightest CP-even Higgs boson of the MSSM is equivalent to the search for the Standard Model Higgs boson.

## 5.2. The radiatively corrected MSSM Higgs sector

When one-loop radiative corrections are incorporated, the Higgs masses and couplings depend on additional parameters of the supersymmetric model that enter via the virtual loops. One of the most striking effects

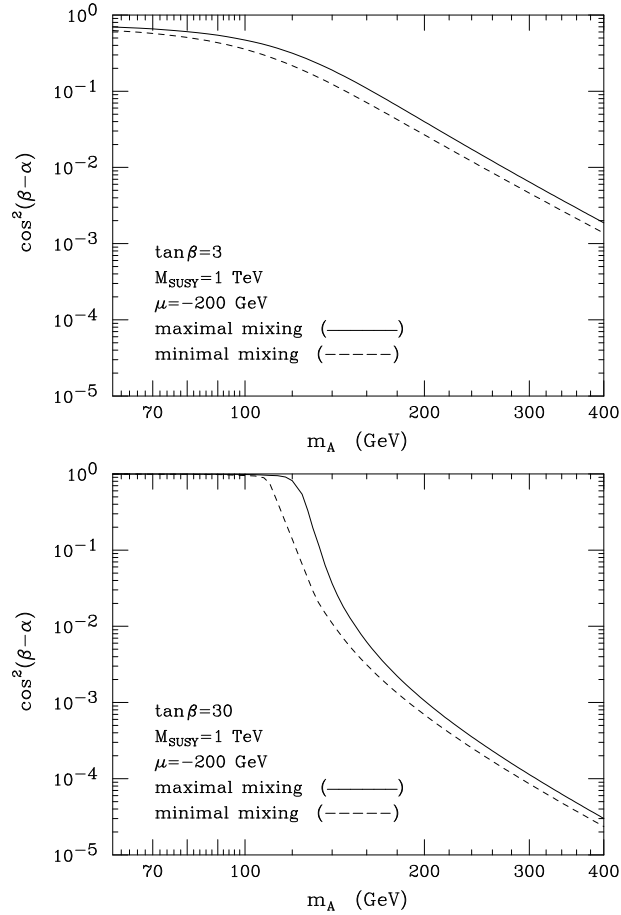


Fig. 10: The value of  $\cos^2(\beta - \alpha)$  is shown as a function of  $m_{A^0}$  for two choices of  $\tan\beta = 3$  and  $\tan\beta = 30$ . When radiative-corrections are included, one can define an approximate loop-corrected angle  $\alpha$  as a function of  $m_{A^0}$ ,  $\tan\beta$  and the MSSM parameters. In the figures above, we have incorporated radiative corrections, assuming that the top-squark masses are given by  $M_{\text{SUSY}} = 1$  TeV. In addition, two extreme cases for the squark mixing parameters are shown (see Section 5.2 for further discussion of the radiative corrections and their dependence on the supersymmetric parameters). The decoupling effect expected from eq. (16), in which  $\cos^2(\beta - \alpha) \propto m_Z^4/m_{A^0}^4$  for  $m_{A^0} \gg m_Z$ , continues to hold even when radiative corrections are included.

of the radiative corrections to the MSSM Higgs sector is the modification of the upper bound of the light CP-even Higgs mass, as first noted in [63]. When  $\tan\beta \gg 1$  and  $m_{A^0} \gg m_Z$ , the *tree-level* prediction of  $m_{h^0} = m_Z$  corresponds to the theoretical upper bound for  $m_{h^0}$ . Including radiative corrections, this theoretical upper bound is increased, primarily because of an incomplete cancellation of the top-quark and top-squark (stop) loops. (These contributions would cancel if supersymmetry were exact.) The relevant parameters that govern the stop sector are the average of the two stop squared-masses:  $M_{\text{SUSY}}^2 \equiv \frac{1}{2}(M_{\tilde{t}_1}^2 + M_{\tilde{t}_2}^2)$ , and the off-diagonal element of the stop squared-mass matrix:  $m_t X_t \equiv m_t(A_t - \mu \cot\beta)$ , where  $A_t$  is a soft supersymmetry-breaking trilinear scalar interaction term, and  $\mu$  is the supersymmetric Higgs mass parameter. The qualitative behavior of the radiative corrections can be most easily seen in the large top squark mass limit, where, in addition, the splitting of the two diagonal entries and the off-diagonal entry of the stop squared-mass matrix are both small in comparison to  $M_{\text{SUSY}}^2$ . In this case, the upper bound on the lightest CP-even Higgs mass is approximately given by

$$m_{h^0}^2 \lesssim m_Z^2 + \frac{3g^2 m_t^4}{8\pi^2 m_W^2} \left[ \ln \left( \frac{M_{\text{SUSY}}^2}{m_t^2} \right) + \frac{X_t^2}{M_{\text{SUSY}}^2} \left( 1 - \frac{X_t^2}{12M_{\text{SUSY}}^2} \right) \right]. \quad (21)$$

More complete treatments of the radiative corrections include the effects of stop mixing, renormalization group improvement, and the leading two-loop contributions, and imply that these corrections somewhat overestimate the true upper bound of  $m_{h^0}$  (see [64] for the most recent results). Nevertheless, eq. (21) correctly illustrates some noteworthy features of the more precise result. First, the increase of the light CP-even Higgs mass bound beyond  $m_Z$  can be significant due to the  $m_t^4$  enhancement of the one-loop radiative correction. Second, the dependence of the light Higgs mass on the stop mixing parameter  $X_t$  implies that (for a given value of  $M_{\text{SUSY}}$ ) the upper bound of the light Higgs mass initially increases with  $X_t$  and reaches its *maximal* value at  $X_t \simeq \sqrt{6}M_{\text{SUSY}}$ . This point is referred to as the *maximal mixing* case (whereas  $X_t = 0$  is called the *minimal mixing* case).

Taking  $m_{A^0}$  large, fig. 11 illustrates that the maximal value of the lightest CP-even Higgs mass bound is realized in the case of maximal mixing at large  $\tan\beta$ . Allowing for the uncertainty in the measured value of  $m_t$  and the uncertainty inherent in the theoretical analysis, one finds for  $M_{\text{SUSY}} \lesssim 2$  TeV that  $m_{h^0} \lesssim m_h^{\text{max}}$ , where

$$\begin{aligned} m_h^{\text{max}} &\simeq 122 \text{ GeV}, & \text{minimal stop mixing,} \\ m_h^{\text{max}} &\simeq 135 \text{ GeV}, & \text{maximal stop mixing.} \end{aligned} \quad (22)$$

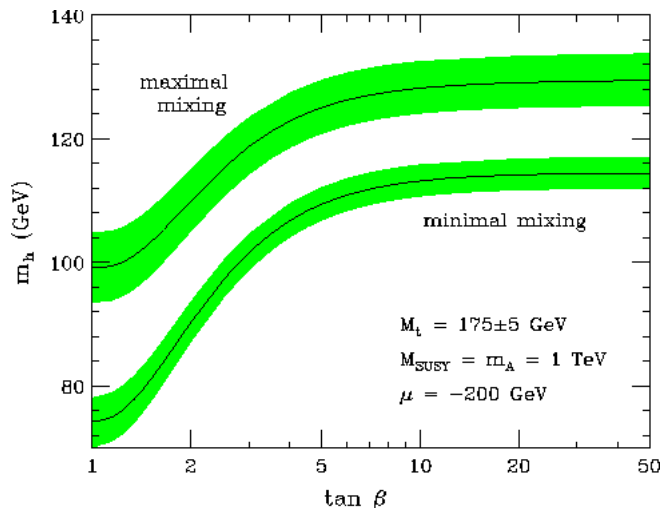


Fig. 11: The radiatively corrected light CP-even Higgs mass is plotted as a function of  $\tan\beta$ , for the maximal mixing [upper band] and minimal mixing cases. The impact of the top quark mass is exhibited by the shaded bands; the central value corresponds to  $m_t = 175$  GeV, while the upper [lower] edge of the bands correspond to increasing [decreasing]  $m_t$  by 5 GeV.

The  $h^0$  mass bound in the MSSM quoted above does not apply to non-minimal supersymmetric extensions of the Standard Model. If additional Higgs singlet and/or triplet fields are introduced, then new Higgs self-coupling parameters appear, which are not significantly constrained by present data. For example, in the simplest non-minimal supersymmetric extension of the Standard Model (NMSSM), the addition of a complex Higgs singlet field  $S$  adds a new Higgs self-coupling parameter,  $\lambda_S$  [65]. The mass of the lightest neutral Higgs boson can be raised arbitrarily by increasing the value of  $\lambda_S$ , analogous to the behavior of the Higgs mass in the Standard Model. Under the assumption that all couplings stay perturbative up to the Planck scale, one finds in nearly all cases that  $m_{h^0} \lesssim 200$  GeV, independent of the details of the low-energy supersymmetric model [66]. Moreover, if the perturbative unification scale is significantly lower than the Planck scale, then the lower bound on the Higgs mass can be substantially larger [67].

Radiative corrections also modify the tree-level expressions for  $m_{H^0}$  and  $m_{H^\pm}$  [eqs. (11) and (9)]. However, since  $m_{H^0} \simeq m_{H^\pm} \simeq m_{A^0}$  when  $m_{A^0} \gg m_Z$ , the impact of the radiative corrections on the heavier Higgs masses

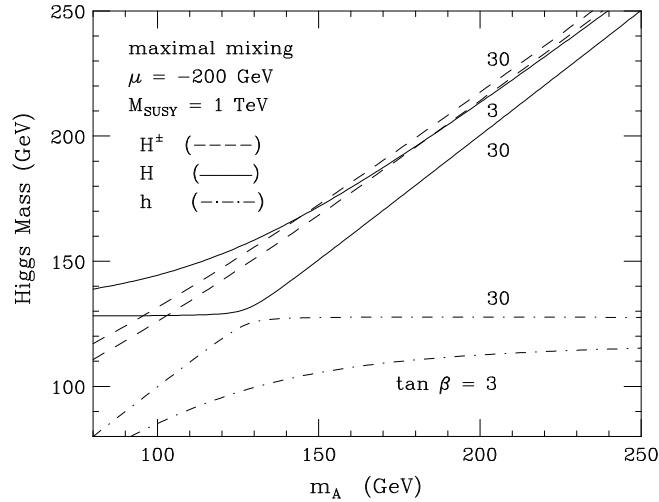


Fig. 12: Lightest CP-even Higgs mass ( $m_{h^0}$ ), heaviest CP-even Higgs mass ( $m_{H^0}$ ) and charged Higgs mass ( $m_{H^\pm}$ ) as a function of  $m_{A^0}$  for two choices of  $\tan\beta = 3$  and  $\tan\beta = 30$ . The slight increase in the charged Higgs mass as  $\tan\beta$  is increased from 3 to 30 is a consequence of the radiative corrections.

is less pronounced than those described above. In fig. 12, we exhibit the masses of the CP-even neutral and the charged Higgs masses as a function of  $m_{A^0}$ . Note that  $m_{H^0} \geq m_h^{\max}$  for all values of  $m_{A^0}$  and  $\tan\beta$ , where  $m_h^{\max}$  is to be evaluated depending on the top-squark mixing, as indicated in eq. (22).

Radiative corrections also significantly modify the tree-level values of the Higgs boson couplings to fermion pairs and to vector boson pairs. As discussed above, the tree-level Higgs couplings depend crucially on the value of  $\cos(\beta - \alpha)$ . In the first approximation, when radiative corrections of the Higgs squared-mass matrix are computed, the diagonalizing angle  $\alpha$  is modified. This provides one important source of the radiative corrections of the Higgs couplings. In fig. 10, we show the effect of radiative corrections on the value of  $\cos(\beta - \alpha)$  as a function of  $m_{A^0}$  for different values of the squark mixing parameters and  $\tan\beta$ . One can then insert the radiatively corrected value of  $\alpha$  into eqs. (17)–(19) to obtain radiatively improved couplings of Higgs bosons to vector bosons and to fermions.

At large  $\tan\beta$ , there is another potentially important class of radiative corrections in addition to those that enter through the modified value of  $\alpha$ .

These corrections arise in the relation between  $m_b$  and  $\tan\beta$  and depend on the details of the MSSM spectrum (which enter via loop-effects). At tree level, the Higgs couplings to  $b\bar{b}$  are proportional to the Higgs–bottom–quark Yukawa coupling,  $h_b$ . Deviations from the tree-level relation between  $h_b$  and  $m_b$  [eq. (7)] due to radiative corrections are calculable and finite [68–72]. One of the fascinating properties of such corrections is that in certain cases the corrections do *not* vanish in the limit of large supersymmetric mass parameters. These corrections grow with  $\tan\beta$  and therefore can be significant in the large  $\tan\beta$  regime. In the supersymmetric limit, bottom quarks only couple to  $\Phi_d^0$ . However, supersymmetry is broken and the bottom quark will receive a small coupling to  $\Phi_u^0$  from radiative corrections,

$$-\mathcal{L}_{\text{Yukawa}} \simeq h_b \Phi_d^0 b\bar{b} + (\Delta h_b) \Phi_u^0 b\bar{b}. \quad (23)$$

Because the Higgs doublet acquires a vacuum expectation value, the bottom quark mass receives an extra contribution equal to  $(\Delta h_b)v_u$ . Although  $\Delta h_b$  is one-loop suppressed with respect to  $h_b$ , for sufficiently large values of  $\tan\beta$  ( $v_u \gg v_d$ ) the contribution to the bottom quark mass of both terms in eq. (23) may be comparable in size. This induces a large modification in the tree level relation,

$$m_b = \frac{h_b v_d}{\sqrt{2}} (1 + \Delta_b), \quad (24)$$

where  $\Delta_b \equiv (\Delta h_b) \tan\beta/h_b$ . The function  $\Delta_b$  contains two main contributions: one from a bottom squark–gluino loop (depending on the two bottom squark masses  $M_{\tilde{b}_1}$  and  $M_{\tilde{b}_2}$  and the gluino mass  $M_{\tilde{g}}$ ) and another one from a top squark–higgsino loop (depending on the two top squark masses  $M_{\tilde{t}_1}$  and  $M_{\tilde{t}_2}$  and the higgsino mass parameter  $\mu$ ). The explicit form of  $\Delta_b$  at one-loop in the limit of  $M_S \gg m_b$  is given by [69–71]:

$$\Delta_b \simeq \frac{2\alpha_s}{3\pi} M_{\tilde{g}} \mu \tan\beta I(M_{\tilde{b}_1}, M_{\tilde{b}_2}, M_{\tilde{g}}) + \frac{Y_t}{4\pi} A_t \mu \tan\beta I(M_{\tilde{t}_1}, M_{\tilde{t}_2}, \mu), \quad (25)$$

where  $\alpha_s = g_s^2/4\pi$ ,  $Y_t \equiv h_t^2/4\pi$ , and contributions proportional to the electroweak gauge couplings have been neglected. In addition, the function  $I$  is defined by

$$I(a, b, c) = \frac{a^2 b^2 \ln(a^2/b^2) + b^2 c^2 \ln(b^2/c^2) + c^2 a^2 \ln(c^2/a^2)}{(a^2 - b^2)(b^2 - c^2)(a^2 - c^2)}, \quad (26)$$

and is manifestly positive. Note that the Higgs coupling proportional to  $\Delta h_b$  is a manifestation of the broken supersymmetry in the low energy theory; hence,  $\Delta_b$  does not decouple in the limit of large values of the supersymmetry breaking masses. Indeed, if all supersymmetry breaking mass



parameters (and  $\mu$ ) are scaled by a common factor, the correction  $\Delta_b$  remains constant.

Similarly to the case of the bottom quark, the relation between  $m_\tau$  and the Higgs–tau–lepton Yukawa coupling  $h_\tau$  is modified:

$$m_\tau = \frac{h_\tau v_d}{\sqrt{2}}(1 + \Delta_\tau). \quad (27)$$

The correction  $\Delta_\tau$  contains a contribution from a tau slepton–neutralino loop (depending on the two stau masses  $M_{\tilde{\tau}_1}$  and  $M_{\tilde{\tau}_2}$  and the mass parameter of the  $\tilde{B}$  (“bino”) component of the neutralino,  $M_1$ ) and a tau sneutrino–chargino loop (depending on the tau sneutrino mass  $M_{\tilde{\nu}_\tau}$ , the mass parameter of the  $\tilde{W}^\pm$  component of the chargino,  $M_2$ , and  $\mu$ ). It is given by [70, 71]:

$$\Delta_\tau = \frac{\alpha_1}{4\pi} M_1 \mu \tan \beta I(M_{\tilde{\tau}_1}, M_{\tilde{\tau}_2}, M_1) - \frac{\alpha_2}{4\pi} M_2 \mu \tan \beta I(M_{\tilde{\nu}_\tau}, M_2, \mu), \quad (28)$$

where  $\alpha_2 \equiv g^2/4\pi$  and  $\alpha_1 \equiv g'^2/4\pi$  are the electroweak gauge couplings. Since corrections to  $h_\tau$  are proportional to  $\alpha_1$  and  $\alpha_2$ , they are typically smaller than the corrections to  $h_b$ .

From eqs. (23) and (24) we can obtain the couplings of the physical neutral Higgs bosons to  $b\bar{b}$ . At large  $\tan \beta$ , the dominant corrections to eq. (19) are displayed below:<sup>6</sup>

$$\begin{aligned} h^0 b\bar{b} &: -\frac{\sin \alpha}{\cos \beta} \frac{1}{1 + \Delta_b} \left[ 1 - \frac{\Delta_b \cot \alpha}{\tan \beta} \right], \\ H^0 b\bar{b} &: \frac{\cos \alpha}{\cos \beta} \frac{1}{1 + \Delta_b} \left[ 1 + \frac{\Delta_b \tan \alpha}{\tan \beta} \right], \\ A^0 b\bar{b} &: \gamma_5 \frac{\tan \beta}{1 + \Delta_b}, \end{aligned} \quad (29)$$

where  $\Delta_b \propto \tan \beta$  [see eq. (25)]. Similarly, the neutral Higgs couplings to  $\tau^+ \tau^-$  are modified by replacing  $\Delta_b$  in eq. (29) with  $\Delta_\tau$  [70, 71]. The corresponding radiative corrections to the couplings of the neutral Higgs bosons to  $t\bar{t}$  are not  $\tan \beta$ -enhanced (see [73] for a useful approximation for these corrections). One can also derive radiatively corrected couplings of the charged Higgs boson to fermion pairs [74, 75]. The tree-level couplings of the charged Higgs boson to fermion pairs are modified accordingly by replacing  $m_b \rightarrow m_b/(1 + \Delta_b)$  and  $m_\tau \rightarrow m_\tau/(1 + \Delta_\tau)$ , respectively.

<sup>6</sup>A better approximation in which non-leading terms at large  $\tan \beta$  are kept can be found in [73].

One consequence of the above results is that the neutral Higgs coupling to  $b\bar{b}$  (which is expected to be the dominant decay mode over nearly all of the MSSM Higgs parameter space), can be significantly suppressed at large  $\tan\beta$  [76–78] if  $\Delta_b \simeq \mathcal{O}(1)$ . For example, eq. (29) implies that  $g_{h^0 b\bar{b}} \simeq 0$  if  $\tan\alpha = \Delta_b/\tan\beta$ . Inserting this result into the corresponding expression for the  $h^0\tau^+\tau^-$  coupling, it follows that

$$g_{h^0\tau^+\tau^-} \simeq \frac{\sqrt{2}m_\tau \cos\alpha}{v \sin\beta} \left( \frac{\Delta_\tau - \Delta_b}{1 + \Delta_\tau} \right), \quad [\text{if } g_{h^0 b\bar{b}} \simeq 0]. \quad (30)$$

Similarly,  $g_{H^0 b\bar{b}} \simeq 0$  if  $\tan\alpha = -\tan\beta/\Delta_b$ . Inserting this result into the corresponding expression for the  $H^0\tau^+\tau^-$  coupling, it follows that

$$g_{H^0\tau^+\tau^-} \simeq \frac{\sqrt{2}m_\tau \sin\alpha}{v \sin\beta} \left( \frac{\Delta_\tau - \Delta_b}{1 + \Delta_\tau} \right), \quad [\text{if } g_{H^0 b\bar{b}} \simeq 0]. \quad (31)$$

In both cases, we see that although the Higgs coupling to  $b\bar{b}$  can be strongly suppressed for certain parameter choices, the corresponding Higgs coupling to  $\tau^+\tau^-$  may be unsuppressed. In such cases, the  $\tau^+\tau^-$  decay mode can be the dominant Higgs decay channel for the CP-even Higgs boson with SM-like couplings to gauge bosons.

Near the decoupling limit,  $\cot\alpha \cot\beta = -1 + \mathcal{O}(m_Z^2/m_{A^0}^2)$  [after an appropriate manipulation of eq. (16)]. Inserting this result into eq. (29), one can check that the  $h^0 b\bar{b}$  coupling does indeed approach its Standard Model value. However, because  $\Delta_b \propto \tan\beta$ , the deviation of the  $h^0 b\bar{b}$  coupling from the corresponding SM result is of  $\mathcal{O}(m_Z^2 \tan\beta/m_{A^0}^2)$ . That is, at large  $\tan\beta$ , the approach to decoupling may be “delayed” [79], depending on the values of other MSSM parameters that enter the radiative corrections.

### 5.3. MSSM Higgs boson decay modes

In this section, we consider the decay properties of the three neutral Higgs bosons ( $h^0$ ,  $H^0$  and  $A^0$ ) and of the charged Higgs pair ( $H^\pm$ ). Let us start with the lightest state,  $h^0$ . When  $m_{A^0} \gg m_Z$ , the decoupling limit applies, and the couplings of  $h^0$  to SM particles are nearly indistinguishable from those of  $h_{\text{SM}}$ . If some superpartners are light, there may be some additional decay modes, and hence the  $h^0$  branching ratios would be different from the corresponding Standard Model values, even though the partial widths to Standard Model particles are the same. Furthermore, loops of light charged or colored superpartners could modify the  $h^0$  coupling to photons and/or gluons, in which case the one-loop  $gg$  and  $\gamma\gamma$  decay rates would also be different. On the other hand, if all superpartners are heavy,

all the decay properties of  $h^0$  are essentially those of the SM Higgs boson, and the discussion of Section 3.1 applies.

For  $m_{A^0} \gg m_Z$ , the heavier Higgs states,  $H^0$ ,  $A^0$  and  $H^\pm$ , are roughly mass-degenerate and have negligible couplings to vector boson pairs. In particular,  $\Gamma(H^0 \rightarrow VV) \ll \Gamma(h_{\text{SM}} \rightarrow VV)$ , while the couplings of  $A^0$  and  $H^\pm$  to the gauge bosons are loop-suppressed. The couplings of  $H^0$ ,  $A^0$  and  $H^\pm$  to down-type (up-type) fermions are significantly enhanced (suppressed) relative to those of  $h_{\text{SM}}$  if  $\tan\beta \gg 1$ . Consequently, the decay modes  $H^0, A^0 \rightarrow b\bar{b}$ ,  $\tau^+\tau^-$  dominate the neutral Higgs decay modes for moderate-to-large values of  $\tan\beta$  below the  $t\bar{t}$  threshold, while  $H^\pm \rightarrow \tau^+\nu$  dominates the charged Higgs decay below the  $t\bar{b}$  threshold.

For values of  $m_{A^0}$  of order  $m_Z$ , all Higgs boson states lie below 200 GeV in mass and would be accessible at the LC. In this parameter regime, there is a significant area of the parameter space in which none of the neutral Higgs boson decay properties approximates those of  $h_{\text{SM}}$ . For example, when  $\tan\beta$  is large, supersymmetry-breaking effects can significantly modify the  $b\bar{b}$  and/or the  $\tau^+\tau^-$  decay rates with respect to those of  $h_{\text{SM}}$ . Additionally, the heavier Higgs bosons can decay into lighter Higgs bosons. Examples of such decay modes are:  $H^0 \rightarrow h^0h^0$ ,  $A^0A^0$ , and  $ZA^0$ , and  $H^\pm \rightarrow W^\pm h^0$ ,  $W^\pm A^0$  (although in the MSSM, the Higgs branching ratio into vector boson–Higgs boson final states, if kinematically allowed, rarely exceeds a few percent). The decay of the heavier Higgs boson into two lighter Higgs bosons can provide information about Higgs self-couplings. For values of  $\tan\beta \lesssim 5$ , the branching ratio of  $H^0 \rightarrow h^0h^0$  is dominant for a Higgs mass range of  $200 \text{ GeV} \lesssim m_{H^0} \lesssim 2m_t$ . The dominant radiative corrections to this decay arise from the corrections to the self-interaction  $\lambda_{H^0h^0h^0}$  in the MSSM and are large [80].

The phenomenology of charged Higgs bosons is less model-dependent, and is governed by the values of  $\tan\beta$  and  $m_{H^\pm}$ . Because the  $H^\pm$  couplings are proportional to fermion masses, the decays to third-generation quarks and leptons are dominant. In particular, for  $m_{H^\pm} < m_t + m_b$  (so that the channel  $H^\pm \rightarrow t\bar{b}$  is closed),  $H^\pm \rightarrow \tau^+\nu_\tau$  is favored if  $\tan\beta \gtrsim 1$ , while  $H^\pm \rightarrow c\bar{s}$  is favored if  $\tan\beta$  is small. Indeed,  $\text{BR}(H^\pm \rightarrow \tau^+\nu_\tau) \simeq 1$  if  $\tan\beta \gtrsim 5$ . These results apply generally to Type-II two-Higgs doublet models. For  $m_{H^\pm} \gtrsim 200 \text{ GeV}$  (the precise value depends on  $\tan\beta$ ), the decay  $H^\pm \rightarrow t\bar{b} \rightarrow W^\pm b\bar{b}$  is the dominant decay mode.

In addition to the above decay modes, there exist new Higgs decay channels that involve supersymmetric final states. Higgs decays into charginos, neutralinos and third-generation squarks and sleptons can become impor-

tant, once they are kinematically allowed [81]. For Higgs masses below 130 GeV, the range of supersymmetric parameter space in which supersymmetric decays are dominant is rather narrow when the current bounds on supersymmetric particle masses are taken into account. One interesting possibility is a significant branching ratio of  $h^0 \rightarrow \tilde{\chi}^0 \tilde{\chi}^0$ , which could arise for values of  $m_{h^0}$  near its upper theoretical limit. Such an invisible decay mode could be detected at the LC by searching for the missing mass recoiling against the  $Z$  in  $e^+e^- \rightarrow h^0 Z$ .

#### 5.4. MSSM Higgs boson production at the LC

For  $m_{A^0} \gtrsim 150$  GeV, fig. 10 shows that the MSSM Higgs sector quickly approaches the decoupling limit, where the properties of  $h^0$  approximately coincide with those of  $h_{\text{SM}}$ . In contrast,  $|\cos(\beta - \alpha)| \ll 1$  implies that the  $H^0 VV$  couplings are highly suppressed [see eq. (17)], and the  $A^0 VV$  couplings are loop-suppressed. Thus, the Higgsstrahlung and vector-boson-fusion cross-sections for  $h_{\text{SM}}$  production also apply to  $h^0$  production, but these are not useful for  $H^0$  and  $A^0$  production. For the heavier neutral Higgs bosons, the most robust production mechanism is  $e^+e^- \rightarrow Z^* \rightarrow H^0 A^0$ , which is not suppressed since the  $ZH^0 A^0$  coupling is proportional to  $\sin(\beta - \alpha)$ , as indicated in eq. (18). Radiatively corrected cross-sections for  $e^+e^- \rightarrow Zh^0$ ,  $ZH^0$ ,  $H^0 A^0$ , and  $h^0 A^0$  have been obtained in [82]. The charged Higgs boson is also produced in pairs via  $s$ -channel photon and  $Z$  exchange. However, since  $m_{H^0} \simeq m_{A^0} \simeq m_{H^\pm}$  in the decoupling limit,  $H^0 A^0$  and  $H^+ H^-$  production are kinematically allowed only when  $m_{A^0} \lesssim \sqrt{s}/2$ .<sup>7</sup> In  $\gamma\gamma$  collisions, one can extend the Higgs mass reach for the neutral Higgs bosons. As described in Section 11, the  $s$ -channel resonant production of  $H^0$  and  $A^0$  (due primarily to the top and bottom-quark loops in the one-loop Higgs- $\gamma\gamma$  triangle) can be detected for some choices of  $m_{A^0}$  and  $\tan\beta$  if the heavy Higgs masses are less than about 80% of the initial  $\sqrt{s}$  of the primary  $e^+e^-$  system. The corresponding cross sections are a few fb [14,83].

If  $m_{A^0} \lesssim 150$  GeV, deviations from the decoupling limit become more pronounced, and  $H^0$  can now be produced via Higgsstrahlung and vector boson fusion at an observable rate. In addition, the factor of  $\cos(\beta - \alpha)$  in the  $Zh^0 A^0$  coupling no longer significantly suppresses  $h^0 A^0$  production. Finally, if  $m_{H^\pm} \lesssim 170$  GeV, the charged Higgs boson will also be produced in  $t \rightarrow H^+ b$ . In the non-decoupling regime, all non-minimal Higgs states can be directly produced and studied at the LC.

<sup>7</sup>The pair production of scalars is P-wave suppressed near threshold, so in practice the corresponding Higgs mass reach is likely to be somewhat lower than  $\sqrt{s}/2$ .

Higgs boson production in association with a fermion-antifermion pair can also be considered. Here, the new feature is the possibility of enhanced Higgs–fermion Yukawa couplings. Consider the behavior of the Higgs couplings at large  $\tan\beta$ , where some of the Higgs couplings to down type fermion pairs (denoted generically by  $b\bar{b}$ ) can be significantly enhanced.<sup>8</sup> Let us examine two particular regions with large  $\tan\beta$ . In the decoupling limit (where  $m_{A^0} \gg m_Z$  and  $|\cos(\beta - \alpha)| \ll 1$ ), it follows from eq. (19) that the  $b\bar{b}H^0$  and  $b\bar{b}A^0$  couplings have equal strength and are significantly enhanced by a factor of  $\tan\beta$  relative to the  $b\bar{b}h_{\text{SM}}$  coupling, while the  $b\bar{b}h^0$  coupling is given by the corresponding Standard Model value. If  $m_{A^0} \lesssim m_Z$  and  $\tan\beta \gg 1$ , then  $|\sin(\beta - \alpha)| \ll 1$ , as implied by fig. 10, and  $m_{h^0} \simeq m_{A^0}$ . In this case, the  $b\bar{b}h^0$  and  $b\bar{b}A^0$  couplings have equal strength and are significantly enhanced (by a factor of  $\tan\beta$ )<sup>9</sup> relative to the  $b\bar{b}h_{\text{SM}}$  coupling. Note that in both cases above, only two of the three neutral Higgs bosons have enhanced couplings to  $b\bar{b}$ . If  $\phi$  is one of the two neutral Higgs bosons with enhanced  $b\bar{b}\phi$  couplings, then the cross-section for  $e^+e^- \rightarrow f\bar{f}\phi$  ( $f = b$  or  $\tau$ ) will be significantly enhanced relative to the corresponding Standard Model cross-section by a factor of  $\tan^2\beta$ . The phase-space suppression is not as severe as in  $e^+e^- \rightarrow t\bar{t}\phi$  (see fig. 5), so this process could extend the mass reach of the heavier neutral Higgs states at the LC given sufficient luminosity. The production of the charged Higgs boson via  $e^+e^- \rightarrow t\bar{b}H^-$  is also enhanced by  $\tan^2\beta$ , although this process has a more significant phase-space suppression because of the final state top quark. If any of these processes can be observed, it would allow for a direct measurement of the corresponding Higgs–fermion Yukawa coupling.

## 6. MSSM Higgs boson searches before the LC

### 6.1. Direct search limits from LEP

Although no direct experimental evidence for the Higgs boson yet exists, there are both experimental as well as theoretical constraints on the parameters of the MSSM Higgs sector. Experimental limits on the charged

<sup>8</sup>We do not consider the possibility of  $\tan\beta \ll 1$ , which would lead to enhanced Higgs couplings to up-type fermions. As previously noted, models of low-energy supersymmetry tend to favor the parameter regime of  $1 \lesssim \tan\beta \lesssim m_t/m_b$ . Moreover, some of the low  $\tan\beta$  region is already ruled out by the MSSM Higgs search (see Section 6.1).

<sup>9</sup>However in this case, the value of the  $b\bar{b}H^0$  coupling can differ from the corresponding  $b\bar{b}h_{\text{SM}}$  coupling when  $\tan\beta \gg 1$ , since in case (ii), where  $|\sin(\beta - \alpha)| \ll 1$ , the product  $\tan\beta \sin(\beta - \alpha)$  need not be particularly small.

and neutral Higgs masses have been obtained at LEP. For the charged Higgs boson,  $m_{H^\pm} > 78.6$  GeV [84]. This is the most model-independent bound. It is valid for more general non-supersymmetric two-Higgs doublet models and assumes only that the  $H^+$  decays dominantly into  $\tau^+\nu_\tau$  and/or  $c\bar{s}$ . The LEP limits on the masses of  $h^0$  and  $A^0$  are obtained by searching simultaneously for  $e^+e^- \rightarrow Z \rightarrow Zh^0$  and  $e^+e^- \rightarrow Z \rightarrow h^0A^0$ . Radiative corrections can be significant, as shown in Section 5.2, so the final limits depend on the choice of MSSM parameters that govern the radiative corrections. The third generation squark parameters are the most important of these. The LEP Higgs working group [85] quotes limits for the case of  $M_{\text{SUSY}} = 1$  TeV in the maximal-mixing scenario, which corresponds to the choice of third generation squark parameters that yields the largest corrections to  $m_{h^0}$ . The present LEP 95% CL lower limits are  $m_{A^0} > 91.9$  GeV and  $m_{h^0} > 91.0$  GeV. The theoretical upper bound on  $m_{h^0}$  as a function of  $\tan\beta$ , exhibited in fig. 11, can then be used to exclude a region of  $\tan\beta$  in which the predicted value of  $m_{h^0}$  lies below the experimental bound. Under the same MSSM Higgs parameter assumptions stated above, the LEP Higgs search excludes the region  $0.5 < \tan\beta < 2.4$  at 95% CL.

In discussing Higgs discovery prospects at the Tevatron and LHC, we shall quote limits based on the assumption of  $M_{\text{SUSY}} = 1$  TeV and maximal squark mixing. This tends to be a conservative assumption; that is, other choices give sensitivity to *more* of the  $[m_{A^0}, \tan\beta]$  plane. However, there are other parameter regimes where certain Higgs search strategies become more difficult. While these issues are of vital importance to the Tevatron and LHC Higgs searches, they are much less important at the LC.

## 6.2. MSSM Higgs searches at the Tevatron

The Tevatron SM Higgs search can be reinterpreted in terms of the search for the CP-even Higgs boson of the MSSM. Since the theoretical upper bound was found to be  $m_{h^0} \lesssim 135$  GeV (for  $M_{\text{SUSY}} < 2$  TeV), only the Higgs search of the low-mass region,  $100 \text{ GeV} \lesssim m_{h^0} \lesssim 135$  GeV, applies. In the MSSM at large  $\tan\beta$ , the enhancement of the  $A^0b\bar{b}$  coupling (and a similar enhancement of either the  $h^0b\bar{b}$  or  $H^0b\bar{b}$  coupling) provides a new search channel:  $q\bar{q}, gg \rightarrow b\bar{b}\phi$ , where  $\phi$  is a Higgs boson with enhanced couplings to  $b\bar{b}$ . Combining both sets of analyses, the Tevatron Higgs Working Group [47] obtained the expected 95% CL exclusion and  $5\sigma$  Higgs discovery contours for the maximal mixing scenario as a function of total integrated luminosity per detector (combining both CDF and D0 data sets).

With  $5 \text{ fb}^{-1}$  of integrated luminosity per experiment, it is possible to

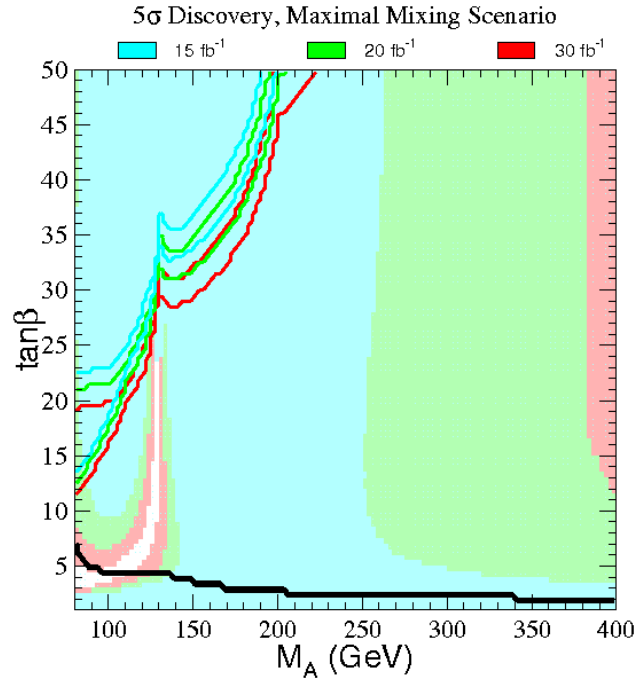


Fig. 13: The  $5\sigma$  discovery region in the  $m_{A^0}$ - $\tan\beta$  plane, for the maximal mixing scenario and two different search channels:  $q\bar{q} \rightarrow V\phi$  ( $\phi = h^0, H^0$ ),  $\phi \rightarrow b\bar{b}$  (shaded regions) and  $gg, q\bar{q} \rightarrow b\bar{b}\phi$  ( $\phi = h^0, H^0, A^0$ ),  $\phi \rightarrow b\bar{b}$  (region in the upper left-hand corner bounded by the solid lines). Different integrated luminosities are explicitly shown by the color coding. The two sets of lines (for a given color) correspond to the CDF and  $D\mathcal{O}$  simulations, respectively. The region below the solid black line near the bottom of the plot is excluded by the absence of observed  $e^+e^- \rightarrow Z\phi$  events at LEP. Taken from [47].

test nearly the entire MSSM Higgs parameter space, and obtain a 95% CL exclusion limit if no signal is observed. To assure discovery of a CP-even Higgs boson at the  $5\sigma$  level, the luminosity requirement becomes very important. Fig. 13 shows that a total integrated luminosity of about  $20 \text{ fb}^{-1}$  per experiment is necessary in order to assure a significant, although not exhaustive, coverage of the MSSM parameter space. If the anticipated  $15 \text{ fb}^{-1}$  integrated luminosity is achieved, the discovery reach will significantly extend beyond that of LEP. Nevertheless, the MSSM Higgs boson could still evade capture at the Tevatron. One would then turn to the LHC to try to obtain a definitive Higgs boson discovery.

### 6.3. MSSM Higgs searches at the LHC

The potential of the LHC to discover one or more of the MSSM Higgs bosons has been exhaustively studied for the minimal and maximal mixing scenarios described above. One of the primary goals of these studies has been to demonstrate that at least one of the MSSM Higgs bosons will be observable by ATLAS and CMS for any possible choice of  $\tan\beta$  and  $m_{A^0}$  consistent with bounds coming from current LEP data. In order to establish such a “no-lose” theorem, an important issue is whether or not the Higgs bosons have substantial decays to supersymmetric particle pairs. It is reasonable to suppose that these decays will be absent or relatively insignificant for the light  $h^0$ . Current mass limits on supersymmetric particles are such that only  $h^0 \rightarrow \tilde{\chi}_1^0 \tilde{\chi}_1^0$  is not kinematically excluded, and this possibility arises only in a very limited class of models. For  $m_{A^0} \gtrsim 200$  GeV, decays of the  $A^0, H^0, H^\pm$  to supersymmetric particles (especially pairs of light charginos/neutralinos) are possible, but the branching ratios are generally not significantly large. In all such cases, the discovery limits we discuss below would only be slightly weakened. Furthermore, at high  $\tan\beta$  the enhancement of the  $b\bar{b}$  and  $\tau^+\tau^-$  couplings of the heavy  $A^0$  and  $H^0$  imply that supersymmetric decay modes will not be important even when  $m_{A^0} \sim m_{H^0} \sim m_{H^\pm} \gg m_Z$ . We will summarize the LHC discovery prospects for the MSSM Higgs bosons assuming that supersymmetric decays are not significant.

One of the primary Higgs discovery modes is detection of the relatively SM-like  $h^0$  using the same modes as employed for a light  $h_{\text{SM}}$ . Based on fig. 14 (which assumes  $L = 300 \text{ fb}^{-1}$ ) [86], we see that for  $m_{A^0} \gtrsim 180$  GeV, the  $h^0$  will be detected via  $gg, WW \rightarrow h^0$  and  $Wh^0, t\bar{t}h^0$  with  $h^0 \rightarrow \gamma\gamma$ , while the  $t\bar{t}h^0$  with  $h^0 \rightarrow b\bar{b}$  mode is viable down to  $m_{A^0} \gtrsim 100\text{--}120$  GeV, depending on  $\tan\beta$ . Similar results have been obtained by CMS [87]. There are also many possibilities for detecting the other MSSM Higgs bosons. First, there is a small domain in which  $m_{A^0} \lesssim 130$  GeV, but yet  $m_{A^0}$  is still large enough for consistency with LEP limits, in which  $t \rightarrow bH^\pm$  discovery will be possible. However, the most interesting alternative detection modes are based on  $gg \rightarrow A^0, H^0$  and  $gb \rightarrow H^\pm t$  production. We focus first on the former. For low-to-moderate  $\tan\beta$  values, the channels  $H^0 \rightarrow ZZ^{(*)} \rightarrow 4\ell$ ,  $H^0 \rightarrow h^0 h^0 \rightarrow b\bar{b}\gamma\gamma$  and  $A^0 \rightarrow Zh^0 \rightarrow \ell\ell b\bar{b}$  are viable when  $m_{A^0} \lesssim 2m_t$ , whereas the  $A^0, H^0 \rightarrow t\bar{t}$  modes are viable for  $m_{A^0} > 2m_t$ . For large enough  $\tan\beta$ , the  $gg \rightarrow A^0, H^0 \rightarrow \tau^+\tau^-, \mu^+\mu^-$  discovery modes become viable. For the  $gb \rightarrow H^\pm t$  process, the  $H^\pm \rightarrow tb$  decays provide a  $5\sigma$  signal both for



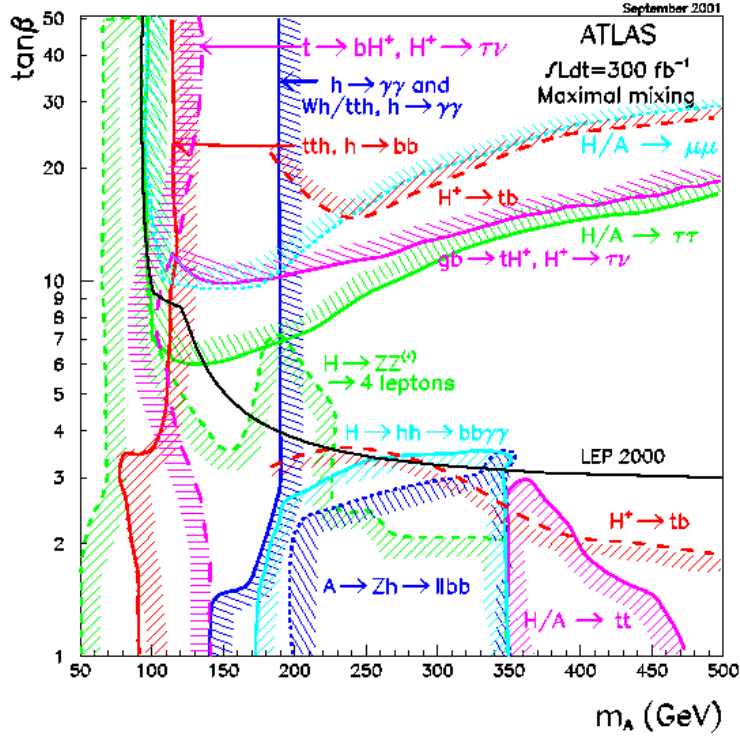


Fig. 14:  $5\sigma$  discovery contours for MSSM Higgs boson detection in various channels are shown in the  $[m_{A^0}, \tan\beta]$  parameter space, assuming maximal mixing and an integrated luminosity of  $L = 300 \text{ fb}^{-1}$  for the ATLAS detector. Taken from [86].

low-to-moderate  $\tan\beta \lesssim 2-3$  and for high  $\tan\beta \gtrsim 15-25$ , depending upon mass. In addition, the  $H^\pm \rightarrow \tau^\pm\nu$  decay mode yields a viable signal for  $\tan\beta \gtrsim 7-12$ . Of course, if the plot were extended to higher  $m_{A^0}$ , the minimum  $\tan\beta$  value required for  $H^0, A^0$  or  $H^\pm$  detection would gradually increase.

We noted earlier that the present LEP limits imply that  $\tan\beta > 2.4$  in the case of maximal mixing and  $M_{\text{SUSY}} = 1 \text{ TeV}$  (with even more stringent limits possible in other regions of the supersymmetric parameter space). Thus, it is very likely that  $\tan\beta$  and  $m_{A^0}$  will be in one of two regions: (a) the increasingly large (as  $m_{A^0}$  increases) wedge of moderate  $\tan\beta > 3$  in which only the  $h^0$  will be detected; or (b) the high  $\tan\beta$  region for which

the  $gg \rightarrow H^0, A^0 \rightarrow \tau^+\tau^-, \mu^+\mu^-$  and  $gb \rightarrow H^\pm t \rightarrow \tau^\pm \nu t, tbt$  modes are viable as well. If the  $H^0, A^0, H^\pm$  are heavy and cannot be detected either at the LHC (because  $\tan\beta$  is not large enough) or at the LC (because they are too heavy to be pair-produced), precision measurements of the  $h^0$  branching ratios and other properties will be particularly crucial. The precision measurements might provide the only means for constraining or approximately determining the value of  $m_{A^0}$  aside from possible direct detection in  $\gamma\gamma \rightarrow H^0, A^0$  production. Expected LC precisions are such that deviations of  $h^0$  branching ratios from the predicted SM values can be detected (in the maximal mixing scenario) for  $m_{A^0} \lesssim 600$  GeV [73].

At the LHC there is another important possibility for  $h^0$  detection. Provided that the mass of the second-lightest neutralino exceeds that of the lightest neutralino (the LSP) by at least  $m_{h^0}$ , gluino and squark production will lead to chain decays in which  $\tilde{\chi}_2^0 \rightarrow h^0 \tilde{\chi}_1^0$  occurs with substantial probability. In this way, an enormous number of  $h^0$ 's can be produced, and the  $h^0 \rightarrow b\bar{b}$  decay mode will produce a dramatic signal [88].

## 7. Non-exotic extended Higgs sectors

In this section, we consider the possibility of extending only the Higgs sector of the SM, leaving unchanged the gauge and fermionic sectors of the SM. We will also consider extensions of the two-doublet Higgs sector of the MSSM.

The simplest extensions of the minimal one-doublet Higgs sector of the SM contain additional doublet and/or singlet Higgs fields. Such extended Higgs sectors will be called non-exotic (to distinguish them from exotic Higgs sectors with higher representations, which will be considered briefly in Section 8). Singlet-only extensions have the advantage of not introducing the possibility of charge violation, since there are no charged Higgs bosons. In models with more than one Higgs doublet, tree-level Higgs-mediated flavor-changing neutral currents are present unless additional symmetries (*e.g.*, discrete symmetries or supersymmetry) are introduced to restrict the form of the tree-level Higgs-fermion interactions [89]. Extensions containing additional doublet fields allow for spontaneous and explicit CP violation within the Higgs sector. These could be the source of observed CP-violating phenomena. Such models require positive squared-masses for the charged Higgs boson(s) in order to avoid spontaneous breaking of electric charge conservation.

Extensions of the SM Higgs sector containing doublets and singlets can certainly be considered on a purely *ad hoc* basis. But there are also many dynamical models in which the effective low-energy sector below some scale  $\Lambda$  of order 1 to 10 TeV, or higher, consists of the SM fermions and gauge bosons plus an extended Higgs sector. Models with an extra doublet of Higgs fields include those with new strong forces, in which the effective Higgs doublet fields are composites containing new heavier fermions. The heavy fermions should be vector-like to minimize extra contributions to precision electroweak observables. In many of these models, the top quark mixes with the right-handed component of a new vector-like fermion. The top quark could also mix with the right-handed component of a Kaluza-Klein (KK) excitation of a fermion field, so that Higgs bosons would be composites of the top quark and fermionic KK excitations. (For a review and references to the literature, see [90].) Although none of these (non-perturbative) models have been fully developed, they do provide significant motivation for studying the Standard Model with a Higgs sector containing extra doublets and/or singlets if only as the effective low-energy theory below a scale  $\Lambda$  in the TeV range.

When considering Higgs sectors in the context of a dynamical model with strong couplings at scale  $\Lambda$ , restrictions on Higgs self-couplings and Yukawa couplings, which would arise by requiring perturbativity for such couplings up to some large GUT scale, do not apply. At most, one should only demand perturbativity up to the scale  $\Lambda$  at which the new (non-perturbative) dynamics enter and the effective theory breaks down.

The minimal Higgs sector of the MSSM is a Type-II two-doublet model, where one neutral Higgs doublet ( $\Phi_d^0$ ) couples at tree level only to down quarks and leptons while the other ( $\Phi_u^0$ ) couples only to up quarks. Non-minimal extended Higgs sectors are also possible in low-energy supersymmetric models. Indeed, string theory realizations of low-energy supersymmetry often contain many extra singlet, doublet and even higher representations, some of which can yield light Higgs bosons (see, *e.g.*, [91]). However, non-singlet Higgs representations spoil gauge coupling unification, unless additional intermediate-scale matter fields are added to restore it. A particularly well-motivated extension is the inclusion of a single extra complex singlet Higgs field, often denoted  $S$ . Including  $S$ , the superpotential for the theory can contain the term  $\lambda_S H_u H_d S$ , which can then provide a natural source of a weak scale value for the  $\mu$  parameter appearing in the bilinear superpotential form  $\mu H_u H_d$  required in the MSSM. A weak-scale value for  $s \equiv \langle S^0 \rangle$ , where  $S^0$  is the scalar component of the superfield  $S$ , is natural

and yields an effective  $\mu = \lambda_S s$ . This extension of the MSSM is referred to as the next-to-minimal supersymmetric model, or NMSSM, and has received considerable attention. For an early review and references, see [1].

### 7.1. The decoupling limit

In many extended Higgs sector models, the most natural parameter possibilities correspond to a decoupling limit in which there is only one light Higgs boson, with Yukawa and vector boson couplings close to those of the SM Higgs boson. In contrast, all the other Higgs bosons are substantially heavier (than the  $Z$ ) with negligibly small relative mass differences, and with suppressed vector boson couplings (which vanish in the exact limit of decoupling). By assumption, the decoupling limit assumes that all Higgs self-couplings are kept fixed and perturbative in size.<sup>10</sup> In the MSSM, such a decoupling limit arises for  $m_{A^0} \gg m_Z$ , and quickly becomes a very good approximation for  $m_{A^0} \gtrsim 150$  GeV.

The decoupling limit can be evaded in special cases, in which the scalar potential exhibits a special form (*e.g.*, a discrete symmetry can forbid certain terms). In such models, there could exist regions of parameter space in which all but one Higgs boson are significantly heavier than the  $Z$ , but the light scalar state does *not* possess SM-like properties [92]. A complete exposition regarding the decoupling limit in the two-Higgs doublet model, and special cases that evade the limit can be found in [62].

### 7.2. Constraints from precision electroweak data and LC implications

In the Standard Model, precision electroweak constraints require  $m_{h_{\text{SM}}} \lesssim 193$  GeV at 95% CL. This is precisely the mass region preferred in the MSSM and its extensions. However, in models of general extended Higgs sectors with only weak doublet and singlet representations, there are more complicated possibilities. First, it could be that there are several, or even many, Higgs bosons that couple to vector bosons and it is only their average mass weighted by the square of their  $VV$  coupling strength (relative to the SM strength) that must obey the SM Higgs mass limit. Second, there can be weak isospin violations either within the Higgs sector itself or involving extra dynamics (for example related to the composite Higgs

---

<sup>10</sup>In the decoupling limit, the heavier Higgs bosons may have enhanced couplings to fermions (*e.g.*, at large  $\tan\beta$  in the two-Higgs doublet model). We assume that these couplings also remain perturbative.

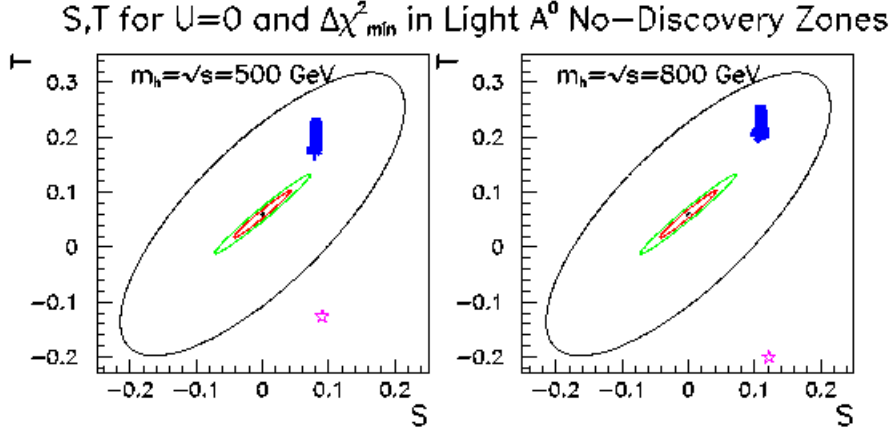


Fig. 15: The outer ellipses show the 90% CL region from current precision electroweak data in the  $S, T$  plane for  $U = 0$  relative to a central point defined by the SM prediction with  $m_{h_{\text{SM}}} = 115$  GeV. The blobs of points show the  $S, T$  predictions for 2HDM models with a light  $A^0$  and with  $\tan\beta$  such that the  $A^0$  cannot be detected in  $b\bar{b}A^0$  or  $t\bar{t}A^0$  production at either the LC or the LHC; the mass of the SM-like  $h^0$  is set equal to  $\sqrt{s} = 500$  GeV (left) or 800 GeV (right) and  $m_{H^\pm}$  and  $m_{H^0}$  have been chosen to minimize the  $\chi^2$  of the full precision electroweak fit. The innermost (middle) ellipse shows the 90% (99.9%) CL region for  $m_{h_{\text{SM}}} = 115$  GeV after the Giga- $Z$  operation and a  $\Delta m_W \lesssim 6$  MeV threshold scan measurement. The stars to the bottom right show the  $S, T$  predictions in the case of the SM with  $m_{h_{\text{SM}}} = 500$  GeV (left) or 800 GeV (right). This figure is from [93].

approach) can compensate for the excessive deviations predicted if there is a SM-like Higgs boson with mass substantially above 200 GeV.

A particularly simple example of this latter possibility arises in the context of the two-Higgs doublet model (2HDM) [92] and is illustrated in fig. 15. Consider a 2HDM in which one of the CP-even neutral Higgs bosons has SM-like couplings but has mass just above a particular presumed value of  $\sqrt{s}$  (500 or 800 GeV) for the linear collider. In addition, focus on cases in which there is a lighter  $A^0$  or  $h^0$  with no  $VV$  coupling (for either, we use the notation  $\hat{h}$ ) and in which all other Higgs bosons have mass larger than  $\sqrt{s}$ . Next, isolate mass and  $\tan\beta$  choices for which detection of the  $\hat{h}$  will also be impossible at the LC. Finally, scan over masses of the heavy Higgs bosons so as to achieve the smallest precision electroweak  $\Delta\chi^2$  relative to

that found in the Standard Model for  $m_{h_{\text{SM}}} = 115$  GeV [93]. For  $\hat{h} = A^0$ , the blobs of overlapping points in fig. 15 indicate the  $S, T$  values for the optimal choices and lie well within the current 90% CL ellipse. The heavy Higgs boson with SM couplings gives a large positive contribution to  $S$  and large negative contribution to  $T$ , and in the absence of the other Higgs bosons would give the  $S, T$  location indicated by the star. However, there is an additional positive contribution to  $T$  arising from a slight mass non-degeneracy among the heavier Higgs bosons. For instance, for the case of a light  $\hat{h} = A^0$ , the  $h^0$  is heavy and SM-like and  $\Delta\rho \equiv \alpha\Delta T$ , where

$$\Delta T = \frac{1}{16\pi m_W^2 \cos^2 \theta_W} \left\{ \frac{\cos^2 \theta_W}{\sin^2 \theta_W} \left( \frac{m_{H^\pm}^2 - m_{H^0}^2}{2} \right) - 3m_W^2 \left[ \ln \frac{m_{h^0}^2}{m_W^2} + \frac{1}{6} + \frac{1}{\sin^2 \theta_W} \ln \frac{m_W^2}{m_Z^2} \right] \right\} \quad (32)$$

can be adjusted by an appropriate choice of  $m_{H^\pm}^2 - m_{H^0}^2$  to place the prediction in the  $S$ - $T$  plane at the location of the blob in fig. 15. Indeed, even if the “light” decoupled Higgs boson is not so light, but rather has mass equal to  $\sqrt{s}$  (and is therefore unobservable), one can still obtain adequate agreement with current precision electroweak data. Fortunately, one can only push this scenario so far. To avoid moving beyond the current 90% ellipse (and also to maintain perturbativity for the Higgs self-couplings), the Higgs with SM-like  $VV$  coupling must have mass  $\lesssim 1$  TeV.

In composite Higgs models with extra fermions, there are similar non-degeneracies of the fermions that can yield a similar positive contribution to  $\Delta T$ . As reviewed in [28], consistency with current precision electroweak data inevitably constrains parameters so that some type of new physics (including a possible heavy scalar sector) would again have to lie below a TeV or so. Future Giga- $Z$  and  $W$ -threshold measurements could provide much stronger constraints on these types of models, as discussed in Section 10. Moreover, such measurements would become a priority if a heavy SM Higgs boson is found at the LHC, but no other new physics (needed for a consistent explanation of the precision electroweak data) is discovered.

### 7.3. Constraints on Higgs bosons with $VV$ coupling

In the MSSM, we know that the Higgs boson(s) that carry the  $VV$  coupling must be light: if  $m_{A^0}$  is large (the decoupling limit) then it is the mass-bounded  $h^0$  that has all the  $VV$  coupling strength; if  $m_{A^0} \lesssim 2m_Z$ , then the  $H^0$  can share the  $VV$  coupling with the  $h^0$ , but then  $m_{H^0}$

cannot be larger than about  $2m_Z$ . In the NMSSM, assuming Higgs-sector CP conservation, there are 3 neutral CP-even Higgs bosons,  $h_{1,2,3}$  ( $m_1 < m_2 < m_3$ ), which can share the  $VV$  coupling strength. One can show (see [94] for a recent update) that the masses of the  $h_i$  with substantial  $VV$  coupling are strongly bounded from above. This result generalizes to the most general supersymmetric Higgs sector as follows. Labeling the neutral Higgs bosons by  $i$  with masses  $m_{h_i}$  and denoting the  $ZZ$  squared-coupling relative to the SM by  $K_i$ , it can be shown that [95]

$$\sum_i K_i \geq 1, \quad \sum_i K_i m_{h_i}^2 \leq m_B^2. \quad (33)$$

where the value of  $m_B$  depends somewhat on the low-energy supersymmetric model. That is, the aggregate strength of the  $VV$  squared-coupling of all the neutral Higgs bosons is at least that of the SM, and the squared-masses of the neutral  $h_i$  weighted by the squared-couplings must lie below a certain bound. A value of  $m_B \sim 200$  GeV in eq. (33) is obtained [66] by assuming that the low-energy supersymmetric theory remains perturbative up to the GUT scale of order  $10^{19}$  GeV. This value of  $m_B$  applies for the most general possible Higgs representations (including triplets) in the supersymmetric Higgs sector and for arbitrary numbers of representations. If only doublet and singlet representations are allowed, the bound would be lower. The value of  $m_B \sim 200$  GeV also applies to general Higgs-sector-only extensions of the SM by requiring consistency with precision electroweak constraints *and* assuming the absence of a large contribution to  $T$  from the Higgs sector itself or from new physics, such as discussed in Section 7.2.

#### 7.4. Detection of non-exotic extended Higgs sector scalars at the Tevatron and LHC

In the case of extended Higgs sectors, all of the same processes as discussed for the SM and MSSM will again be relevant. However, one can no longer guarantee Higgs discovery at the Tevatron and/or LHC. In particular, if there are many Higgs bosons sharing the  $WW, ZZ$  coupling, Higgs boson discovery based on processes that rely on the  $VV$  coupling could be much more difficult than in models with just a few light Higgs bosons with substantial  $VV$  coupling. This is true even if the sum rule of eq. (33) applies. For example, in the NMSSM, the addition of one singlet to the minimal two-doublet Higgs structure allows for parameter choices such that no Higgs boson can be discovered at the LHC [96,97] using any of the processes considered for SM Higgs and MSSM Higgs detection. The problematical re-

gions of parameter space originally discussed in [96] were those in which the  $\gamma\gamma$  decay channel signals for the CP-even Higgs bosons are decreased (because of decreased  $W$ -loop contribution to the coupling) and a moderate value of  $\tan\beta$  was chosen so that  $t\bar{t}$ +Higgs processes are weak and  $b\bar{b}$ +Higgs processes are insufficiently enhanced. However, as shown in [97], the recent addition of the  $t\bar{t}h \rightarrow t\bar{t}b\bar{b}$  and, especially, the  $W^*W^* \rightarrow h \rightarrow \tau^+\tau^-$  discovery modes to the list of viable channels by the CMS and ATLAS collaborations means that discovery of at least one NMSSM Higgs bosons would be possible in all the “bad” parameter regions found in [96]. However, [97] also finds that there are parameter choices (explicitly excluded in the study of [96]) such that the CP-even Higgs bosons decay primarily to a pair of CP-odd Higgs bosons. Discovery techniques for this type of final state have not been developed for the LHC.

However, in other cases, the Tevatron and LHC could observe signals not expected in an approximate decoupling limit. For example, in the 2HDM model discussed earlier the light  $\hat{h}$  with no  $VV$  couplings decays via  $\hat{h} \rightarrow b\bar{b}, \tau^+\tau^-$  and discovery in  $t\bar{t}\hat{h}, b\bar{b}\hat{h}$  and even  $gg \rightarrow \hat{h}$  [98] is possible, though certainly not guaranteed. Further, in these models there is a heavy neutral Higgs boson having the bulk of the  $VV$  coupling and (for consistency with current precision electroweak constraints or with perturbativity) a mass less than about 1 TeV. This latter Higgs boson would be detected at the LHC using  $gg, WW$  fusion production and  $ZZ \rightarrow 4\ell, WW \rightarrow 2j\ell\nu, \dots$  decay modes, just like a heavy SM Higgs boson.

### 7.5. LC production mechanisms for non-exotic extended Higgs sector scalars

Any physical Higgs eigenstate with substantial  $WW$  and  $ZZ$  coupling will be produced in Higgsstrahlung and  $WW$  fusion at the LC. Although there could be considerable cross section dilution and/or resonance peak overlap, the LC will nonetheless always detect a signal. This has been discussed for the MSSM in Section 5.4. In the NMSSM, if one of the heavier CP-even  $h_i$  has most of the  $VV$  coupling, the strong bound on its mass [94] noted earlier implies that it will be detected at any LC with  $\sqrt{s} > 350$  GeV within a small fraction of a year when running at planned luminosities [99]. The worst possible case is that in which there are many Higgs bosons with  $VV$  coupling with masses spread out over a large interval with separation smaller than the mass resolution. In this case, the Higgs signal becomes a kind of continuum distribution. Still, in [95] it is shown that the sum rule of eq. (33) guarantees that the Higgs continuum signal will still be



detectable for sufficient integrated luminosity,  $L \gtrsim 200 \text{ fb}^{-1}$ , as a broad excess in the recoil mass spectrum of the  $e^+e^- \rightarrow ZX$  process. (In this case,  $WW$  fusion events do *not* allow for the reconstruction of Higgs events independently of the final state Higgs decay channel.) As already noted, the value of  $m_B \sim 200 \text{ GeV}$  appearing in eq. (33) can be derived from the constraints of perturbative evolution up to some high energy (GUT or Planck) scale for the most general Higgs sector in supersymmetric theories. The same bound on  $m_B$  is also required by precision electroweak data for general SM Higgs sector extensions, at least in theories that do not have a large positive contribution to  $T$  from a non-decoupling structure in the Higgs sector or from new physics not associated with the Higgs sector.

Other production modes of relevance include Higgs pair production [100], single Higgs production in association with  $t\bar{t}$  [44, 45, 101–106] and with  $b\bar{b}$  [104–107]. In multi-doublet models,  $t\bar{b}H^-/b\bar{t}H^+$  [44, 108, 109] and  $\tau\nu H^\pm$  [108, 110, 111] production are also present (and in some cases  $c\bar{b}H^-/b\bar{c}H^+$  production is competitive [111]). The associated production of a charged Higgs boson and gauge boson has also been studied [112]. However, none of these modes are guaranteed to be either kinematically accessible at the LC or to have a sufficiently high event rate to be observed (if kinematically allowed). Regardless of the production process, relevant decay channels could include cases where heavier Higgs bosons decay to lighter ones. If observed, such decays would provide vital information on Higgs self-couplings [113].

It is also important to consider the production processes that are most relevant for those Higgs bosons (denoted  $\hat{h}$ ) which do not have substantial  $VV$  couplings. Such processes have particular relevance in the non-decoupling scenario for the general 2HDM model discussed earlier. In this scenario,  $\hat{h}$  is the only Higgs boson light enough to be produced at an LC with  $\sqrt{s} \lesssim 1 \text{ TeV}$ , but it cannot be produced and detected in  $WW$  fusion or Higgsstrahlung. Since the other Higgs bosons are heavy, the  $\hat{h}$  also cannot be produced in association with another Higgs boson. As shown in [92, 105], the  $b\bar{b}\hat{h}$  and  $t\bar{t}\hat{h}$  processes will also not be detectable at the LC if  $\tan\beta$  is moderate in value. The most interesting tree-level processes are then those based on the quartic couplings  $WW\hat{h}\hat{h}$  and  $ZZ\hat{h}\hat{h}$  required by gauge invariance [114]. These couplings allow for  $WW \rightarrow \hat{h}\hat{h}$  fusion and  $Z^* \rightarrow Z\hat{h}\hat{h}$  production, respectively. The exact cross sections for these processes are only mildly sensitive to the masses of the other heavier Higgs bosons via 2HDM Higgs self-couplings. Of course, phase space restrictions imply an upper limit on the  $\hat{h}$  masses that can be probed in this way.

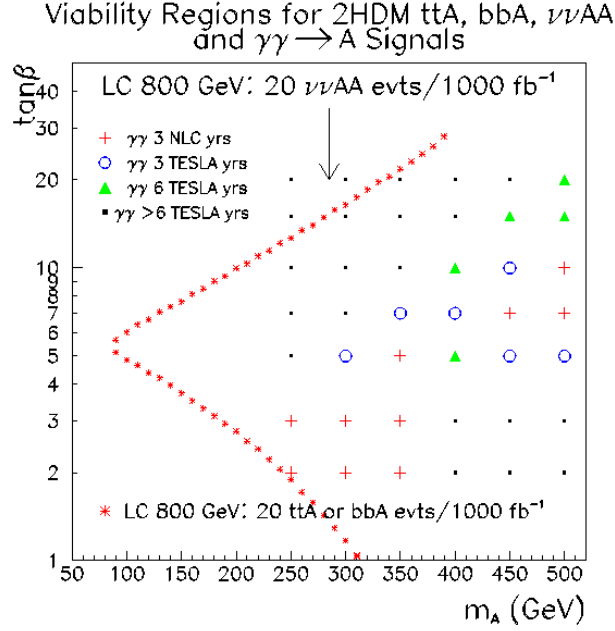


Fig. 16: The stars form an outline of a wedge of  $[m_{A^0}, \tan \beta]$  parameter space inside which the LC operating at  $\sqrt{s} = 800$  GeV yields fewer than 20 events per 1000  $\text{fb}^{-1}$  in both the  $t\bar{t}A^0$  and  $b\bar{b}A^0$  production modes. Also shown by the arrow is the  $m_{A^0}$  value above which the process  $e^+e^- \rightarrow \nu\bar{\nu}A^0A^0$  yields fewer than 20 events per 1000  $\text{fb}^{-1}$ . The + symbols on the grid of  $[m_{A^0}, \tan \beta]$  values show the points for which a  $4\sigma$  signal for  $\gamma\gamma \rightarrow A^0$  would be achieved using LC operation at  $\sqrt{s} = 630$  GeV after three years of operation assuming running conditions and strategies as specified in [17] using the NLC-based design of the  $\gamma\gamma$  collider. (The nominal  $e^+e^-$  luminosity for the underlying NLC design employed is 220  $\text{fb}^{-1}$  per year at  $\sqrt{s} = 500$  GeV.) The circles (triangles) show the additional points that would yield a  $4\sigma$  signal for twice (four times) the integrated luminosity of the current NLC  $\gamma\gamma$  interaction region design. The small squares show the additional points sampled in the study of [17]. This figure was taken from [115].

The case of  $\hat{h} = A^0$  is illustrated in figs. 16 and 17 [115]. Fig. 16 shows the wedge region in which fewer than 20 events per 1000  $\text{fb}^{-1}$  are obtained in  $b\bar{b}A^0$  and  $t\bar{t}A^0$  production at  $\sqrt{s} = 800$  GeV. Fig. 17 shows the  $m_{A^0}$  values for which fewer than 20 events are obtained in  $Z^* \rightarrow ZA^0A^0$  and  $W^*W^* \rightarrow A^0A^0$  production at  $\sqrt{s} = 500$  GeV and 800 GeV. Thus, single  $A^0$  discovery is not possible via any of the above processes in the region of the

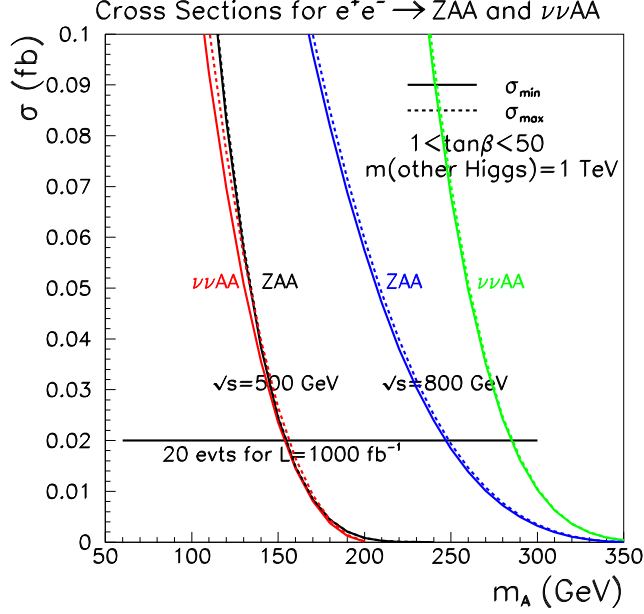


Fig. 17: The cross sections for  $e^+e^- \rightarrow ZA^0A^0$  and  $e^+e^- \rightarrow \nu\bar{\nu}A^0A^0$  as a function of  $m_{A^0}$  are shown, assuming a 2HDM model with a heavy SM-like  $h^0$ . We have taken  $m_{h^0} = m_{H^0} = m_{H^\pm} = 1$  TeV. Maximum and minimum values found after scanning  $1 \leq \tan\beta \leq 50$  are shown for  $\sqrt{s} = 500$  GeV and 800 GeV. The variation with  $\tan\beta$  arises from small contributions associated with exchanges of the heavy Higgs bosons. The 20 event level for  $L = 1000 \text{ fb}^{-1}$  is indicated. Taken from [115].

wedge with  $m_{A^0} \gtrsim 300$  GeV. With the  $\gamma\gamma$  collider option at the LC, we note that  $\gamma\gamma \rightarrow A^0$  can provide a signal for the decoupled  $A^0$  over a significant portion of the wedge region. The results from a realistic study of [17] are illustrated in fig. 16, which focuses on  $m_{A^0} \geq 250$  GeV. In particular, the operation of the  $\gamma\gamma$  collider for two years using a polarization configuration for the electron beams and laser photons yielding a broad  $E_{\gamma\gamma}$  spectrum and one year using a configuration yielding a peaked spectrum is assumed. The pluses indicate  $4\sigma$  discovery points after three years of operation (assuming that the machine operates for  $10^7$  sec during one calendar year) in the appropriate configurations at the NLC. The results of fig. 16 employ the  $E_{\gamma\gamma}$  luminosity spectra as computed in [17] based on the particular laser and interaction region design that is discussed in more detail in Section 11.

A factor of two higher  $\gamma\gamma$  luminosity, as might be achievable at TESLA or through further design improvement at the NLC, would allow  $4\sigma$  discovery for the additional points indicated by the circles. The corresponding results for a decoupled CP-even  $\hat{h} = h^0$  are similar.

## 8. Exotic Higgs sectors and other possibilities

As we have seen, there are many scenarios and models in which the Higgs sector is more complicated than the one-Higgs-doublet of the Standard Model. Supersymmetry requires at least two Higgs doublets. Even in the absence of supersymmetry, a two-doublet Higgs sector allows for CP-violating phenomena. Singlets can also be added without altering the tree-level prediction of  $\rho = 1$ . However, the possibility of Higgs representations with still higher weak isospin (left-handed, denoted by  $L$ ) and/or hypercharge should not be ignored. Indeed, for judicious choices of the numbers and types of such representations, gauge coupling unification (although at scales below  $10^{15}$  GeV) is possible without introducing supersymmetry [116]. The main drawback of introducing scalars of this type is that, for triplets and most higher representations, if the vacuum expectation value of the neutral Higgs field member of the representation is non-zero ( $v_L \neq 0$ ) then  $\rho$  becomes infinitely renormalized and can no longer be computed [117]. In this case,  $\rho$  becomes an independent input parameter to the theory. Triplets have received the most attention, as they arise naturally in left-right symmetric extensions of the Standard Model gauge group [118]. (These and other models that utilize Higgs triplets are reviewed in [1].) In this section we will also briefly consider the Higgs-like pseudo-Nambu-Goldstone bosons that arise in generic technicolor theories.

### 8.1. A triplet Higgs sector

Including a single complex SU(2)-triplet Higgs representation, in addition to some number of doublets and singlets, results in six additional physical Higgs eigenstates:  $H^{--,++}$ ,  $H^{-,+}$ ,  $H^0$  and  $H^{0'}$ . All but the doubly-charged states can mix with the doublet/singlet Higgs states under some circumstances. Even if  $v_L \neq 0$  for the neutral field,  $\rho = 1$  can be preserved at tree level if, in addition, a real triplet field is also included [119, 120]. However,  $\rho$  will still be infinitely renormalized at one-loop unless  $v_L = 0$  is chosen. Left-right (L-R) symmetric models capable of yielding the see-saw mechanism for neutrino mass generation *require* two triplet Higgs repre-

representations (an L-triplet and an R-triplet). The large see-saw mass entry,  $M$ , arises from a “Majorana coupling” which L-R symmetry requires to be present for both the L-triplet and R-triplet representations.<sup>11</sup> Again,  $\rho$  will not be altered if  $v_L = 0$ , but  $v_R$  must be non-zero and large for large  $M$ . We will briefly discuss the phenomenology of an L-triplet; the corresponding phenomenology of the R-triplet is quite different. (See [1] for a review.)

The resulting Higgs phenomenology can be very complex. We focus on the most unequivocal signal for a triplet representation, namely observation of a doubly-charged Higgs boson. Pair production,  $Z^* \rightarrow H^{++}H^{--}$  would be visible at the LHC for  $m_{H^{--}} \lesssim 1$  TeV [116], but has limited mass reach,  $m_{H^{--}} < \sqrt{s}/2$ , at the LC. Fortunately, single production of a doubly-charged Higgs boson at the LC is also generally possible. In particular, the generically-allowed Majorana coupling leads to an  $e^-e^- \rightarrow H^{--}$  coupling and the possibility of  $s$ -channel resonance production of the  $H^{--}$  in  $e^-e^-$  collisions. Observation of this process would provide a dramatic confirmation of the presence of the Majorana coupling and, in many cases, the ability to actually measure its magnitude. For a discussion and review, see [121]. If the  $H^{--}$  is heavy *and* has significant  $W^-W^-$  coupling (requiring  $v_L \neq 0$ ), then it can become broad and the  $s$ -channel resonant production cross section is suppressed (see, *e.g.*, [122]) and might not be observable. Another production mechanism sensitive to the  $e^-e^- \rightarrow H^{--}$  coupling that might be useful in such an instance is  $e^-e^- \rightarrow H^{--}Z$ , and  $e^-e^- \rightarrow H^-W^-$  will be sensitive to the  $e^-e^- \rightarrow H^-$  coupling that would be present for the  $H^-$  member of the triplet representation [123]. Using just the Majorana coupling, doubly-charged Higgs bosons can also be produced via  $e^-e^- \rightarrow e^+H^{--}$  and  $e^+e^- \rightarrow e^+e^+H^{--}$  [124] and the singly-charged members of the same representation can be produced in  $e^-e^- \rightarrow H^-W^-$  [123].

Despite the loss of predictivity for  $\rho$ , it could be that non-zero  $v_L$  is Nature’s choice. In this case, the  $e^-e^-$  collider option again has some unique advantages. The neutral, singly-charged and doubly-charged Higgs bosons of the triplet representation can *all* be produced (via  $ZZ$  fusion,  $W^-Z$  fusion and  $W^-W^-$  fusion, respectively). For example, [125] studies  $W^-W^- \rightarrow H^{--}$  fusion.

---

<sup>11</sup>The so-called Majorana couplings correspond to the terms in the Yukawa interactions in which a fermion bilinear of lepton number  $+2$  or  $-2$  (*e.g.*, the latter contains  $\nu\nu$  and  $e^-e^-$ ) couples to the triplet fields. When the neutral component of the R-triplet acquires a vacuum expectation value, a Majorana mass term for the right-handed neutrino is generated, and lepton number is spontaneously broken. In this model B – L is a spontaneously broken gauged U(1) symmetry.

## 8.2. Pseudo Nambu Goldstone bosons

In the context of technicolor and related theories, the lowest-mass states are typically a collection of pseudo-Nambu-Goldstone bosons, of which the lightest is very possibly a state  $P^0$  which can have mass below 200 GeV and couplings and other properties not unlike those of a light SM-like Higgs boson. Typically, its  $WW, ZZ$  coupling is very small (arising via loops or anomalies), while its  $b\bar{b}$  coupling can be larger. The phenomenology of such a  $P^0$  was studied in [126, 127]. The best modes for detection of the  $P^0$  at the LC are  $e^+e^- \rightarrow \gamma P^0 \rightarrow \gamma b\bar{b}$  and  $\gamma\gamma \rightarrow P^0 \rightarrow b\bar{b}$ . Since the  $P^0$  is likely to be discovered at the LHC in the  $\gamma\gamma$  final state, we will know ahead of time of its existence, and precision measurements of its properties would be a primary goal of the LC. High integrated luminosity would be required.

## 9. LC Measurements of Higgs Boson Properties

In addition to the observation of one or more Higgs boson(s), an essential part of the LC physics program consists of measuring the mass, width, and couplings of the Higgs boson(s) with precision, and the determination of the scalar potential that gives rise to electroweak symmetry breaking.

Determinations of the Higgs couplings are needed to demonstrate that a Higgs boson generates mass for vector bosons, charged leptons, and up- and down-type quarks. Whether there is only one Higgs doublet can be checked if the ratios of measured branching ratios of directly coupled particles are indeed proportional to the ratios of the squared-masses. Small variations can distinguish between a SM Higgs and  $h^0$  of the MSSM with couplings close to the SM Higgs boson. Couplings are determined through measurements of Higgs branching ratios and cross sections. Higgs bosons are also expected to couple to themselves, and this self-coupling  $\lambda$  can only be explored through the direct production of two or more Higgs bosons. It is in this category of *direct* and *model independent* determination of many absolute couplings (and not just their ratios) that the strength of the LC Higgs physics program really stands out.

Details of some of the studies can be found in [128] and a comprehensive description of European studies using results of the simulated TESLA detector can be found in [129]. North American studies consider simulations of detectors with capabilities as described elsewhere [10]. The program of measurements of Higgs boson properties strongly impacts detector design. Measurement of branching ratios into fermions requires sophisticated ver-

tex detectors to separate  $b$  from  $c$  (and gluon) jets. Precise recoil mass measurements opposite leptons need excellent momentum resolution (particularly for  $\mu^+\mu^-$ ) from charged particle tracking. The performance of the combined tracking and calorimetry systems needs to result in precise jet-jet invariant masses, missing mass measurements, and the ability to separate hadronic  $W$  from hadronic  $Z$  decays.

The specific measurements used to determine the Higgs couplings to vector bosons, fermions and scalars are significantly different depending on the mass of the Higgs boson. A generic neutral CP-even Higgs boson will be denoted by  $h$  in this section. We treat three cases separately: a light Higgs boson ( $m_h < 2m_W$ ), an intermediate mass Higgs boson ( $2m_W \leq m_h < 2m_t$ ), and a heavy Higgs boson ( $m_h \geq 2m_t$ ).

### 9.1. Mass

In the Standard Model, the Higgs mass determines all its other properties. Thus, the precision of the mass measurement affects the comparison of theory and experiment, for example, in a global fit of cross sections, branching ratios, and precision electroweak data. Similarly, in the MSSM or other models with extended Higgs sectors, the masses of all the Higgs bosons are an important input to determining the underlying model parameters.

For this fundamental mass measurement, the LC can exploit recoils against a  $Z$  (independently of Higgs decay), and event reconstruction plus kinematic constraints can improve resolution and clean up mass tails. For a light or intermediate mass Higgs boson, optimal running conditions would have smaller center-of-mass energy (*e.g.*,  $\sqrt{s} = 350$  GeV for better momentum resolution), and possess as small a level of beamstrahlung as possible. Under such conditions, one can precisely measure the recoil mass in  $e^+e^- \rightarrow Zh$  events opposite to the reconstructed leptonic decay  $Z \rightarrow e^+e^-$  or  $\mu^+\mu^-$ , with the additional advantage of decay mode independence. Accuracy can be improved by reconstructing specific decay modes, leading for example to a four-jet topology where effective (5-C) kinematic constrained fits can be employed.

Fig. 18 shows the distribution of the recoil mass,

$$M_{\text{recoil}} = \sqrt{s - 2\sqrt{s} \cdot E_{\ell^+\ell^-} + M_{\ell^+\ell^-}^2}, \quad (34)$$

in a simulation of the “Large” Linear Collider Detector (LCD) [130] for Higgs masses between 115 and 160 GeV [131]. Using fits of Monte Carlo shape templates and an integrated luminosity of  $500 \text{ fb}^{-1}$ , precisions of

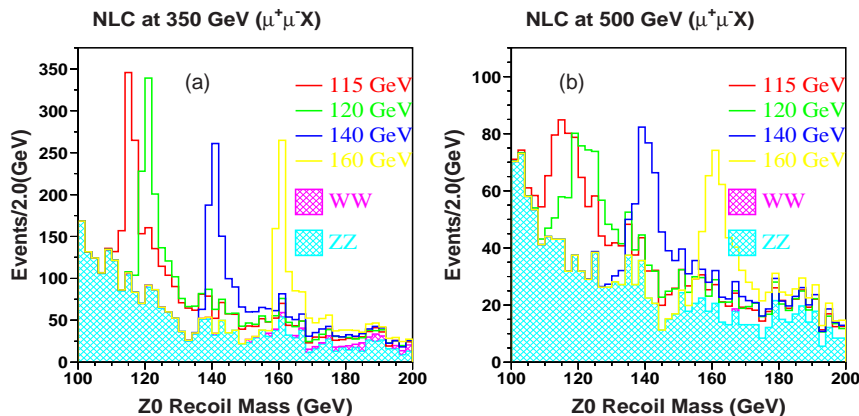


Fig. 18: Recoil mass from a pair of leptons simulated in the LCD Large detector for different Higgs masses at (a)  $\sqrt{s} = 350$  GeV and (b) 500 GeV. Taken from [131].

$\Delta m_{h_{\text{SM}}} \simeq 60$  MeV at  $\sqrt{s} = 350$  GeV and  $\Delta m_{h_{\text{SM}}} \simeq 120$  MeV at  $\sqrt{s} = 500$  GeV have been estimated for either the  $e^+e^-$  or  $\mu^+\mu^-$  mode.

Realistic simulations have also been made of the LCD Large detector for the process  $Zh \rightarrow q\bar{q}h$  resulting in four jets. Fig. 19(a) shows the jet-jet invariant mass distribution for pairs of jets for Higgs with  $m_{h_{\text{SM}}} = 115$  GeV recoiling against a  $Z$  that has been reconstructed from its hadronic decay mode [132]. A clean Higgs signal with a mass resolution of approximately 2 GeV is observed. The central Higgs mass is shifted down due to the loss of low energy charged and neutral particles in the simulated event reconstruction. A low mass tail of the Higgs signal arises from missing neutrinos in semi-leptonic  $b$  and  $c$  quark decays. Using neural net tags and full kinematic fitting [133], the mass peak shown in fig. 19(b) is obtained for  $m_{h_{\text{SM}}} = 120$  GeV,  $\sqrt{s} = 500$  GeV, and  $500 \text{ fb}^{-1}$  resulting in  $\Delta m_{h_{\text{SM}}} \simeq 50$  MeV. With the possibility of a second lower-energy interaction point, scans across the  $Zh$  threshold may be attractive. With a total integrated luminosity of  $100 \text{ fb}^{-1}$ ,  $\Delta m_{h_{\text{SM}}} \simeq 100$  MeV at  $m_{h_{\text{SM}}} = 150$  GeV is achievable [134], competitive with the methods above.

More work is necessary to confirm analogous precisions for heavier Higgs bosons and MSSM Higgs bosons with different decay modes and possible near-mass degeneracies. The number of  $Zh$  events with  $Z \rightarrow \ell^+\ell^-$  for an intermediate mass ( $m_h > 2m_W$ ) or heavy Higgs ( $m_h > 2m_t$ ) with SM cou-



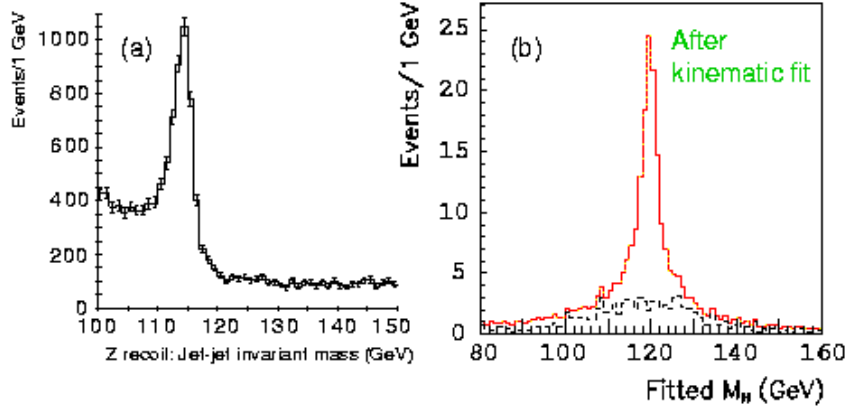


Fig. 19: (a) Jet-jet invariant mass of the jets recoiling from a  $Z$  reconstructed hadronically simulated in the LCD Large detector,  $m_{h_{SM}} = 115$  GeV [132]. (b) Direct reconstruction of the four-jet  $q\bar{q}h_{SM}$  state simulated in the LCD Large detector after fitting with full kinematic constraints,  $m_{h_{SM}} = 120$  GeV [133].

pling plummets quickly [135]. In this case, and for the decays  $h \rightarrow ZZ$ , hadronic decays of the  $Z$  would have to be considered to gain sufficient statistics. For the heavier MSSM Higgs boson states, European studies [136] have shown typical mass precisions of  $\Delta m_{H^\pm}$  and  $\Delta m_{A^0, H^0}$  of around 1 GeV for  $500 \text{ fb}^{-1}$ , but at  $\sqrt{s} = 800$  GeV.

## 9.2. Coupling Determinations – Light Higgs Boson

### 9.2.1. Cross Sections

For Higgs masses below  $2m_W$ , the couplings  $g_{hZZ}$  and  $g_{hWW}$  are best measured through measurements of the Higgsstrahlung and  $WW$  fusion cross sections, respectively. These cross sections are also critical in the extraction of branching ratios since the experimental measurement will be a product of cross section and branching ratio.

Measurement of the Higgsstrahlung cross section is best addressed via the recoil mass method outlined above [131]. To reduce the contribution from the  $WW$  fusion process, it is best to run at a lower energy, *i.e.*,  $\sqrt{s} = 350$  GeV, and to examine recoil against  $\mu^+\mu^-$  to avoid large Bhabha backgrounds. A simulation based on the LCD Large detector with  $500 \text{ fb}^{-1}$  finds  $\Delta\sigma/\sigma \simeq 3\%$  [4.7%] at  $\sqrt{s} = 350$  [500] GeV, as shown in fig. 20(a). These results agree roughly with estimates from European studies [137].

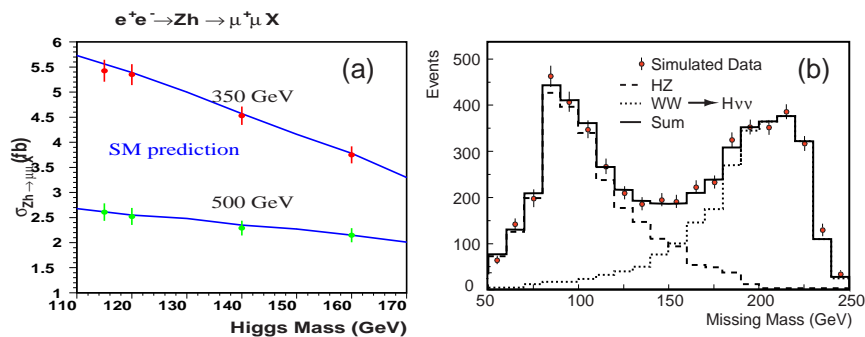


Fig. 20: (a) Cross section measurement for  $500 \text{ fb}^{-1}$  [131] and (b) separation of Higgsstrahlung and  $WW$  fusion ( $\sqrt{s} = 350 \text{ GeV}$ ) through a fit after background subtraction [138], both simulated in the LCD Large detector.

With efficient and pure  $b$ -jet tagging, events due to the process  $e^+e^- \rightarrow W^+W^-\nu\bar{\nu} \rightarrow \nu\bar{\nu}h \rightarrow \nu\bar{\nu}b\bar{b}$  can be separated from those due to Higgsstrahlung,  $Zh \rightarrow \nu\bar{\nu}h \rightarrow \nu\bar{\nu}b\bar{b}$  by examining the missing mass distribution and fitting to the expected shapes of a peak at  $m_Z$  from Higgsstrahlung and the higher missing masses from  $WW$  fusion. This technique has been confirmed with simulations of the LCD Large detector as shown in fig. 20(b) [138]. With  $500 \text{ fb}^{-1}$  and a precision of  $\delta\text{BR}(h_{\text{SM}} \rightarrow b\bar{b})/\text{BR} \simeq 3\%$  (see below), the fusion-process cross section with this analysis can be found with a precision  $\Delta\sigma/\sigma = 3.5\%$  for  $m_{h_{\text{SM}}} = 120 \text{ GeV}$ .

### 9.2.2. Branching Ratios

A key advantage of the linear collider in Higgs studies is the attractive situation of identifying Higgsstrahlung  $Zh$  events through the tag of the  $Z$  decays. This selection is largely independent of the decay mode of the  $h$  and simplifies the measurement of Higgs boson branching ratios.

Small beam sizes, the possibility of a first measurement as close as 1 cm from the beam axis, and sophisticated pixel vertex detectors allow for efficient and clean separation of quark flavors. Separate tagging of  $b$  and  $c$  jets is possible. By assumption, jets that are not identified as heavy flavor are assumed to be gluon jets, since the Higgs partial width into  $gg$  dominates the width into light quark pairs.

In a study [139] of vertexing in a CCD vertex detector in a standard

Table 1: Predicted branching ratio precisions in the LCD Large detector and typical vertex detector configuration for  $500 \text{ fb}^{-1}$  and  $\sqrt{s} = 500 \text{ GeV}$  [142].

	$m_{h_{\text{SM}}} = 120 \text{ GeV}$		$m_{h_{\text{SM}}} = 140 \text{ GeV}$	
	BR	$\delta\text{BR}/\text{BR}$	BR	$\delta\text{BR}/\text{BR}$
$h_{\text{SM}} \rightarrow b\bar{b}$	$(69 \pm 2.0)\%$	2.9%	$(34 \pm 1.3)\%$	3.8%
$h_{\text{SM}} \rightarrow WW^*$	$(14 \pm 1.3)\%$	10%	$(51 \pm 1.5)\%$	3.0%
$h_{\text{SM}} \rightarrow c\bar{c}$	$(2.8 \pm 1.1)\%$	39%	$(1.4 \pm 0.64)\%$	44%
$h_{\text{SM}} \rightarrow gg$	$(5.2 \pm 0.93)\%$	18%	$(3.5 \pm 0.79)\%$	23%
$h_{\text{SM}} \rightarrow \tau^+\tau^-$	$(7.1 \pm 0.56)\%$	8.0%	$(3.6 \pm 0.38)\%$	10%

configuration of a LCD detector (C1 in [140]), topological vertexing [141] with neural net selection [see fig. 21(a)] was used for flavor (or anti-flavor, *i.e.*, veto  $WW^*$ ) tagging. Assuming  $500 \text{ fb}^{-1}$  and 80% polarization, results shown in Table 1 were obtained (and include the most recent updated branching ratio precisions of [142]). These results have been checked to scale roughly with other studies [143–145] as  $(\sigma \int \mathcal{L} dt)^{-1/2}$ , with the results of [145] (that includes  $h_{\text{SM}}\nu\bar{\nu}$ ) being noticeably better for  $c\bar{c}$  and  $gg$  with errors as shown in fig. 21. As described in more detail in Section 9.2.5, these branching ratio measurements can then be used to either distinguish a SM Higgs boson from an MSSM Higgs boson, or to probe higher mass states and extract MSSM parameters such as  $m_{A^0}$  even if  $A^0$  is not accessible.

With enough data and good charged particle momentum resolution, even the rare decay mode into  $\mu^+\mu^-$  can be observed. As shown in fig. 22, for a Higgs boson mass of 120 GeV where the Standard Model branching ratio is predicted to be only  $3 \times 10^{-4}$ , the signal can be extracted from the underlying background with more than  $5\sigma$  significance with  $1000 \text{ fb}^{-1}$  [146]. For this channel, there are clear advantages to running at multi-TeV energies where precisions could be reached to extend the test of the Higgs mechanism of mass generation in the lepton sector by checking if  $g_{h_{\text{SM}}\mu\mu}/g_{h_{\text{SM}}\tau\tau} = m_\mu/m_\tau$ .

For lighter Higgs bosons, the coupling to top quarks is still accessible via the radiative process  $t\bar{t}h$  described below or indirectly through  $\text{BR}(h \rightarrow gg)$ . An accessible decay mode for light Higgs bosons is  $h \rightarrow \gamma\gamma$  requiring excellent electromagnetic calorimetry in the detector. For a SM Higgs boson in a typical LCD detector, this is a difficult measurement requiring a great deal of luminosity, which is best for masses around 120 GeV [147], as shown in fig. 23. A higher luminosity study [148] with  $1000 \text{ fb}^{-1}$  and  $m_{h_{\text{SM}}} = 120 \text{ GeV}$  for the TESLA detector finds  $\delta\text{BR}/\text{BR} = 14\%$ . A gamma-gamma col-

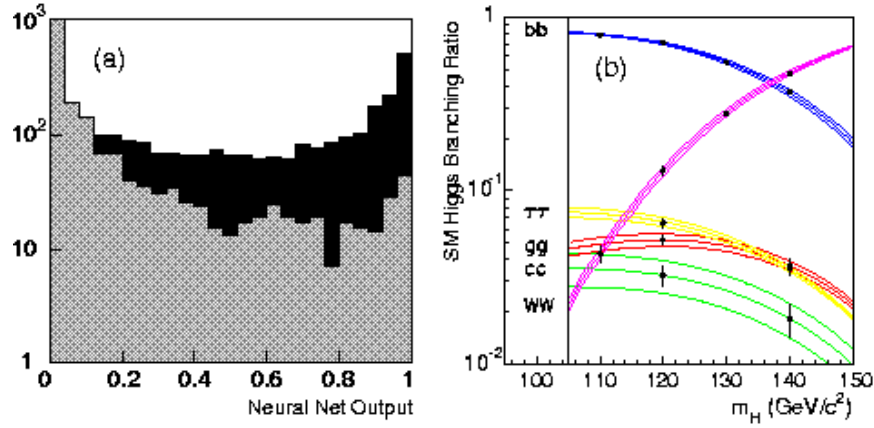


Fig. 21: (a) For the simulated LCD Large detector with CCD vertex detector, neural net  $h_{\text{SM}} \rightarrow c\bar{c}$  output for  $h_{\text{SM}} \rightarrow c\bar{c}$  events (dark) compared to output for  $h_{\text{SM}} \rightarrow b\bar{b}$  events (gray). Taken from [140]. (b) Variation of branching ratios with SM Higgs mass (bands are  $1\sigma$  uncertainties on the predictions) and measurement precisions in the TESLA detector (points with error bars). Taken from [145].

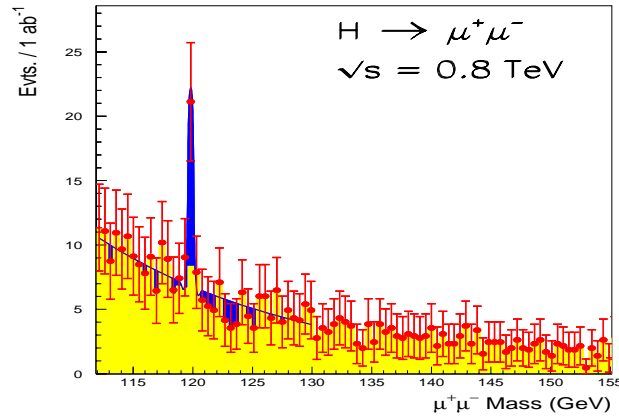


Fig. 22: Distribution of the  $\mu^+\mu^-$  invariant mass for  $m_{h_{\text{SM}}} = 120 \text{ GeV}$ . The points with error bars represent 1000 fb<sup>-1</sup> of data. Taken from [146].

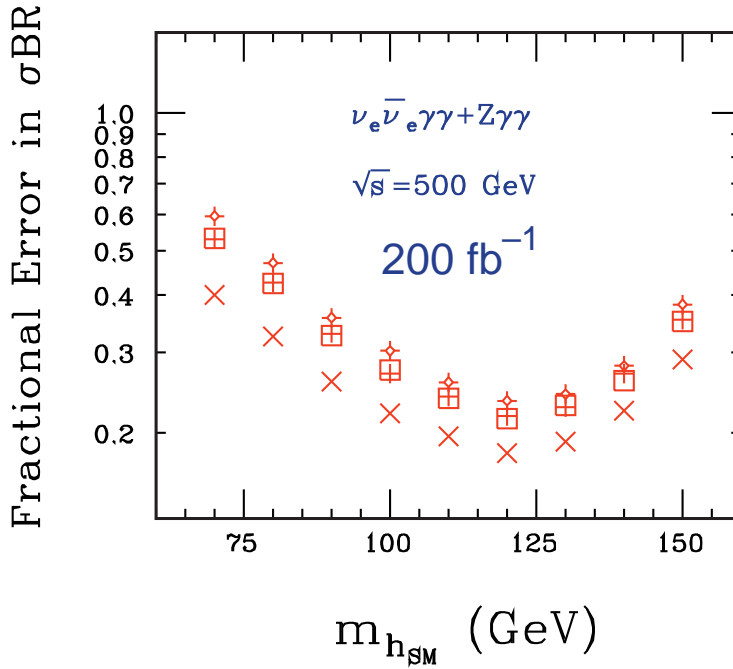


Fig. 23: Fractional error on the branching ratio  $BR(h_{SM} \rightarrow \gamma\gamma)$ . The open squares are for a typical LCD detector electromagnetic energy resolution of  $\Delta E/E = 10\%/\sqrt{E} \oplus 1.0\%$ . Taken from [147].

lider, discussed in Section 11, would be a more powerful tool for determining the Higgs coupling to photons.

Invisible Higgs boson decay channels, if significant, pose a difficult challenge for the LHC Higgs search. [149]. Possible invisible final states include neutralinos [150], majorons [151], heavy neutrinos [152], or the disappearance of the Higgs boson due to Higgs-radion mixing [153]. Likewise, the LHC Higgs search will be difficult if the  $b\bar{b}$ ,  $WW^*$ ,  $ZZ^*$  and  $\gamma\gamma$  decay channels are significantly suppressed (in which case, *e.g.*, Higgs decay into light hadronic jets could be dominant [154]). The LC can close these loopholes and measure the branching ratio easily even for branching ratios as small as 5% as shown in fig. 24 for a relatively narrow Higgs state using the recoil mass method and demanding no detector activity opposite the  $Z$  [155], or by comparing the number of events tagged with  $Z \rightarrow \ell^+\ell^-$  with the total number of observed Higgs decays into known states.

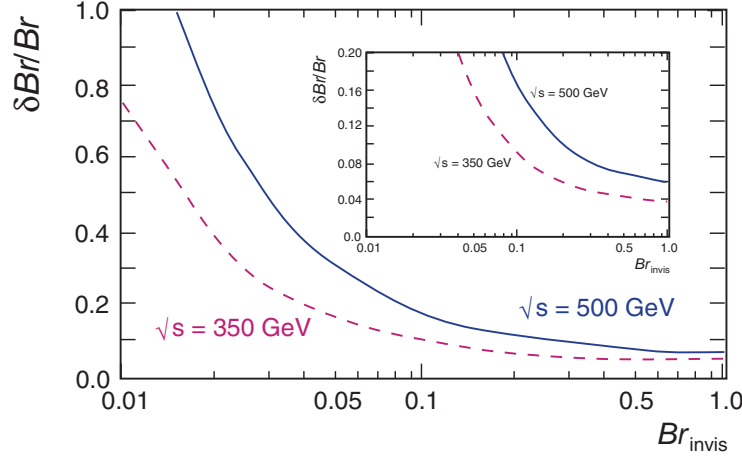


Fig. 24: Fractional error on a Higgs invisible branching ratio for  $m_h = 120$  GeV and  $500 \text{ fb}^{-1}$  of data. The asymptotic value as the branching ratio (Br) approaches unity is due solely to the statistical uncertainty in  $\sigma(hZ)$ . A blow-up of the region of  $\delta Br/Br \leq 0.2$  is also shown. Taken from [155]

### 9.2.3. Radiative Production, $t\bar{t}h$

For a light Higgs boson, production through radiation off a top quark is feasible [44, 45, 101–106], resulting in a final state of  $t\bar{t}h$ , thus allowing for a determination of the Yukawa top quark coupling  $g_{htt}$ . For a SM-like Higgs boson with  $m_h = 120$  GeV, the  $t\bar{t}h$  cross section is roughly 10 times larger at  $\sqrt{s} = 700\text{--}800$  GeV than at 500 GeV. At  $\sqrt{s} = 800$  GeV, a statistical error of  $\delta g_{htt}/g_{htt} \sim 5\%$  was estimated [102] for  $L = 500 \text{ fb}^{-1}$  on the basis of an optimal-observable analysis [156]. At  $\sqrt{s} = 500$  GeV, a statistical error of  $\delta g_{htt}/g_{htt} \simeq 21\%$  is estimated [103, 104] using a total integrated luminosity of  $1000 \text{ fb}^{-1}$ . A more sophisticated analysis using neural net selections, full simulation, and the same integrated luminosity at  $\sqrt{s} = 800$  GeV finds a total error of 6% on the coupling [157].

### 9.2.4. Self-Coupling

To fully delineate the Higgs sector, it is essential to measure the shape of the Higgs potential. The cross section for double Higgs production (*e.g.*,  $Zhh$ ) is related to the triple Higgs coupling  $g_{hhh}$ , which in turn is related

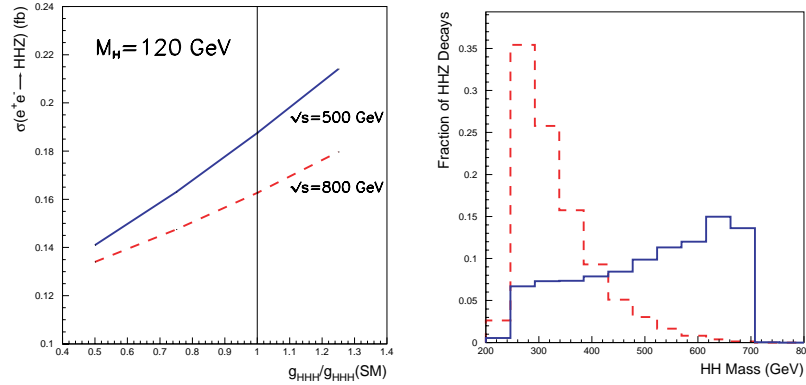


Fig. 25: (a) Dependence of the  $hhZ$  cross section on the triple Higgs coupling, normalized to its SM value for the indicated mass and  $\sqrt{s}$  values. (b) Distribution of the  $hh$  invariant mass in  $hhZ$  events from diagrams containing the triple Higgs vertex (solid line) compared to that from other diagrams (dashed line). Both plots have been taken from [161].

to the spontaneous symmetry breaking shape of the Higgs potential [158]. In the MSSM, a variety of double Higgs production processes [113] would be required to determine  $g_{hhh}$ ,  $g_{hAA}$ , *etc.*

These cross sections are low, and high integrated luminosity is needed, bolstered by polarization and neural net selections. Experimental studies [159,160] indicate that for a SM-like Higgs boson with  $m_h = 120$  GeV at  $\sqrt{s} = 500$  GeV and  $1000 \text{ fb}^{-1}$ , a precision of  $\delta g_{hhh}/g_{hhh} = 23\%$  is possible. A measurement of the double Higgs production cross section to extract  $g_{hhh}$  has to deal with dilution due to the existence of diagrams that lead to the same final states but that do not include a triple Higgs vertex [see fig. 25(a)], so additional kinematical variables can be considered to enhance sensitivity to the signal. A study considering the  $h$  decay angle in the  $hh$  rest frame and the  $hh$  invariant mass [fig. 25(b)] has shown improved separation and an increased precision of  $\delta g_{hhh}/g_{hhh} = 20\%$  [161] for the same mass, energy, and integrated luminosity as above. The regions of accessibility in the MSSM parameter space for the MSSM Higgs self-couplings have also been performed [113,162].

With the cross section for SM triple Higgs production so low [ $\sigma(Zhhh) < 0.001 \text{ fb}$ ], measurement of the quartic coupling  $g_{hhhh}$  is hopeless with currently envisioned luminosities.

### 9.2.5. Implications for the MSSM Higgs Sector

The discussion of light Higgs coupling determinations has been based on the assumption that the actual Higgs couplings to fermions, vector bosons and scalars are close to the corresponding Standard Model expectations. In Section 7.1, it was argued that such an expectation is rather generic, and applies to the decoupling limit of models of Higgs physics beyond the Standard Model. In particular, the decoupling limit of the MSSM Higgs sector sets in rather rapidly once  $m_{A^0} \gtrsim 150$  GeV [see Section 5.1]. Since  $m_{h^0} \lesssim 135$  GeV in the MSSM [eq. (22)], the precision study of  $h^0$  using the techniques discussed above can distinguish between  $h^0$  and  $h_{\text{SM}}$  with a significance that depends on how close the model is to the decoupling limit. Said another way, the detection of deviations in the Higgs couplings from their Standard Model predictions would yield evidence for the existence of the non-minimal Higgs sector, and in the context of the MSSM would provide constraints on the value of  $m_{A^0}$  (with some dependence on  $\tan\beta$  and other MSSM parameters that enter in the Higgs radiative corrections).

In [73], the potential impact of precision Higgs measurements at the LC on distinguishing  $h^0$  from  $h_{\text{SM}}$  was examined. The fractional deviation of the  $h^0$  branching ratios into a given final state from the corresponding result for  $h_{\text{SM}}$  (assuming the same Higgs mass in both cases) is defined as:  $\delta\text{BR} \equiv (\text{BR}_{\text{MSSM}} - \text{BR}_{\text{SM}})/\text{BR}_{\text{SM}}$ . For the MSSM Higgs boson decay, both  $m_{h^0}$  and the corresponding branching ratios were computed including the radiative corrections due to the virtual exchange of Standard Model and supersymmetric particles, as described in Section 5.2. Thus, the  $h^0$  branching ratios depend on  $m_{A^0}$  and  $\tan\beta$  (which fix the tree-level MSSM Higgs sector properties) and a variety of MSSM parameter that govern the loop corrections. Four scenarios were considered: the minimal and maximal top-squark mixing cases [see eq. (22) and surrounding text], and two additional cases with large  $|\mu| = |A_t|$  (for  $\mu A_t < 0$  and two possible sign choices of  $\mu$ ), where  $\mu$  and  $A_t$  control the top-squark mixing. In the latter two scenarios, significant renormalization of the CP-even Higgs mixing angle  $\alpha$  and  $\Delta_b$  [see eq. (29)] can arise.

In fig. 26, contours of  $\delta\text{BR}$  are plotted for three  $h^0$  decay modes:  $b\bar{b}$ ,  $WW^*$  and  $gg$ . The contours shown correspond roughly to the  $1\sigma$  and  $2\sigma$  measurements claimed by [145], rescaled for the LC at  $\sqrt{s} = 500$  GeV (see also the  $b\bar{b}$  and  $WW^*$  branching ratio precisions given in Table 1). In the minimal and maximal scenarios, the dependence on  $m_{A^0}$  is nearly independent of  $\tan\beta$ , and demonstrates that one can achieve sensitivity to values



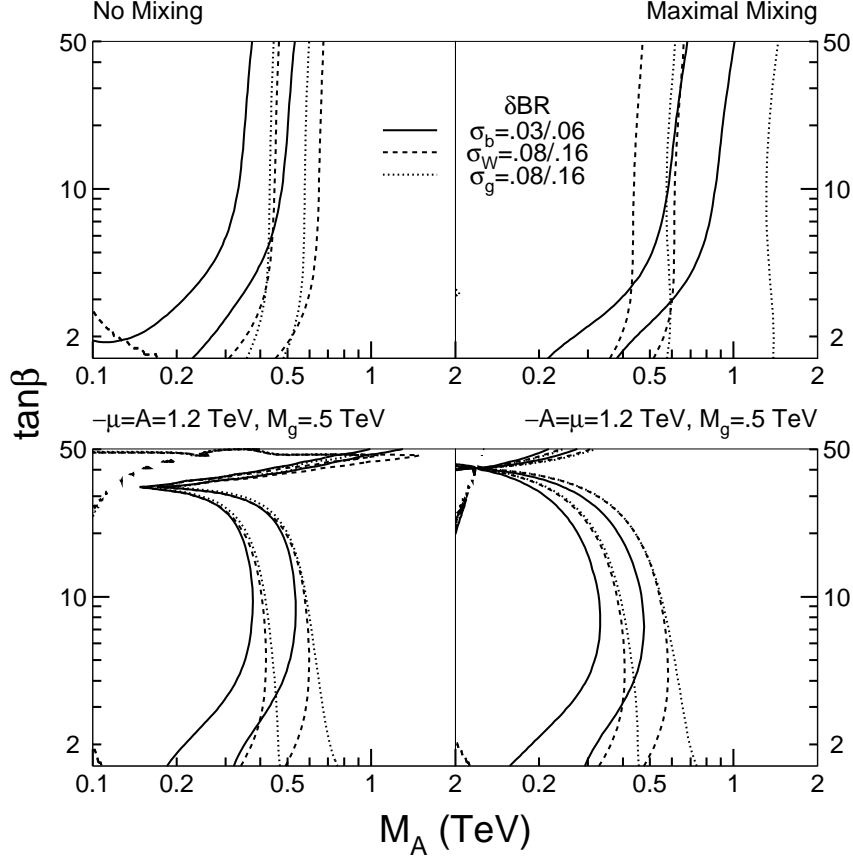


Fig. 26: Contours of  $\delta\text{BR}(b\bar{b}) = 3$  and 6% (solid),  $\delta\text{BR}(WW^*) = 8$  and 16% (dashed) and  $\delta\text{BR}(gg) = 8$  and 16% (dotted) [BR deviations are defined in the text] in the no (*i.e.* minimal) mixing scenario (top left), the maximal mixing scenario (top right), and the large  $\mu$  and  $A_t$  scenario with  $\mu = -A_t = 1.2$  TeV (bottom left) and  $\mu = -A_t = -1.2$  TeV (bottom right). Taken from [73].

of  $m_{A^0}$  that lie significantly beyond  $\sqrt{s}/2$  where direct production at the LC via  $e^+e^- \rightarrow H^0A^0$  is kinematically forbidden. However in some MSSM parameter regimes [*e.g.*, the case of large  $\mu = -A_t$  as shown in fig. 26(c) and (d)], a region of  $\tan\beta$  may yield almost no constraint on  $m_{A^0}$ . This is due to the phenomenon of  $m_{A^0}$ -independent (or premature) decoupling [73] in which  $\cos(\beta - \alpha)$  [which controls the departure from the decoupling limit]

vanishes at a particular value of  $\tan\beta$  independently of the value of  $m_{A^0}$ . Thus, a measured deviation of Higgs branching ratios that distinguishes  $h^0$  from  $h_{\text{SM}}$  can place significant constraints on the heavier non-minimal Higgs states, although the significance of the resulting constraints can depend in a nontrivial way on the value of the MSSM parameters that control the Higgs radiative corrections.

### 9.3. Coupling Determinations – Intermediate Mass Higgs Boson

For  $m_h < 2m_W$ , there are many possible branching ratio measurements at the LC (see Table 1). This rich phenomenology allows for the determination of Higgs couplings to many of the fermions and bosons. For larger masses, decays to  $f\bar{f}$  become rarer until the threshold for decays into top is crossed. In this intermediate mass range, the LC can measure the  $W$  and  $Z$  couplings more precisely than the LHC both through Higgs production rates and via branching ratios for decays into these bosons. Whether the observed Higgs boson fully generates the  $W$  and  $Z$  mass can then be checked.

We have noted in Section 2 that precision electroweak measurements in the framework of the Standard Model imply that  $m_{h_{\text{SM}}} \lesssim 193$  GeV at 95% CL [24]. Thus, any Higgs boson observed with a mass much greater than this would imply new physics. At this point, measurements from a Giga- $Z$  dataset would be particularly useful to probe this new sector.

#### 9.3.1. Cross Sections

Techniques described earlier [131, 138] for cross section measurements of both the Higgsstrahlung and  $W$ -fusion processes, with subsequent Higgs decays into  $b\bar{b}$ , can still be performed for the lower portion of the intermediate mass range below  $m_{h_{\text{SM}}} = 160$  GeV. Even in this intermediate mass range, it is beneficial to run at the peak of the cross section at roughly  $m_h + m_Z + 50$  GeV. Typical precisions of  $\Delta\sigma(Zh_{\text{SM}})/\sigma(Zh_{\text{SM}}) \simeq 5\%$  and  $\Delta\sigma(\nu\bar{\nu}h_{\text{SM}})/\sigma(\nu\bar{\nu}h_{\text{SM}}) \simeq 17\%$  for  $m_{h_{\text{SM}}} = 160$  GeV at  $\sqrt{s} = 350$  GeV with  $500 \text{ fb}^{-1}$  can be obtained.

For heavier Higgs bosons in this mass range, cross sections for both Higgsstrahlung and  $W$ -fusion will need to be extracted from these processes followed by  $h \rightarrow WW^*$  decays for example as described in [144]. Couplings determined from  $t\bar{t}h$  and  $Zhh$  production would clearly need higher center-of-mass energy.

### 9.3.2. Branching Ratios

Using Higgsstrahlung events at an optimal  $\sqrt{s}$ , the statistical error on  $\text{BR}(h_{\text{SM}} \rightarrow b\bar{b})$  is still only 6.5% at  $m_{h_{\text{SM}}} = 160$  GeV [145]. At  $\sqrt{s} = 500$  GeV, with leptonic decays of the  $Z$  only, the statistical error on this branching ratio reaches 25% at  $m_{h_{\text{SM}}} \simeq 165$  GeV with  $250 \text{ fb}^{-1}$  and remains below 30% for  $m_{h_{\text{SM}}} < 200$  GeV with  $2000 \text{ fb}^{-1}$  [135]. However, in addition to the leptonic decays of the  $Z$ , hadronic decays can also be used to effectively tag the associated  $Z$ . Extrapolating from full LCD detector simulations, it is conservatively estimated that including the hadronic decays of the  $Z$  results in an increase in signal statistics above background by a factor of four. With these assumptions and  $500 \text{ fb}^{-1}$ , again with the optimal  $\sqrt{s} \simeq 350$  GeV, the error on the  $b\bar{b}$  branching ratio can then be estimated to reach 25% at  $m_{h_{\text{SM}}} \simeq 200$  GeV. Measurement of branching ratios to  $c\bar{c}$ ,  $\tau^+\tau^-$ ,  $gg$ , and  $\gamma\gamma$  does not seem feasible in this mass range.

Branching ratios into vector bosons can be measured with good precision in this intermediate mass range. For  $m_{h_{\text{SM}}} = 160$  GeV and  $500 \text{ fb}^{-1}$ , a predicted excellent precision of 2.1% on  $\text{BR}(h_{\text{SM}} \rightarrow WW)$ , has been reported [144] and extrapolated estimated precisions of better than 7% over the mass range of 150 to 200 GeV [135].

To measure  $\text{BR}(h \rightarrow ZZ)$ , it will be necessary to distinguish hadronic  $Z$  decays from hadronic  $W$  decays, serving as an important benchmark for electromagnetic and hadronic calorimetry. With the same luminosity, and assuming that this separation allows one to identify one of the two  $Z$ 's in the Higgs decays (through leptons or  $b\bar{b}$ ) 40% of the time, the statistical uncertainty of this branching ratio would be approximately 8% for  $m_{h_{\text{SM}}} \simeq 210$  GeV [135] degrading to 17% for  $m_{h_{\text{SM}}} = 160$  GeV [129] where the branching ratio into  $Z$ 's is still small.

## 9.4. Coupling Determinations – Heavy Higgs Boson

If a SM-like Higgs boson is heavy (*i.e.*,  $m_h > 2m_t$ ), then new physics beyond the Standard Model must exist (*e.g.*, see Section 7.2; other examples of possible new physics effects are surveyed in [28, 163]). High-statistics measurements at the  $Z$  peak would again be useful to elucidate these effects.

### 9.4.1. Cross Sections

As a specific case, for  $m_h = 500$  GeV at  $\sqrt{s} = 800$  GeV, a SM-like Higgs boson would have a width of 70 GeV and dominant decay modes into  $W^+W^-$

(55%),  $ZZ$  (25%), and  $t\bar{t}$  (20%). The production cross section for  $Zh$  would be 6 fb, but production would be dominated by  $\nu\bar{\nu}h$  production at 10 fb. With  $1000 \text{ fb}^{-1}$ , one expects 400  $Zh$  events where the  $Z$  decays to  $e^+e^-$  or  $\mu^+\mu^-$ . With reasonable selection and acceptance cuts, a measurement of  $\sigma(Zh)$  to better than 7% should be feasible. See [163] for an independent assessment of the LC discovery reach for a heavy Higgs boson.

#### 9.4.2. Branching Ratios

The LHC will have great difficulty distinguishing  $h \rightarrow t\bar{t}$  decays due to huge QCD  $t\bar{t}$  backgrounds. On the other hand, this mode should be observable at the LC. In the SM, the important coupling  $g_{tth_{\text{SM}}}^2 \simeq 0.5$  can be compared to  $g_{bb_{\text{SM}}}^2 \simeq 4 \times 10^{-4}$ . If the Higgs boson is heavier than 350 GeV, it will be possible to obtain a good determination of the top-Higgs Yukawa coupling. Full simulations are needed for heavy Higgs decays into top, but with reasonable assumptions, one can expect a statistical error of  $\delta\text{BR}/\text{BR} \simeq 14\%$  with  $500 \text{ fb}^{-1}$  [135]. Simulations using the TESLA detector of the  $W^+W^- \rightarrow h_{\text{SM}} \rightarrow t\bar{t}$  process with  $1000 \text{ fb}^{-1}$  and 6-jet final states show impressive signal significance for  $\sqrt{s} = 1000 \text{ GeV}$  and reasonably good significance at  $\sqrt{s} = 800 \text{ GeV}$  [164]. These studies find that a relative error in the top quark Yukawa coupling measurement better than 10% can be achieved for Higgs masses in the 350–500 GeV and 350–650 GeV ranges at  $\sqrt{s} = 800 \text{ GeV}$  and  $1000 \text{ GeV}$ , respectively.

Again assuming detector performance allowing for separation of hadronic  $W$  and  $Z$  decays, and using production through  $W$ -fusion, similar techniques for extracting  $\text{BR}(h_{\text{SM}} \rightarrow t\bar{t})$  can be applied resulting in estimates on  $\text{BR}(h_{\text{SM}} \rightarrow W^+W^-)$  and  $\text{BR}(h_{\text{SM}} \rightarrow ZZ)$  as shown in Table 2.

### 9.5. Summary of Couplings

The relative measurement errors for a SM Higgs at various masses are summarized in Table 2. As much as possible, the entries in this compilation have been collected from LCD detector simulations, particularly for lighter masses. For uniformity, the entries have been scaled to  $500 \text{ fb}^{-1}$ , except where noted otherwise. The significant measurements of many branching ratios, couplings and the total width demonstrates the strength of the LC Higgs program.

Just as the computer program ZFITTER [165] is used with  $Z$  mass, widths, asymmetries and branching ratios to make global fits for  $Z$  couplings, a program HFITTER [128] is now available that performs a global

Table 2: Summary of measurement precisions for the properties of a SM-like Higgs boson,  $h$ , for a range of Higgs boson masses. Unless otherwise noted (see footnotes below the table),  $\sqrt{s} = 500$  GeV and the total integrated luminosity is taken to be  $500 \text{ fb}^{-1}$ .

$\Delta m_h$	$\simeq 120$ MeV (recoil against leptons from $Z$ ) $\simeq 50$ MeV (direct reconstruction)				
$m_h$ (GeV)	120	140	160	200	400–500
$\sqrt{s}$ (GeV)	500				800
$\Delta\sigma(Zh)/\sigma(Zh)$	4.7%	6.5%	6%	7%	10%
$\Delta\sigma(\nu\bar{\nu}h)\text{BR}(b\bar{b})/\sigma\text{BR}$	3.5%	6%	17%	–	–
$\delta g_{hxx}/g_{hxx}$ (from BR's)					
$t\bar{t}$	6–21% †	–	–	–	10%
$b\bar{b}$	1.5%	2%	3.5%	12.5%	–
$c\bar{c}$	20%	22.5%	–	–	–
$\tau^+\tau^-$	4%	5%	–	–	–
$\mu^+\mu^-$	15% ‡	–	–	–	–
$WW^{(*)}$	4.5%	2%	1.5%	3.5%	8.5%
$ZZ^{(*)}$	–	–	8.5%	4%	10%
$gg$	10%	12.5%	–	–	–
$\gamma\gamma$	7%	10%	–	–	–
$g_{hhh}$	20% §	–	–	–	–
$\Gamma_{\text{tot}}$ ††	10.1%	8.2%	12.9%	10.6%	22.3%

† The range of  $ht\bar{t}$  couplings is obtained from  $e^+e^- \rightarrow t\bar{t}h$ , with  $\sqrt{s} = 500$ – $800$  GeV and  $1000 \text{ fb}^{-1}$  of data.

‡ based on  $\sqrt{s} = 800$  GeV and  $1000 \text{ fb}^{-1}$  of data.

§ based on  $\sqrt{s} = 500$  GeV and  $1000 \text{ fb}^{-1}$  of data.

†† indirect determination from  $\Gamma(VV^*)/\text{BR}(VV^*)$ ,  $V = W, Z$ .

fit taking into account correlations between measurements of Higgs boson properties. Individual couplings of the Higgs boson can then be extracted optimally, for example through the correct combination of cross section and branching ratio measurements for such couplings as  $g_{hWW}$  and  $g_{hZZ}$ . Such precision fits can be used to probe indirectly for higher-mass states.

## 9.6. Total Width

For light Higgs bosons, the predicted SM width is far too small to be measured directly (and any anomalously wide state will indicate new

physics), but the combination of branching ratios and coupling measurements allows the indirect and *model-independent* measurement of the total width through  $\Gamma_{\text{tot}} = \Gamma(h \rightarrow X)/\text{BR}(h \rightarrow X)$ . For  $m_{h_{\text{SM}}} < 115$  GeV, the total width measurement would very likely require a  $\gamma\gamma$  collider, an  $e^+e^-$  LC, and input from the LHC [2]. However, limits from LEP indicating  $m_{h_{\text{SM}}} \gtrsim 115$  GeV would result in a non-negligible branching ratio to  $WW^*$  with the exciting and attractive prospect of an indirect model-independent measurement of the total width using LC measurements alone.

First, measurements of  $\sigma(h\nu\nu) \times \text{BR}(h \rightarrow b\bar{b})$  and  $\text{BR}(h \rightarrow b\bar{b})$  independently (through recoil in Higgsstrahlung) gives  $\Gamma(h \rightarrow WW^*)$ . Using a similar independent measurement of  $\text{BR}(h \rightarrow WW^*)$  then gives the total width through the relation  $\Gamma_{\text{tot}} = \Gamma(h \rightarrow WW^*)/\text{BR}(h \rightarrow WW^*)$ . Similarly, both  $\Gamma(h \rightarrow ZZ^*)$  and  $\text{BR}(h \rightarrow ZZ^*)$  can be determined from the Higgsstrahlung process and used to compute  $\Gamma_{\text{tot}} = \Gamma(h \rightarrow ZZ^*)/\text{BR}(h \rightarrow ZZ^*)$ . These two independent results for  $\Gamma_{\text{tot}}$  can then be combined. The results are summarized in Table 2. Even with as little as  $200 \text{ fb}^{-1}$ ,  $\Gamma_{\text{tot}}$  can be found to approximately 10% for  $m_{h_{\text{SM}}} = 120$  GeV, improving to  $\sim 7\%$  for  $m_{h_{\text{SM}}} \sim 150$  GeV. Even better precision can be attained with the introduction of some model assumptions in the value used for  $\Gamma(h_{\text{SM}} \rightarrow WW^*)$ , *i.e.*, assuming the SU(2) relation between  $W$  and  $Z$  couplings along with  $\sigma_{\text{meas}}(Zh_{\text{SM}})$ , or else by using its SM value directly as a consistency check.

For  $m_{h_{\text{SM}}} \gtrsim 205$  GeV,  $\Gamma_{\text{tot}}(h_{\text{SM}}) > 2$  GeV and the total width could be directly resolved with typical LCD detector resolutions. The variations of precision for indirect and direct measurements for different values of  $m_{h_{\text{SM}}}$  and inputs from different machines are examined in [2, 166]. The jet-jet mass resolution assumed in [2] has been verified by full simulations [132] in the LCD Large Detector resulting in estimated direct measurements of the total width reaching minimum values of  $\simeq 6\%$  in the mass range of 240–280 GeV with  $200 \text{ fb}^{-1}$ . A more complete analysis for  $m_{h_{\text{SM}}} = 240$  GeV, where the predicted SM Higgs width is 3.4 GeV, fits to a convolution of resolution and a Breit-Wigner as shown in fig. 27 to find  $\Delta\Gamma_{h_{\text{SM}}}/\Gamma_{h_{\text{SM}}} = 12\%$  [167]. The indirect determination described above can also still be pursued and a combination would allow even better precisions.

## 9.7. Quantum Numbers

The spin, parity, and charge conjugation quantum numbers  $J^{PC}$  of a Higgs boson candidate, generically denoted by  $\phi$ , can potentially be determined in a model-independent way. Useful ingredients include the following:

1. If  $\phi$  is produced in  $\gamma\gamma$  collisions, then it cannot have  $J = 1$  and it

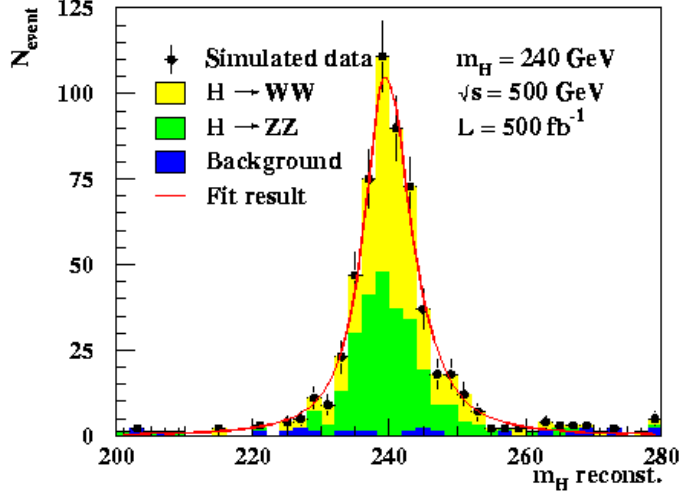


Fig. 27: Fit to the reconstructed  $h_{\text{SM}}$  mass to directly extract  $\Gamma_{h_{\text{SM}}}$  [167].

must have positive  $C$  [168].

2. The behavior of the  $Z\phi$  Higgsstrahlung cross section at threshold constrains the possible values of  $J^{\text{PC}}$  of the state. If the spin of the  $\phi$  is 2 or less, a cross section growing as  $\beta$  indicates a CP-even object, whereas a cross section growing as  $\beta^3$  signals a CP-odd state [169,170] with differences as shown in fig. 28(a).

3. The angular dependence of the  $e^+e^- \rightarrow Z\phi$  cross section depends upon whether the  $\phi$  is CP-even, CP-odd, or a mixture [170–173]. Following [173] we parameterize the  $ZZ\phi$  vertex as

$$\Gamma_{\mu\nu}(k_1, k_2) = a g_{\mu\nu} + b \frac{k_{1\mu} k_{2\nu} - g_{\mu\nu} k_1 \cdot k_2}{m_Z^2} + \tilde{b} \frac{\epsilon_{\mu\nu\alpha\beta} k_1^\alpha k_2^\beta}{m_Z^2}, \quad (35)$$

where  $k_1$  and  $k_2$  are the momenta of the two  $Z$ s. The first term arises from a Standard-Model-like  $ZZ\phi$  coupling, and the last two from effective interactions that could be induced by high-mass virtual particles. With this vertex the Higgsstrahlung cross section becomes

$$\begin{aligned} \frac{d\sigma}{d\cos\theta_Z} \propto & 1 + \frac{p_Z^2}{m_Z^2} \sin^2\theta_Z - 4 \text{Im} \left[ \frac{\tilde{b}}{\tilde{a}} \right] \frac{v_e a_e}{v_e^2 + a_e^2} \frac{p_z \sqrt{s}}{m_Z^2} \cos\theta_Z \\ & + \left| \frac{\tilde{b}}{\tilde{a}} \right|^2 \frac{p_z^2 s}{2m_Z^4} (1 + \cos^2\theta_Z), \end{aligned} \quad (36)$$

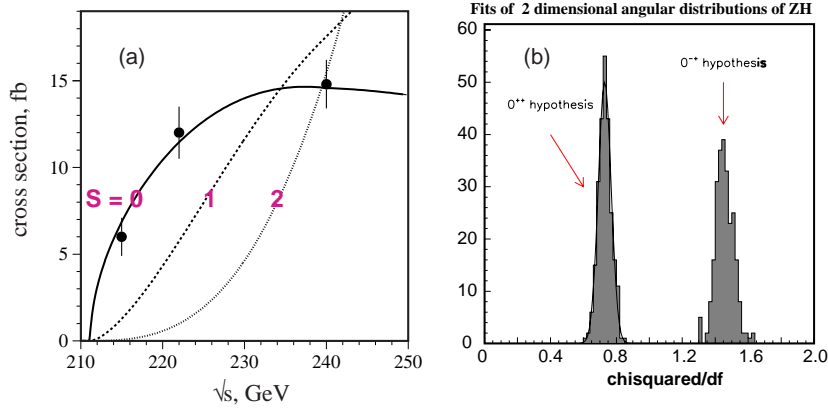


Fig. 28: (a) Behavior of Higgsstrahlung threshold for various spin states along with typical measurement precisions on the cross section. Taken from [169]. (b) Fit to the double-differential angular distribution in  $Z\phi$  events (see text) to distinguish CP-even and CP-odd states. Taken from [135].

where  $\theta_Z$ ,  $p_Z$ , and  $E_Z$  are the scattering angle, momentum, and energy of the final-state  $Z$  boson;  $v_e$  and  $a_e$  are the vector and axial-vector  $Ze^+e^-$  couplings; and  $\tilde{a} \equiv a - bE_Z\sqrt{s}/m_Z^2$ . The term in eq. (36) proportional to  $\cos\theta_Z$  arises from interference between the CP-even and CP-odd couplings in eq. (35). If the CP-odd coupling  $\tilde{b}$  is large enough, it can be extracted from the forward-backward asymmetry. Even upper limits on this asymmetry would be interesting. Note that the CP-even component of a Higgs boson will typically couple at tree level whereas the CP-odd component will only couple via one-loop diagrams (typically dominated by the  $t$  quark loop). As a result, one expects the coupling strength  $\tilde{b}$  to be proportional to  $m_Z^2/s$  times a loop suppression factor. Thus, an asymmetry measurement may be able to provide a crude determination of the  $\tilde{b}/a$  term. If  $\phi$  is a purely CP-odd state with a one-loop coupling, the resulting  $ZA^0$  cross section will simply be too small to provide a useful measurement of the asymmetry.

4. The angular distribution of the fermions in the  $Z \rightarrow f\bar{f}$  decays in  $Z\phi$  production also reflects the CP nature of the state  $\phi$  [171,172]. For the decay  $Z \rightarrow e^+e^-$  or  $\mu^+\mu^-$ , the following angles can be defined: the angle between the initial  $e^-$  and the  $Z$ ; the angle between the final state  $e^-$  or  $\mu^-$  and the direction of motion of the  $Z$ , in the rest frame of the  $Z$ ; and the angle between the  $Z$  production plane and  $Z$  decay plane. Correlations between these angles can be exploited, *e.g.*, a fit to the double-differential angular



distribution of the first two of these angles results in a  $14\sigma$  separation between the  $0^{++}$  (CP-even, scalar) and the  $0^{-+}$  (CP-odd, pseudoscalar) [135], assuming that the  $Z\phi$  cross section is independent of the CP nature of  $\phi$  [see fig. 28(b)]. Even more powerful are fits to the triple-differential angular distribution where sufficient luminosity can uncover non-standard  $ZZ\phi$  couplings. However, this technique again suffers from the difficulty described in the previous item; namely, the CP-odd part of the state  $\phi$  is typically so weakly coupled to  $ZZ$  that there is little sensitivity to the CP-odd component (if there is any significant CP-even component in  $\phi$ ) or little cross section (if  $\phi$  is almost purely CP-odd).

5. If  $\phi$  has significant branching ratios to either  $\tau^+\tau^-$  or  $t\bar{t}$ , channels which are ‘self-analyzing’, then the decay distribution structure can provide a direct determination of the ratio  $b_f/a_f$  in the  $y_f\bar{f}(a_f + ib_f\gamma_5)f\phi$  ( $f = \tau$  or  $t$ ) Yukawa coupling structure of  $\phi$  [174–176]. Detector simulation studies have been made of the specific decay  $\phi \rightarrow \tau^+\tau^- \rightarrow \rho^+\bar{\nu}_\tau\rho^-\nu_\tau$  where likelihood fits were made to angular correlations between decay products of each  $\tau$  [177] resulting in distinguishing the CP nature of the  $\phi$  to a confidence level greater than 95% with  $500\text{ fb}^{-1}$  at  $\sqrt{s} = 500\text{ GeV}$ .

6. The angular distributions in the  $t\bar{t}\phi$  final state, which has adequate cross section for  $\sqrt{s} \gtrsim 800\text{ GeV}$  for modest values of  $m_\phi \lesssim 200\text{ GeV}$ , assuming Yukawa coupling  $y_t\bar{t}(a_t + ib_t\gamma_5)t\phi$  comparable to SM values, appears to provide an excellent means for determining the CP nature of  $\phi$  by allowing one to probe the ratio  $b_t/a_t$  [102, 178]. An observable CP-violating asymmetry in  $t\bar{t}\phi$  production (via a T-odd triple correlation product proposed in [101]) would provide evidence for a CP-violating Higgs sector.

7. It is likely that the CP properties of the  $\phi$  can be well determined using photon polarization asymmetries in  $\gamma\gamma \rightarrow \phi$  collisions [176, 179, 180] (see Section 11).

8. If the  $\phi$  has substantial  $ZZ$  coupling, then  $e^-e^- \rightarrow ZZ e^-e^- \rightarrow \phi e^-e^-$  can be used to probe its CP nature [181] via the energy distributions of the  $\phi$  and the final electrons, which are much harder in the case of a CP-odd state than for a CP-even state. Certain correlations are also useful probes of the CP properties of the  $\phi$ . However, if the CP-odd portion of  $\phi$  couples at one-loop (as expected for a Higgs boson), there will be either little sensitivity to this component or little cross section.

### 9.8. Precision studies of non-SM-like Higgs bosons

We confine our remarks to the two-doublet Higgs model (either the MSSM Higgs sector or a more general 2HDM). In the MSSM, we noted

in Section 5.4 that for  $m_{A^0} \lesssim \sqrt{s}/2$ , as long as one is not too close to threshold, it is possible to observe all Higgs scalars of the non-minimal Higgs sector. In particular, in parameter regions away from the decoupling limit, none of the CP-even Higgs scalars may resemble the SM Higgs boson. Precision studies of all the Higgs bosons will provide a detailed profile of the non-minimal Higgs sector. Once  $m_{A^0} \gtrsim \sqrt{s}/2$ , only the  $h^0$  will be visible at the LC in an approximate decoupling regime (although there may be some possibilities for observing the heavier Higgs states produced singly either in association with a  $b\bar{b}$  pair at large  $\tan\beta$  where the coupling to  $b\bar{b}$  is enhanced, or by  $s$ -channel resonance production at a  $\gamma\gamma$  collider). In the more general 2HDM, the simplest mechanisms for producing the heavier neutral Higgs bosons are  $e^+e^- \rightarrow H^0 A^0$ ,  $e^+e^- \rightarrow H^0 b\bar{b}$ ,  $A^0 b\bar{b}$  and  $e^+e^- \rightarrow H^0 t\bar{t}$ ,  $A^0 t\bar{t}$ . Charged Higgs bosons can be produced via  $e^+e^- \rightarrow H^+ H^-$  and  $e^+e^- \rightarrow H^+ \bar{t}b + H^- t\bar{b}$ . We have seen that none of these processes are guaranteed to be either kinematically accessible or have a useful rate.

Values of  $m_{A^0}$  and  $m_{H^0}$  in excess of 500 GeV to 1 TeV are certainly possible. In such cases, a substantial increase of energy for the LC will be required to observe these states directly, either in association with  $b\bar{b}$  (at large  $\tan\beta$ ) or via  $H^0 A^0$  production. Measuring the former will provide a crucial determination of the  $b\bar{b}$  couplings, which in the given model context will provide a determination of  $\tan\beta$ , with accuracy determined by the production rates. Moreover, if  $H^0$  and  $A^0$  can be produced at a high rate (by whatever process), a detailed study of their branching ratios has the potential for providing vital information regarding the model parameters.

In low-energy supersymmetric models, the heavy  $H^0$ ,  $A^0$  and  $H^\pm$  would generally decay to various pairs of supersymmetric particles as well as to  $b$ 's and  $t$ 's. A study of the relative branching ratios and the rates for specific processes would provide powerful determinations of  $\tan\beta$  and many of the soft-supersymmetry-breaking parameters [182–186]. In addition, at large  $\tan\beta$  the absolute widths of  $H^0$ ,  $A^0$  ( $H^\pm$ ) become large enough to be directly measured in the  $b\bar{b}$  ( $t\bar{t}$ ) final state and provide an excellent determination of  $\tan\beta$  [186].<sup>12</sup> The accuracy in the  $\tan\beta$  measurement that can be achieved after combining all these  $\tan\beta$  determinations in quadrature are illustrated in fig. 29 assuming  $\sqrt{s} = 500$  GeV,  $L = 2000$  fb<sup>-1</sup>, and  $m_{A^0} = 200$  GeV. Excellent precision is achieved at low and high  $\tan\beta$

---

<sup>12</sup>More precisely, what is being measured via the above techniques is the relevant Yukawa coupling, which is determined by  $\tan\beta$  at tree level. At one-loop, radiative corrections must be included in order to convert from the Yukawa coupling to a uniform definition of  $\tan\beta$  [187].

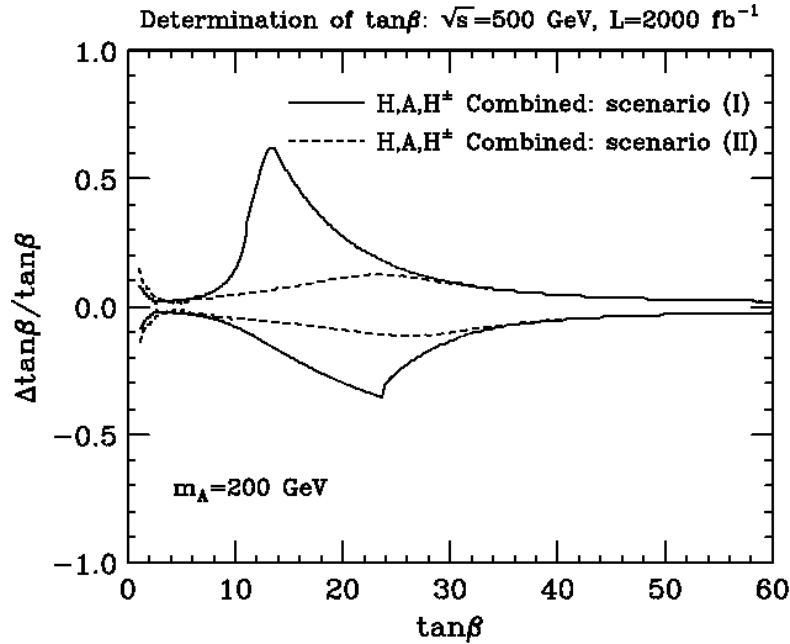


Fig. 29: The accuracy with which  $\tan\beta$  can be measured, assuming  $m_{A^0} = 200$  GeV,  $\sqrt{s} = 500$  GeV and integrated luminosity of  $L = 2000$  fb $^{-1}$ , after combining in quadrature the errors on  $\tan\beta$  from: a) the rate for  $b\bar{b}A^0, b\bar{b}H^0 \rightarrow b\bar{b}b\bar{b}$ ; b) the  $H^0A^0 \rightarrow b\bar{b}b\bar{b}$  rate; c) a measurement of the average  $H^0, A^0$  total width in  $H^0A^0$  production; d) the  $H^+H^- \rightarrow t\bar{t}b\bar{b}$  rate; and e) the total  $H^\pm$  width measured in  $H^+H^- \rightarrow t\bar{t}b\bar{b}$  production. Results are shown for two supersymmetric scenarios: in (I), the  $H^0$  and  $A^0$  do not decay to supersymmetric particles; in (II), there are substantial decays of the  $H^0$  and  $A^0$  to a pair of the lightest supersymmetric particles ( $\tilde{\chi}_1^0\tilde{\chi}_1^0$ ). Taken from [186].

regardless of the specific supersymmetric scenario. However, in the range  $10 < \tan\beta < 30$ , good accuracy in the  $\tan\beta$  measurement is only achieved if there are some supersymmetric decays of  $H^0$  and  $A^0$  against which the corresponding  $b\bar{b}$  decay modes have to compete.

## 10. The Giga-Z option—implications for Higgs physics

Measurements of the effective leptonic mixing angle and the  $W$  boson mass to precisions of  $\delta \sin^2 \theta_{\text{eff}} \simeq 10^{-5}$  and  $\delta m_W \approx 6$  MeV at Giga-Z can be exploited in many ways. The size of the resulting 90% CL ellipses

were shown in fig. 15. These measurements imply that the SM Higgs boson mass can be determined indirectly to a precision of about 7%. A deviation between the directly observed value and the value implied by a global SM fit to Giga- $Z$  data would require new physics beyond the SM.

If new physics is present then it will be possible to obtain information about new high mass scales beyond the direct reach of the collider. For example, in the MSSM such information would be of particular importance if the heavier scalar top quark,  $\tilde{t}_2$ , and the heavy Higgs bosons  $A^0$ ,  $H^0$  and  $H^\pm$  were beyond the kinematical reach of the LC and background problems precluded their observation at the LHC. Similar considerations apply to more general extended Higgs sector models.

### 10.1. Giga- $Z$ and the MSSM

In the MSSM, the relation between  $m_W$  and  $\sin^2 \theta_{\text{eff}}$  is affected by the parameters of the supersymmetric sector, especially the  $\tilde{t}$  sector. At the LC, the mass of the light  $\tilde{t}$ ,  $m_{\tilde{t}_1}$ , and the  $\tilde{t}$  mixing angle,  $\theta_{\tilde{t}}$ , should be measurable very well if the process  $e^+ e^- \rightarrow \tilde{t}_1 \bar{\tilde{t}}_1$  is accessible [188].

In fig. 30 [21], it is demonstrated how *upper* bounds on  $m_{A^0}$  and  $m_{\tilde{t}_2}$  can be derived from measurements of  $m_{h^0}$ ,  $m_W$  and  $\sin^2 \theta_{\text{eff}}$ , supplemented by precise determinations of  $m_{\tilde{t}_1}$  and  $\theta_{\tilde{t}}$ . The most restrictive upper bounds are obtained if  $\tan \beta > 10$  (in this case, one assumes that the value of  $\tan \beta$  would have already been determined from measurements in the gaugino sector [189]). The other parameters values are assumed to have the uncertainties as expected from LHC [190] and the LC [129].

For low  $\tan \beta$  (where the prediction for  $m_{h^0}$  depends sensitively on  $\tan \beta$ ) the heavier  $\tilde{t}$  mass,  $m_{\tilde{t}_2}$ , can be restricted to  $760 \text{ GeV} \lesssim m_{\tilde{t}_2} \lesssim 930 \text{ GeV}$  from the  $m_{h^0}$ ,  $m_W$  and  $\sin^2 \theta_{\text{eff}}$  precision measurements. The mass  $m_{A^0}$  varies between 200 GeV and 1600 GeV. If  $\tan \beta \geq 10$  (where  $m_{h^0}$  has only a mild dependence on  $\tan \beta$ ), the allowed region for the  $\tilde{t}_2$  is much smaller,  $660 \text{ GeV} \lesssim m_{\tilde{t}_2} \lesssim 680 \text{ GeV}$ , and  $m_{A^0}$  is restricted to  $m_{A^0} \lesssim 800 \text{ GeV}$ .

In deriving the bounds on the heavier  $\tilde{t}$  mass,  $m_{\tilde{t}_2}$ , the constraints from  $m_{h^0}$ ,  $\sin^2 \theta_{\text{eff}}$  and  $m_W$  play an important role. For the bounds on  $m_{A^0}$ , the main effect comes from  $\sin^2 \theta_{\text{eff}}$ . The assumed value of  $\sin^2 \theta_{\text{eff}} = 0.23140$  differs slightly from the corresponding value obtained in the SM limit. For this value the (logarithmic) dependence on  $m_{A^0}$  is still large enough [21] so that from the high precision in  $\sin^2 \theta_{\text{eff}}$  at Giga- $Z$  an *upper limit* on  $m_{A^0}$  can be set. With an error in  $\sin^2 \theta_{\text{eff}}$  that would be at least ten times larger at the LC without the Giga- $Z$  mode, no bound on  $m_{A^0}$  could be inferred.

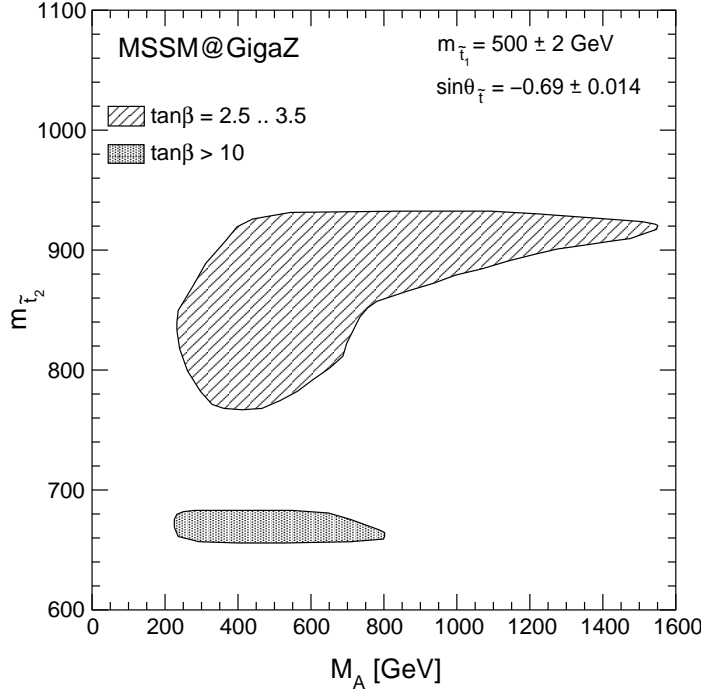


Fig. 30: The region in the  $[m_{A^0}, m_{\tilde{t}_2}]$  parameter space, allowed by  $1\sigma$  errors obtained from the Giga- $Z$  measurements of  $m_W$  and  $\sin^2\theta_{\text{eff}}$ :  $m_W = 80.400 \pm 0.006$  GeV,  $\sin^2\theta_{\text{eff}} = 0.23140 \pm 0.00001$ , and from the LC measurement of  $m_{h^0}$ :  $m_{h^0} = 115 \pm 0.05$  (exp.)  $\pm 0.5$  (theo.) GeV.  $\tan\beta$  is assumed to be  $\tan\beta = 3 \pm 0.5$  or  $\tan\beta > 10$ . The other parameters are given by  $m_{\tilde{t}_1} = 500 \pm 2$  GeV,  $\sin\theta_{\tilde{t}} = -0.69 \pm 0.014$ ,  $A_b = A_t \pm 10\%$ ,  $m_{\tilde{g}} = 500 \pm 10$  GeV,  $\mu = -200 \pm 1$  GeV and  $M_2 = 400 \pm 2$  GeV. Taken from [21].

## 10.2. Giga- $Z$ and non-exotic extended Higgs sectors

Building on the discussion of the general 2HDM given earlier, one can imagine many situations for which the very small Giga- $Z$  90% CL ellipses illustrated in fig. 15 would provide crucial (perhaps the only) constraints. For example, suppose the LHC observes a 1 TeV Higgs boson with very SM-like properties and no other new physics below the few-TeV scale. We have seen that this is possible in the 2HDM scenarios consistent with current precision electroweak constraints. Suppose further that it is not immediately possible to increase  $\sqrt{s}$  sufficiently so that  $h^0 A^0$  production is

allowed (typically requiring  $\sqrt{s} > 1.5$  TeV in these models). Giga- $Z$  measurements would provide strong guidance as to the probable masses of the non-SM-like Higgs bosons of any given non-minimal Higgs sector. However, it must be accepted that a particular Giga- $Z$  result for  $S, T$  might have other non-Higgs interpretations as well.

## 11. The $\gamma\gamma$ collider option

Higgs production in  $\gamma\gamma$  collisions offers a unique capability to measure the two-photon width of the Higgs and to determine its CP composition through control of the photon polarization.

The  $\gamma\gamma$  coupling of a SM-like Higgs boson  $h_{\text{SM}}$  of relatively light mass receives contributions from loops containing any particle whose mass arises in whole or part from the vacuum expectation value of the corresponding neutral Higgs field. A measurement of  $\Gamma(h_{\text{SM}} \rightarrow \gamma\gamma)$  provides the possibility of revealing the presence of arbitrarily heavy particles that acquire mass via the Higgs mechanism.<sup>13</sup> However, because such masses are basically proportional to some coupling times  $v$ , if the coupling is perturbative the masses of these heavy particles are unlikely to be much larger than 0.5–1 TeV. Since  $\text{BR}(h_{\text{SM}} \rightarrow X)$  is entirely determined by the spectrum of light particles, and is thus not affected by heavy states,  $N(\gamma\gamma \rightarrow h_{\text{SM}} \rightarrow X) \propto \Gamma(h_{\text{SM}} \rightarrow \gamma\gamma)\text{BR}(h_{\text{SM}} \rightarrow X)$  will provide an extraordinary probe for such heavy states. Even if there are no new particles that acquire mass via the Higgs mechanism, a precision measurement of  $N(\gamma\gamma \rightarrow \hat{h} \rightarrow X)$  for specific final states  $X$  ( $X = b\bar{b}, WW^*, \dots$ ) can allow one to distinguish between a  $\hat{h}$  that is part of a larger Higgs sector and the SM  $h_{\text{SM}}$ .<sup>14</sup> The deviations from the SM predictions typically exceed 5% if the other heavier Higgs bosons have masses below about 400 GeV.

The predicted rate for Higgs boson production followed by decay to final state  $X$  can be found in [14]. This rate depends strongly on  $d\mathcal{L}_{\gamma\gamma}/dy$ , the differential  $\gamma\gamma$  collider luminosity, where  $y = m_{\hat{h}}/\sqrt{s}$  and  $\sqrt{s}$  is the  $ee$  collider center-of-mass energy. An important parameter to maximize peak luminosity is  $\langle\lambda\lambda'\rangle$ , the average value of the product of the helicities of the two colliding photons after integration over their momentum fractions  $z$  and  $z'$ . Larger values of this parameter also suppress the dominant

<sup>13</sup>Loop contributions from particles that acquire a large mass  $M$  from some other mechanism will decouple as  $M^{-2}$  and  $\Gamma(h_{\text{SM}} \rightarrow \gamma\gamma)$  will not be sensitive to their presence.

<sup>14</sup>It may also be possible to detect some rare Higgs decay modes at the  $\gamma\gamma$  collider. For example, [19] argues that the detection of  $\gamma\gamma \rightarrow h_{\text{SM}} \rightarrow \gamma\gamma$  will be possible.

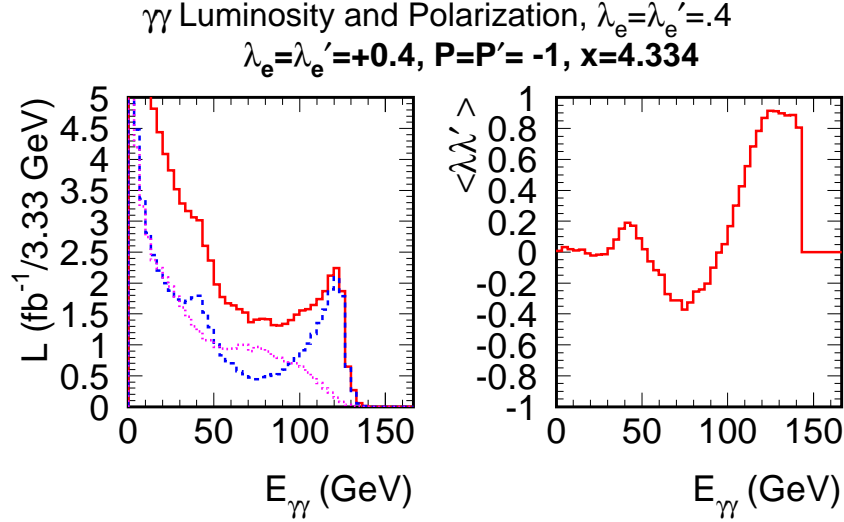


Fig. 31: The CAIN [191] predictions for the  $\gamma\gamma$  luminosity,  $L = d\mathcal{L}/dE_{\gamma\gamma}$ , are plotted in units of  $\text{fb}^{-1}$  per 3.33 GeV bin size, for circularly polarized photons assuming the NLC-based design for the  $\gamma\gamma$  collider [10, 17], with  $\sqrt{s} = 160$  GeV, 80% electron beam polarization, and a 1.054/3 micron laser wavelength. The directions of the photon polarizations and electron helicities have been chosen to produce a peaked  $E_{\gamma\gamma}$  spectrum. Beamstrahlung and other effects are included. The dashed (dotted) curve gives the component of the total luminosity that derives from the  $J_z = 0$  ( $J_z = 2$ ) two-photon configuration. Also plotted is the corresponding value of  $\langle \lambda\lambda' \rangle$  [given by  $\langle \lambda\lambda' \rangle = (L_{J_z=0} - L_{J_z=2}) / (L_{J_z=0} + L_{J_z=2})$ ]. Taken from [17].

$J_z = \pm 2$ ,  $\gamma\gamma \rightarrow b\bar{b}(g)$  background, which is proportional to  $(1 - \langle \lambda\lambda' \rangle)$ . The computation of  $d\mathcal{L}_{\gamma\gamma}/dy$  was first considered in [11, 12]. More realistic determinations [191] including beamstrahlung, secondary collisions between scattered electrons and photons from the laser beam, and other non-linear effects result in a substantial enhancement of the luminosity in the low- $E_{\gamma\gamma}$  region as shown in fig. 31.

The choice of parameters that gives a peaked spectrum is well suited for light Higgs studies. Using the spectrum of fig. 31 as an example, the di-jet invariant mass distributions for the Higgs signal and for the  $b\bar{b}(g)$  background for  $m_{h_{\text{SM}}} = 120$  GeV are shown in fig. 32 [17]. After a nominal year of operation ( $10^7$  sec),  $\Gamma(h_{\text{SM}} \rightarrow \gamma\gamma)\text{BR}(h_{\text{SM}} \rightarrow b\bar{b})$  could be measured

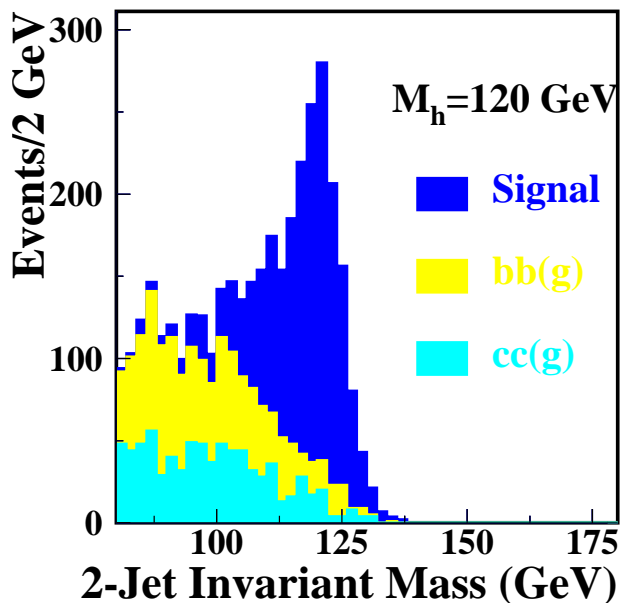


Fig. 32: Higgs signal and heavy quark backgrounds for  $\gamma\gamma \rightarrow h$  in units of events per 2 GeV for a Higgs mass of 120 GeV after one year of running, with the  $\gamma\gamma$  luminosity spectrum of fig. 31. Results are from [17].

with an accuracy of about 2.9%. (The more optimistic error of close to 2%, quoted in [15,192] for  $m_{h_{\text{SM}}} = 120$  GeV, is based upon a significantly higher peak luminosity.) The error for this measurement increases to about 10% for  $m_{h_{\text{SM}}} = 160$  GeV, primarily due to the decrease of the Higgs di-jet branching fraction by a factor of 18.

In many scenarios, it is possible that by combining this result with other types of precision measurements for the SM-like Higgs boson, small deviations can be observed indicating the possible presence of heavier Higgs bosons. For a 2HDM (either the MSSM or a two-Higgs-doublet model with partial decoupling), if  $m_{H^0} \sim m_{A^0} > \sqrt{s}/2$  then  $e^+e^- \rightarrow H^0 A^0$  is not possible. Further, as discussed earlier in association with fig. 16, the alternatives of  $b\bar{b}H^0$  and  $b\bar{b}A^0$  production will only allow  $H^0$  and  $A^0$  detection if  $\tan\beta$  is large [105]. Thus,  $\gamma\gamma \rightarrow H^0, A^0$  may be the only option allowing their



discovery (without a collider with higher  $\sqrt{s}$ ). The back-scattering kinematics are such that a LC for which the maximum energy is  $\sqrt{s} = 630$  GeV can potentially probe Higgs masses as high as 500 GeV in  $\gamma\gamma$  collisions. If  $m_{H^0}$  and  $m_{A^0}$  are known to within roughly 50 GeV on the basis of precision  $h^0$  data, then they will be easily detected by choosing the machine  $\sqrt{s}$  and polarization/helicity configurations that yield a  $E_{\gamma\gamma}$  spectrum peaked near the upper edge of the expected mass range [17, 83]. But, if it happens that no constraints have been placed on the  $H^0, A^0$  masses, then it is most appropriate to run entirely at the maximal  $\sqrt{s}$  and to consider how best to cover the portion of the LHC wedge<sup>15</sup> with  $m_{H^0} \sim m_{A^0} \gtrsim \sqrt{s}/2$  (for which  $H^0 A^0$  pair production is not possible). Assuming a maximum of  $\sqrt{s} = 630$  GeV, the goal would then be to roughly uniformly cover the  $300 \text{ GeV} \lesssim m_{A^0}, m_{H^0} \lesssim 500 \text{ GeV}$  region of the LHC wedge. For this purpose, it is best to run part of the time with polarization/helicity directions that yield a peaked (type-II) spectrum (with peak at  $E_{\gamma\gamma} \sim 500$  GeV for  $\sqrt{s} = 630$  GeV) and roughly three times as long in a polarization/helicity configuration that yields a broad (type-I)  $E_{\gamma\gamma}$  spectrum with good luminosity and substantial  $\langle\lambda\lambda'\rangle$  in the  $350 \lesssim E_{\gamma\gamma} \lesssim 450$  GeV region.

For the NLC-based design of the  $\gamma\gamma$  collider as specified in [10, 17], after roughly four years of total running time (one year with the peaked spectrum and three years with the broad spectrum, assuming that the machine operates  $10^7$  sec per year) one can achieve  $> 4\sigma$  signals (99% exclusion) in  $\gamma\gamma \rightarrow H^0, A^0 \rightarrow b\bar{b}$  for most (all) of the  $[m_{A^0}, \tan\beta]$  LHC wedge region. With twice the luminosity of the nominal NLC design (as might be achieved at TESLA or by using round beams at the NLC), essentially all of the wedge region is covered at the  $5\sigma$  level except for the lowest  $\tan\beta$  values in the  $m_{A^0} > 2m_t$  part of the wedge (where it is anticipated that  $\gamma\gamma \rightarrow H^0, A^0 \rightarrow t\bar{t}$  will yield a viable signal). This is summarized in fig. 33. In fact, for  $H^0, A^0$  discovery, the  $\gamma\gamma$  collider is almost perfectly complementary to the LHC (and also the LC operation in the  $e^+e^-$  collision mode).

The corresponding results for  $\gamma\gamma \rightarrow \hat{h} \rightarrow b\bar{b}$  for the wedge region of a 2HDM model with a light decoupled  $\hat{h}$ , and all other Higgs bosons heavier than  $\sqrt{s}$ , were given earlier in fig. 16. Again, the  $\gamma\gamma$  collider would allow  $\hat{h}$  discovery in a substantial portion of the wedge region in which its discovery would not otherwise be possible.

Once one or more Higgs bosons have been detected, precision studies can

<sup>15</sup>The LHC wedge, discussed in Section 6.3, corresponds to the moderate  $\tan\beta$  large  $m_{A^0}$  wedge-like region in the  $[m_{A^0}, \tan\beta]$  parameter space (see fig. 14) where only the  $h^0$  of the MSSM Higgs sector can be observed.

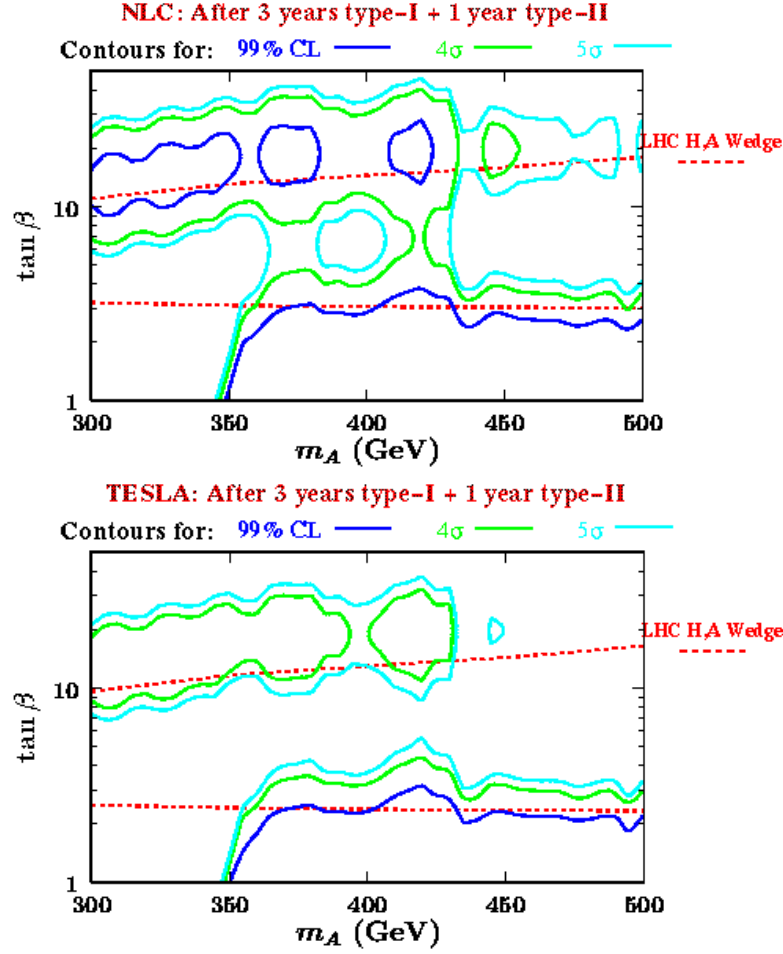


Fig. 33: Assuming a machine energy of  $\sqrt{s} = 630$  GeV and employing only  $\gamma\gamma \rightarrow H^0, A^0 \rightarrow b\bar{b}$ , we show the  $[m_{A^0}, \tan\beta]$  regions for which three years of operation using the type-I  $P\lambda_e, P'\lambda'_e > 0$  polarization configuration and one year of operation using the type-II  $P\lambda_e, P'\lambda'_e < 0$  configuration will yield  $S/\sqrt{B} \geq 5$ ,  $S/\sqrt{B} \geq 4$  or exclude the  $H^0, A^0$  at 99% CL. The dashed curves indicate the wedge region from the LHC plot of fig. 14—the lower curve gives a rough approximation to the LEP (maximal-mixing) limits while the upper curve is that above which  $H^0, A^0 \rightarrow \tau^+\tau^-$  can be directly detected at the LHC. The upper plot is for the NLC-based  $\gamma\gamma$  collider design and the lower plot is that achieved with a factor of 2 increase in luminosity, as might be achieved at TESLA or by using round  $e^-e^-$  beams instead of flat beams at the NLC. Results are from [17] as summarized in [19].

be performed including: determination of CP properties; a detailed scan to separate the  $H^0$  and  $A^0$  in the decoupling limit of a 2HDM; and branching ratios measurements. The branching ratios to supersymmetric final states are especially important for determining the basic supersymmetry breaking parameters [83, 183, 184, 193].

The CP properties can be determined for any spin-0 Higgs  $\hat{h}$  produced in  $\gamma\gamma$  collisions. Since  $\gamma\gamma \rightarrow \hat{h}$  is of one-loop order, whether  $\hat{h}$  is CP-even, CP-odd or a mixture, the CP-even and CP-odd parts of  $\hat{h}$  have  $\gamma\gamma$  couplings of similar size. However, the structure of the couplings is very different:

$$\mathcal{A}_{\text{CP-even}} \propto \vec{\epsilon}_1 \cdot \vec{\epsilon}_2, \quad \mathcal{A}_{\text{CP-odd}} \propto (\vec{\epsilon}_1 \times \vec{\epsilon}_2) \cdot \hat{p}_{\text{beam}}. \quad (37)$$

By adjusting the orientation of the initial laser photon polarization vectors with respect to one another, it is possible to determine the relative CP-even and CP-odd content of the resonance  $\hat{h}$  [179]. If  $\hat{h}$  is a mixture, one can use helicity asymmetries for this purpose [176, 179]. However, if  $\hat{h}$  is either purely CP-even or purely CP-odd, then one must employ transverse linear polarizations [176, 180]. Substantial luminosity with transverse polarization can be obtained, although the spectrum is not peaked (see [17]).

One measure of the CP nature of a Higgs boson is the asymmetry for parallel *vs.* perpendicular orientation of the linear polarizations of the initial laser beams,

$$\mathcal{A} \equiv \frac{N_{\parallel} - N_{\perp}}{N_{\parallel} + N_{\perp}}, \quad (38)$$

which is positive (negative) for a CP-even (odd) state. Since 100% linear polarization for the laser beams translates into only partial linear polarization for the colliding photons, both  $N_{\parallel}$  and  $N_{\perp}$  will be non-zero for the signal. In addition, the heavy quark background contributes to both. The expected value of  $\mathcal{A}$  must be carefully computed for a given model. For the SM Higgs boson with  $m_{h_{\text{SM}}} = 120$  GeV, it is found [17] that  $\mathcal{A}$  can be measured with an accuracy of about 20% in one year of operation using linear polarizations for the two lasers. This measurement would thus provide a moderately strong test of the even-CP nature of  $h_{\text{SM}}$ . Of course, the linear polarization configuration is not ideal for the most accurate determination of  $\Gamma(h_{\text{SM}} \rightarrow \gamma\gamma)\text{BR}(h_{\text{SM}} \rightarrow b\bar{b})$ , but would allow measuring this product with an accuracy of about 8%.

We end by noting that the  $e^{-}\gamma$  and  $e^{-}e^{-}$  collider options are most relevant to exotic Higgs scenarios, as discussed in Section 8.

## 12. Concluding Remarks

The physical origin of electroweak symmetry breaking is not yet known. In all theoretical approaches and models, the dynamics of electroweak symmetry breaking must be revealed at the TeV-scale or below. This energy scale will be thoroughly explored by hadron colliders, starting with the Tevatron and followed later in this decade by the LHC. Even though the various theoretical alternatives can only be confirmed or ruled out by future collider experiments, a straightforward interpretation of the electroweak precision data suggests that electroweak symmetry breaking dynamics is weakly-coupled, and a Higgs boson with mass between 100 and 200 GeV must exist. With the supersymmetric extension of the Standard Model, this interpretation opens the route to grand unification of all the fundamental forces, with the eventual incorporation of gravity in particle physics.

The discovery of the Higgs boson at the Tevatron and/or the LHC is a crucial first step. The measurement of Higgs properties at the LHC will begin to test the dynamics of electroweak symmetry breaking. However, a high-luminosity  $e^+e^-$  linear collider, now under development, is needed for a systematic program of precision Higgs measurements. For example, depending on the value of the Higgs mass, branching ratios and Higgs couplings can be determined in some cases at the level of a few percent. In this way, one can extract the properties of the Higgs sector in a comprehensive way, and establish (or refute) the theory of scalar sector dynamics as the mechanism responsible for generating the fundamental particle masses.

## Acknowledgments

We are very grateful to Andreas Kronfeld who served with us as a co-convenor of the Higgs Working Group of the American Linear Collider Working Group. This chapter is an update of our contribution to the American Linear Collider Working Group Resource Book for Snowmass 2001. We have benefited greatly from Andreas' contributions and counsel. We would also like to thank David Asner, Marcela Carena, Sven Heinemeyer, Heather Logan, Steve Mrenna, Michael Peskin, Carlos Wagner, Georg Weiglein, Dieter Zeppenfeld and Peter Zerwas for fruitful conversations and collaborative efforts that contributed to this work.

J.F.G., H.E.H. and R.V.K. are supported in part by the U.S. Department of Energy under the respective grants DE-FG03-91ER40674, DE-FG03-92ER40689 (Task B) and DE-FG02-91ER40661 (Task A).

## References

1. J.F. Gunion, H.E. Haber, G. Kane and S. Dawson, *The Higgs Hunter's Guide* (Perseus Publishing, Reading, MA, 1990).
2. J.F. Gunion, L. Poggioli, R. Van Kooten, C. Kao, P. Rowson *et al.*, "Higgs boson discovery and properties," in *New Directions for High Energy Physics*, Proceedings of the 1996 DPF/DPB Summer Study on High Energy Physics, Snowmass '96, edited by D.G. Cassel, L.T. Gennari and R.H. Siemann (Stanford Linear Accelerator Center, Stanford, CA, 1997) pp. 541–587 [hep-ph/9703330].
3. H.E. Haber, T. Han, F.S. Merritt, J. Womersley *et al.*, "Weakly coupled Higgs bosons and precision electroweak physics," in *New Directions for High Energy Physics*, Proceedings of the 1996 DPF/DPB Summer Study on High Energy Physics, Snowmass '96, edited by D.G. Cassel, L.T. Gennari and R.H. Siemann (Stanford Linear Accelerator Center, Stanford, CA, 1997) pp. 482–498 [hep-ph/9703391].
4. H. Murayama and M.E. Peskin, *Ann. Rev. Nucl. Part. Sci.* **46**, 533 (1996) [hep-ex/9606003].
5. E. Accomando *et al.* [ECFA/DESY LC Physics Working Group], *Phys. Rep.* **299**, 1 (1998) [hep-ph/9705442].
6. M. Carena and H.E. Haber, FERMILAB-Pub-02/114-T and SCIPP 02/07 [hep-ph/0208209], to appear in *Progress in Particle and Nuclear Physics*, edited by A. Faessler.
7. C. Adolphsen *et al.* [International Study Group Collaboration], "International study group progress report on linear collider development," SLAC-R-559 and KEK-REPORT-2000-7 (April, 2000).
8. N. Akasaka *et al.*, "JLC design study," KEK-REPORT-97-1.
9. R. Brinkmann, K. Flottmann, J. Rossbach, P. Schmuser, N. Walker and H. Weise [editors], "TESLA: The superconducting electron positron linear collider with an integrated X-ray laser laboratory. Technical design report, Part 2: The Accelerator," DESY-01-011 (March, 2001), <http://tesla.desy.de/tdr/>.
10. T. Abe *et al.* [American Linear Collider Working Group Collaboration], SLAC-R-570 (2001) [hep-ex/0106055–58].
11. I.F. Ginzburg, G.L. Kotkin, V.G. Serbo and V.I. Telnov, *Nucl. Instrum. Meth.* **A205**, 47 (1983).
12. I.F. Ginzburg, G.L. Kotkin, S.L. Panfil, V.G. Serbo and V.I. Telnov, *Nucl. Instrum. Meth.* **A219**, 5 (1984).
13. D.L. Borden, D.A. Bauer and D.O. Caldwell, *Phys. Rev.* **D48**, 4018 (1993).
14. J.F. Gunion and H.E. Haber, *Phys. Rev.* **D48**, 5109 (1993).
15. S. Söldner-Rembold and G. Jikia, *Nucl. Instrum. Meth.* **A472**, 133 (2001) [hep-ex/0101056];
16. E. Boos *et al.*, *Nucl. Instrum. Meth. A* **472**, 100 (2001) [hep-ph/0103090]; M. Melles, *Nucl. Instrum. Meth. A* **472**, 128 (2001) [hep-ph/0008125].
17. D. Asner, J. Gronberg and J.F. Gunion, hep-ph/0110320, *Phys. Rev.* **D67** (2003) in press.

18. M.M. Velasco *et al.*, “Photon-Photon and Electron-Photon Colliders with Energies Below a TeV,” in *Proceedings of the APS/DPF/DPB Summer Study on the Future of Particle Physics* (Snowmass 2001), edited by R. Davidson and C. Quigg, E3005 [hep-ph/0111055].
19. D. Asner, B. Grzadkowski, J.F. Gunion, H.E. Logan, V. Martin, M. Schmitt and M.M. Velasco, hep-ph/0208219.
20. U. Baur *et al.*, Report of the P1-WG1 subgroup, “Present and Future Electroweak Precision Measurements and the Indirect Determination of the Mass of the Higgs Boson,” in *Proceedings of the APS/DPF/DPB Summer Study on the Future of Particle Physics* (Snowmass 2001), edited by R. Davidson and C. Quigg, P1WG1 [hep-ph/0202001].
21. J. Erler, S. Heinemeyer, W. Hollik, G. Weiglein and P.M. Zerwas, *Phys. Lett.* **B486**, 125 (2000) [hep-ph/0005024]; J. Erler and S. Heinemeyer, in *Proceedings of the 5th International Symposium on Radiative Corrections* (RADCOR 2000), 11–15 September 2000, edited by H.E. Haber, SLAC-R-579, eConf C000911 [hep-ph/0102083].
22. H.E. Haber and Y. Nir, *Phys. Lett.* **B306**, 327 (1993) [hep-ph/9302228]; H.E. Haber, in *Physics From the Planck Scale to the Electroweak Scale*, Proceedings of the US–Polish Workshop, Warsaw, Poland, September 21–24, 1994, edited by P. Nath, T. Taylor, and S. Pokorski (World Scientific, Singapore, 1995) pp. 49–63 [hep-ph/9501320].
23. For a recent review, see R.N. Mohapatra, in *Supersymmetry, Supersymmetry and Supercolliders*, edited by J. Bagger (World Scientific, Singapore, 1998) [hep-ph/9911272].
24. D. Abbaneo *et al.* [LEP Electroweak Working Group] and N. de Groot *et al.* [SLD Heavy Flavor Group], CERN-EP-2002-091 [hep-ex/0212036]; and additional updates at <http://lepewwg.web.cern.ch/LEPEWWG/>.
25. ALEPH, DELPHI, L3 and OPAL Collaborations, The LEP working group for Higgs boson searches], LHWG Note 2002-01 (July 2002), contributed paper for ICHEP’02 (Amsterdam, July 2002), and additional updates at <http://lephiggs.web.cern.ch/LEPHIGGS/www/welcome.html>; P.A. McNamara and S.L. Wu, *Rept. Prog. Phys.* **65** (2002) 465.
26. E. Farhi and L. Susskind, *Phys. Rep.* **74**, 277 (1981); R.K. Kaul, *Rev. Mod. Phys.* **55**, 449 (1983). For a recent review, see C.T. Hill and E.H. Simmons, FERMI-PUB-02/045-T [hep-ph/0203079].
27. M.E. Peskin and T. Takeuchi, *Phys. Rev. Lett.* **65**, 964 (1990); *Phys. Rev.* **D46**, 381 (1992).
28. M.E. Peskin and J.D. Wells, *Phys. Rev.* **D64**, 093003 (2001) [hep-ph/0101342].
29. See, *e.g.*, A.G. Cohen, in *The Building Blocks of Creation—From Microfermis to Megaparsecs*, Proceedings of the Theoretical Advanced Study Institute (TASI 93) in Elementary Particle Physics, Boulder, CO, 6 June—2 July 1993, edited by S. Raby and T. Walker (World Scientific, Singapore, 1994); C.P. Burgess, in *Proceedings of the 4th International Symposium on Radiative Corrections (RADCOR 98): Applications of Quantum Field Theory to Phenomenology*, Barcelona, Catalonia, Spain, 8–12 September 1998, edited

- by J. Sola (World Scientific, Singapore, 1999) pp. 471–488 [hep-ph/9812470].
30. R. Dashen and H. Neuberger, Phys. Rev. Lett. **50**, 1897 (1983).
  31. T. Hambye and K. Riesselmann, Phys. Rev. **D55**, 7255 (1997) [hep-ph/9610272].
  32. See, *e.g.*, G. Altarelli and G. Isidori, Phys. Lett. **B337**, 141 (1994); J.A. Casas, J.R. Espinosa and M. Quirós, Phys. Lett. **B342**, 171 (1995) [hep-ph/9409458]; **B382**, 374 (1996) [hep-ph/9603227].
  33. W. Langguth, I. Montvay and P. Weisz, Nucl. Phys. **B277**, 11 (1986); A. Hasenfratz, K. Jansen, J. Jersak, C.B. Lang, T. Neuhaus and H. Yoneyama, Nucl. Phys. **B317**, 81 (1989); J. Kuti, L. Lin and Y. Shen, Phys. Rev. Lett. **61**, 678 (1988).
  34. U.M. Heller, M. Klomfass, H. Neuberger and P. Vranas, Nucl. Phys. **B405**, 555 (1993).
  35. M.Lüscher and P. Weisz, Phys. Lett. **B212**, 472 (1988), Nucl. Phys. **B318**, 705 (1989).
  36. J. Shigemitsu, Phys. Lett. **B226**, 364 (1989); W. Bock, A.K. De, C. Frick, K. Jansen and T. Trappenberg, Nucl. Phys. **B371**, 683 (1992); W. Bock, C. Frick, J. Smit and J.C. Vink, Nucl. Phys. **B400**, 309 (1993) [hep-lat/9212026].
  37. K. Riesselmann, hep-ph/9711456.
  38. G. Isidori, G. Ridolfi and A. Strumia, Nucl. Phys. **B609**, 387 (2001) [hep-ph/0104016].
  39. G. 't Hooft, in *Recent Developments in Gauge Theories*, Proceedings of the NATO Advanced Summer Institute, Cargese, 1979, edited by G. 't Hooft *et al.* (Plenum, New York, 1980) p. 135; E. Witten, Nucl. Phys. **B188**, 513 (1981); L. Susskind, Phys. Rep. **104**, 181 (1984).
  40. H.P. Nilles, Phys. Rep. **110**, 1 (1984).
  41. H.E. Haber and G.L. Kane, Phys. Rep. **117**, 75 (1985); S.P. Martin, hep-ph/9709356.
  42. A. Djouadi, J. Kalinowski and M. Spira, Comput. Phys. Commun. **108**, 56 (1998) [hep-ph/9704448]. The HDECAY program is available at <http://home.cern.ch/~mspira/proglist.html>.
  43. T. Han, Int. J. Mod. Phys. **A11**, 1541 (1996) [hep-ph/9601393].
  44. A. Djouadi, J. Kalinowski and P.M. Zerwas, Z. Phys. **C54**, 155 (1992).
  45. S. Dittmaier, M. Kramer, Y. Liao, M. Spira and P. M. Zerwas, Phys. Lett. **B441**, 383 (1998) [hep-ph/9808433].
  46. A. Freitas, W. Hollik, W. Walter and G. Weiglein, Phys. Lett. **B495**, 338 (2000) [hep-ph/0007091]; A. Freitas, S. Heinemeyer, W. Hollik, W. Walter and G. Weiglein, Nucl. Phys. Proc. Suppl. **89**, 82 (2000) [hep-ph/0007129]; and in *Proceedings of the 5th International Symposium on Radiative Corrections* (RADCOR 2000), 11–15 September 2000, edited by H.E. Haber, SLAC-R-579, eConf C000911 [hep-ph/0101260].
  47. M. Carena, J.S. Conway, H.E. Haber and J.D. Hobbs *et al.*, FERMILAB-CONF-00/270-T [hep-ph/0010338].
  48. D. Costanzo, “Higgs Physics at the Large Hadron Collider,” presented at the 36th Rencontres de Moriond on Electroweak Interactions and Unified

- Theories, Les Arcs, France, 10–17 March 2001 [hep-ex/0105033]; V.A. Mitsou, “Search for New Physics with ATLAS at the LHC,” in *From Particles to the Universe*, Proceedings of the 15th Lake Louise Winter Institute, Alberta, Canada, 20–26 February 2000, edited by A. Astbury, B.A. Campbell, F.C. Khanna and M.G. Vincter (World Scientific, Singapore, 2001) [hep-ph/0004161].
49. K. Lassila-Perini, ETH Dissertation thesis No. 12961 (1998). [CERN-THESIS-99-3]; “Higgs Physics at the LHC,” presented at the III International Symposium on LHC Physics and Detectors, Chia, 25–27 October 2001, CMS Conference Report CMS CR 2001/018.
  50. M. Dittmar, *Pramana* **55**, 151 (2000); M. Dittmar and A.-S. Nicollerat, “High Mass Higgs Studies using  $gg \rightarrow h_{\text{SM}}$  and  $qq \rightarrow qqh_{\text{SM}}$  at the LHC,” CMS NOTE 2001/036.
  51. M. Hohlfeld, “On the determination of Higgs parameters in the ATLAS experiment at the LHC,” ATL-PHYS-2001-004.
  52. D. Zeppenfeld, R. Kinnunen, A. Nikitenko and E. Richter-Was, *Phys. Rev.* **D62**, 013009 (2000) [hep-ph/0002036].
  53. D. Zeppenfeld, “Higgs Couplings at the LHC,” in *Proceedings of the APS/DPF/DPB Summer Study on the Future of Particle Physics* (Snowmass 2001), edited by R. Davidson and C. Quigg, SNOWMASS-2001-P123 [hep-ph/0203123].
  54. A. De Roeck, presentations for the ATLAS Collaboration at the International Workshop on Linear Colliders, *Workshop on Physics and Experiments with Future Electron-Positron Linear Colliders*, 26–30 August, 2002, Jeju Island, Korea; and private communications.
  55. O.J. Éboli and D. Zeppenfeld, *Phys. Lett.* **B495**, 147 (2000) [hep-ph/0009158].
  56. L.J. Hall and M.B. Wise, *Nucl. Phys.* **B187**, 397 (1981).
  57. For a review of the two-Higgs-doublet model, see Chapter 4 of [1].
  58. K. Inoue, A. Kakuto, H. Komatsu, and S. Takeshita, *Prog. Theor. Phys.* **67**, 1889 (1982); R. Flores and M. Sher, *Ann. Phys. (NY)* **148**, 95 (1983).
  59. J.F. Gunion and H.E. Haber, *Nucl. Phys.* **B272**, 1 (1986); **B278**, 449 (1986) [E: **B402**, 567 (1993)].
  60. V.D. Barger, J.L. Hewett and R.J.N. Phillips, *Phys. Rev.* **D41** (1990) 3421.
  61. B. Schrempp and M. Wimmer, *Prog. Part. Nucl. Phys.* **37** (1996) 1 [hep-ph/9606386].
  62. J.F. Gunion and H.E. Haber, SCIPP-02/10 and UCD-2002-10 [hep-ph/0207010], *Phys. Rev. D*, in press.
  63. H.E. Haber and R. Hempfling, *Phys. Rev. Lett.* **66**, 1815 (1991); Y. Okada, M. Yamaguchi and T. Yanagida, *Prog. Theor. Phys.* **85**, 1 (1991); J. Ellis, G. Ridolfi and F. Zwirner, *Phys. Lett.* **B257**, 83 (1991).
  64. S. Heinemeyer, W. Hollik and G. Weiglein, *Phys. Rev.* **D58**, 091701 (1998) [hep-ph/9803277]; *Phys. Lett.* **B440**, 296 (1998) [hep-ph/9807423]; *Eur. Phys. J.* **C9**, 343 (1999) [hep-ph/9812472]; M. Carena, H.E. Haber, S. Heinemeyer, W. Hollik, C.E.M. Wagner and G. Weiglein, *Nucl. Phys.* **B580**, 29 (2000) [hep-ph/0001002]; R.-J. Zhang, *Phys. Lett.* **B447**, 89 (1999) [hep-



- ph/9808299]; J.R. Espinosa and R.-J. Zhang, *JHEP* **0003**, 026 (2000) [hep-ph/9912236]; *Nucl. Phys.* **B586**, 3 (2000) [hep-ph/0003246]; J.R. Espinosa and I. Navarro, *Nucl. Phys.* **B615**, 82 (2001) [hep-ph/0104047]; G. Degrassi, P. Slavich and F. Zwirner, *Nucl. Phys.* **B611**, 403 (2001) [hep-ph/0105096]; A. Brignole, G. Degrassi, P. Slavich and F. Zwirner, *Nucl. Phys.* **B631**, 195 (2002) [hep-ph/0112177]; *Nucl. Phys.* **B643**, 79 (2002) [hep-ph/0206101]; G. Degrassi, S. Heinemeyer, W. Hollik, P. Slavich and G. Weiglein, hep-ph/0212020; Computer programs developed for computing the radiatively-corrected Higgs masses, FeynHiggs and FeynHiggsFast, are described respectively in S. Heinemeyer, W. Hollik and G. Weiglein, *Comput. Phys. Commun.* **124**, 76 (2000) [hep-ph/9812320]; and CERN-TH-2000-055 [hep-ph/0002213].
65. J. Ellis, J.F. Gunion, H.E. Haber, L. Roszkowski and F. Zwirner, *Phys. Rev.* **D39**, 844 (1989). For a recent treatment and guide to the literature see: C. Panagiotakopoulos and A. Pilaftsis, *Phys. Rev.* **D63**, 055003 (2001) [hep-ph/0008268]. A detailed discussion of NMSSM phenomenology can be found in U. Ellwanger, M. Rausch de Traubenberg and C.A. Savoy, *Nucl. Phys.* **B492**, 21 (1997) [hep-ph/9611251].
  66. J.R. Espinosa and M. Quirós, *Phys. Rev. Lett.* **81**, 516 (1998) [hep-ph/9804235]; M. Masip, *Phys. Rev. Lett.* **B444**, 352 (1998) [hep-ph/9810303].
  67. K. Tobe and J.D. Wells, *Phys. Rev.* **D66**, 013010 (2002) [hep-ph/0204196].
  68. J.A. Coarasa, R.A. Jiménez and J. Solà, *Phys. Lett.* **B389**, 312 (1996) [hep-ph/9511402]; R.A. Jiménez and J. Solà, *Phys. Lett.* **B389**, 53 (1996) [hep-ph/9511292]; A. Bartl, H. Eberl, K. Hikasa, T. Kon, W. Majerotto and Y. Yamada, *Phys. Lett.* **B378**, 167 (1996) [hep-ph/9511385].
  69. R. Hempfling, *Phys. Rev.* **D49**, 6168 (1994); L. Hall, R. Rattazzi and U. Sarid, *Phys. Rev.* **D50**, 7048 (1994) [hep-ph/9306309].
  70. M. Carena, M. Olechowski, S. Pokorski and C.E.M. Wagner, *Nucl. Phys.* **B426**, 269 (1994) [hep-ph/9402253].
  71. D. Pierce, J. Bagger, K. Matchev, and R. Zhang, *Nucl. Phys.* **B491**, 3 (1997) [hep-ph/9606211].
  72. S. Heinemeyer, W. Hollik and G. Weiglein, *Eur. Phys. J.* **C16**, 139 (2000) [hep-ph/0003022].
  73. M. Carena, H.E. Haber, H.E. Logan and S. Mrenna, *Phys. Rev.* **D65**, 055005 (2002) [E: **D65**, 099902 (2002)] [hep-ph/0106116].
  74. M. Carena, D. Garcia, U. Nierste and C.E.M. Wagner, *Nucl. Phys.* **B577**, 88 (2000) [hep-ph/9912516].
  75. H. Eberl, K. Hidaka, S. Kraml, W. Majerotto and Y. Yamada, *Phys. Rev.* **D62**, 055006 (2000) [hep-ph/9912463].
  76. M. Carena, S. Mrenna and C.E.M. Wagner, *Phys. Rev.* **D60**, 075010 (1999) [hep-ph/9808312]; *Phys. Rev.* **D62**, 055008 (2000) [hep-ph/9907422].
  77. H. Baer and J.D. Wells, *Phys. Rev.* **D57**, 4446 (1998) [hep-ph/9710368]; W. Loinaz and J. D. Wells, *Phys. Lett.* **B445**, 178 (1998) [hep-ph/9808287].
  78. J.L. Diaz-Cruz, H.-J. He, T. Tait and C.P. Yuan, *Phys. Rev. Lett.* **80**, 4641 (1998) [hep-ph/9802294]; C. Balázs, J.L. Diaz-Cruz, H.-J. He, T. Tait and C.P. Yuan, *Phys. Rev.* **D59**, 055016 (1999) [hep-ph/9807349].

79. H.E. Haber, M.J. Herrero, H.E. Logan, S. Peñaranda, S. Rigolin and D. Temes, *Phys. Rev.* **D63**, 055004 (2001) [hep-ph/0007006].
80. P.H. Chankowski, S. Pokorski and J. Rosiek, *Nucl. Phys.* **B423**, 497 (1994).
81. A. Djouadi, P. Janot, J. Kalinowski and P.M. Zerwas, *Phys. Lett.* **B376**, 220 (1996) [hep-ph/9603368]; A. Djouadi, J. Kalinowski, P. Ohmann and P.M. Zerwas, *Z. Phys.* **C74**, 93 (1997) [hep-ph/9605339].
82. S. Heinemeyer, W. Hollik, J. Rosiek and G. Weiglein, *Eur. Phys. J.* **C19**, 535 (2001) [hep-ph/0102081].
83. M.M. Mühlleitner, M. Krämer, M. Spira and P.M. Zerwas, *Phys. Lett.* **B508**, 311 (2001) [hep-ph/0101083].
84. ALEPH, DELPHI, L3 and OPAL Collaborations, The LEP working group for Higgs boson searches], LHWG Note 2001-05 (July 2001), [hep-ex/0107031].
85. ALEPH, DELPHI, L3 and OPAL Collaborations, The LEP working group for Higgs boson searches], LHWG Note 2001-04 (July 2001), [hep-ex/0107030].
86. Fig. 14 was provided by E. Richter-Was and F. Gianotti on behalf of the ATLAS collaboration.
87. D. Denegri *et al.*, “Summary of the CMS Discovery Potential for the MSSM SUSY Higgses,” CMS NOTE 2001/032 [hep-ph/0112045].
88. I. Hinchliffe, F.E. Paige, M.D. Shapiro, J. Soderqvist and W. Yao, *Phys. Rev.* **D55**, 5520 (1997) [hep-ph/9610544]; S. Abdullin *et al.* [CMS Collaboration], *J. Phys.* **G28**, 469 (2002) [hep-ph/9806366].
89. S.L. Glashow and S. Weinberg, *Phys. Rev.* **D15**, 1958 (1977); E.A. Paschos, *Phys. Rev.* **D15**, 1966 (1977).
90. B.A. Dobrescu, FERMILAB-CONF-99-051 [hep-ph/9903407]; and in *Physics and experiments with future linear  $e^+e^-$  colliders*, Proceedings of the 5th International Linear Collider Workshop, Batavia, IL, USA, 2000, edited by A. Para and H.E. Fisk (American Institute of Physics, New York, 2001), pp. 113–121 [hep-ph/0103038].
91. M. Cvetič, H. Lu, C.N. Pope, A. Sadzadeh and T.A. Tran, *Nucl. Phys.* **B586**, 275 (2000) [hep-th/0003103].
92. P. Chankowski, T. Farris, B. Grzadkowski, J.F. Gunion, J. Kalinowski and M. Krawczyk, *Phys. Lett.* **B496**, 195 (2000) [hep-ph/0009271].
93. J.F. Gunion, in *Physics and experiments with future linear  $e^+e^-$  colliders*, Proceedings of the 5th International Linear Collider Workshop, Batavia, IL, USA, 2000, edited by A. Para and H.E. Fisk (American Institute of Physics, New York, 2001), pp. 231–236 [hep-ph/0012199].
94. U. Ellwanger and C. Hugonie, *Eur. Phys. J.* **C25** (2002) 297 [hep-ph/9909260].
95. J.R. Espinosa and J.F. Gunion, *Phys. Rev. Lett.* **82**, 1084 (1999) [hep-ph/9807275].
96. J.F. Gunion, H.E. Haber and T. Moroi, “Will at least one of the Higgs bosons of the next-to-minimal supersymmetric extension of the Standard Model be observable at LEP2 or the LHC?”, in *New Directions for High Energy Physics*, Proceedings of the 1996 DPF/DPB Summer Study on High

- Energy Physics, Snowmass '96, edited by D.G. Cassel, L.T. Gennari and R.H. Siemann (Stanford Linear Accelerator Center, Stanford, CA, 1997) [hep-ph/9610337].
97. U. Ellwanger, J.F. Gunion and C. Hugonie, hep-ph/0111179.
  98. J.F. Gunion and B. Grzadkowski, work in progress.
  99. J. Kamoshita, Y. Okada and M. Tanaka, Phys. Lett. **B328**, 67 (1994) [hep-ph/9402278].
  100. J.F. Gunion, L. Roszkowski, A. Turski, H.E. Haber, G. Gamberini, B. Kayser, S.F. Novaes, F.I. Olness and J. Wudka, Phys. Rev. **D38**, 3444 (1988).
  101. S. Bar-Shalom, D. Atwood, G. Eilam, R.R. Mendel and A. Soni, Phys. Rev. **D53**, 1162 (1996) [hep-ph/9508314].
  102. J.F. Gunion, B. Grzadkowski and X. He, Phys. Rev. Lett. **77** (1996) 5172 [hep-ph/9605326].
  103. S. Dawson and L. Reina, Phys. Rev. **D57** (1998) 5851 [hep-ph/9712400]; Phys. Rev. **D59**, 054012 (1999) [hep-ph/9808443]; H. Baer, S. Dawson, and L. Reina, Phys. Rev. **D61**, 0113002 (2000) [hep-ph/9906419].
  104. S. Dawson and L. Reina, Phys. Rev. **D60**, 015003 (1999) [hep-ph/9812488].
  105. B. Grzadkowski, J.F. Gunion and J. Kalinowski, Phys. Lett. **B480**, 287 (2000) [hep-ph/0001093].
  106. S. Dittmaier, M. Kramer, Y. Liao, M. Spira and P.M. Zerwas, Phys. Lett. **B478**, 247 (2000) [hep-ph/0002035].
  107. U. Cotti, A. Gutierrez-Rodriguez, A. Rosado and O.A. Sampayo, Phys. Rev. **D59**, 095011 (1999) [hep-ph/9902417].
  108. S. Kanemura, S. Moretti and K. Odagiri, JHEP **0102**, 011 (2001) [hep-ph/0012030].
  109. B.A. Kniehl, F. Madricardo and M. Steinhauser, Phys. Rev. **D66**, 054016 (2002) [hep-ph/0205312].
  110. A. Gutierrez-Rodriguez and O. A. Sampayo, Phys. Rev. **D62**, 055004 (2000); S. Moretti, Eur. Phys. J. direct **C4**, 15 (2002) [hep-ph/0206208].
  111. H.J. He and C.-P. Yuan, Phys. Rev. Lett. **83**, 28 (1999) [hep-ph/9810367]; H.J. He, S. Kanemura and C.-P. Yuan, Phys. Rev. Lett. **89**, 101803 (2002) [hep-ph/0203090]; and hep-ph/0209376.
  112. S.H. Zhu, hep-ph/9901221; A. Arhrib, M. Capdequi Peyranère, W. Hollik and G. Moulhaka, Nucl. Phys. **B581**, 34 (2000) [hep-ph/9912527]; S. Kanemura, Eur. Phys. J. **C17**, 473 (2000) [hep-ph/9911541]; H.E. Logan and S. Su, Phys. Rev. **D66**, 035001 (2002) [hep-ph/0203270]; **D67**, 017703 (2003) [hep-ph/0206135].
  113. A. Djouadi, H.E. Haber and P.M. Zerwas, Phys. Lett. **B375**, 203 (1996) [hep-ph/9602234]; P. Osland and P.N. Pandita, Phys. Rev. **D59**, 055013 (1999) [hep-ph/9806351]; A. Djouadi, W. Kilian, M. Mühlleitner and P.M. Zerwas, Eur. Phys. J. **C10**, 27 (1999) [hep-ph/9903229]; F. Boudjema and A. Semenov, Phys. Rev. **D66**, 095007 (2002) [hep-ph/0201219].
  114. H.E. Haber and Y. Nir, Phys. Lett. **B306**, 327 (1993) [hep-ph/9302228].
  115. T. Farris, J.F. Gunion and H.E. Logan, "Higgs sectors in which the only light Higgs boson is CP-odd and linear collider strategies for its discov-

- ery,” in *Proceedings of the APS/DPF/DPB Summer Study on the Future of Particle Physics* (Snowmass 2001), edited by R. Davidson and C. Quigg, SNOWMASS-2001-P121 [hep-ph/0202087].
116. J.F. Gunion, C. Loomis and K.T. Pitts, “Searching for doubly-charged Higgs bosons at future colliders,” in *New Directions for High Energy Physics*, Proceedings of the 1996 DPF/DPB Summer Study on High Energy Physics, Snowmass '96, edited by D.G. Cassel, L.T. Gennari and R.H. Siemann (Stanford Linear Accelerator Center, Stanford, CA, 1997), pp. 603–607 [hep-ph/9610237].
  117. J.F. Gunion, R. Vega and J. Wudka, *Phys. Rev.* **D43**, 2322 (1991).
  118. R.N. Mohapatra, *Fortsch. Phys.* **31**, 185 (1983); J.F. Gunion, J. Grifols, A. Mendez, B. Kayser and F. Olness, *Phys. Rev.* **D40**, 1546 (1989); N.G. Deshpande, J.F. Gunion, B. Kayser and F. Olness, *Phys. Rev.* **D44**, 837 (1991).
  119. H. Georgi and M. Machacek, *Nucl. Phys.* **B262**, 463 (1985).
  120. M.S. Chanowitz and M. Golden, *Phys. Lett.* **B165**, 105 (1985).
  121. J.F. Gunion, *Int. J. Mod. Phys.* **A11**, 1551 (1996) [hep-ph/9510350]; **A13**, 2277 (1998) [hep-ph/9803222]; F. Cuyppers and M. Raidal, *Nucl. Phys.* **B501**, 3 (1997) [hep-ph/9704224]; P.H. Frampton, *Int. J. Mod. Phys.* **A15**, 2455 (2000) [hep-ph/0002017].
  122. J. Gluza, *Phys. Lett.* **B403**, 304 (1997) [hep-ph/9704202].
  123. R.A. Alanakian, *Phys. Lett.* **B436**, 139 (1998) [hep-ph/9706383].
  124. G. Barenboim, K. Huitu, J. Maalampi and M. Raidal, *Phys. Lett.* **B394**, 132 (1997) [hep-ph/9611362].
  125. V.D. Barger, J.F. Beacom, K. Cheung and T. Han, *Phys. Rev.* **D50**, 6704 (1994) [hep-ph/9404335].
  126. R. Casalbuoni, A. Deandrea, S. De Curtis, D. Dominici, R. Gatto and J.F. Gunion, *Nucl. Phys.* **B555**, 3 (1999) [hep-ph/9809523].
  127. K. Lane, K.R. Lynch, S. Mrenna and E.H. Simmons, *Phys. Rev.* **D66**, 015001 (2002) [hep-ph/0203065].
  128. K. Desch, and M. Battaglia, in *Physics and experiments with future linear  $e^+e^-$  colliders*, Proceedings of the 5th International Linear Collider Workshop, Batavia, IL, USA, 2000, edited by A. Para and H.E. Fisk (American Institute of Physics, New York, 2001), pp. 312–316; M. Battaglia and K. Desch, in *ibid.*, pp. 163–182 [hep-ph/0101165].
  129. R.D. Heuer, D.J. Miller, F. Richard and P.M. Zerwas [editors], “TESLA: The superconducting electron positron linear collider with an integrated X-ray laser laboratory. Technical design report, Part 3: Physics at an  $e^+e^-$  Linear Collider,” DESY-01-011 (March, 2001), <http://tesla.desy.de/tdr/> [hep-ph/0106315].
  130. LCD refers to “Linear Collider Detector” as defined by the North American simulation studies, see <http://www-sldnt.slac.stanford.edu/nld/>.
  131. H. Yang and K. Riles, “Impact of Tracker Design on Higgs Mass and Cross Section Resolutions,” in *Proceedings of the APS/DPF/DPB Summer Study on the Future of Particle Physics* (Snowmass 2001), edited by R. Davidson and C. Quigg, SNOWMASS-2001-E3040.

132. M. Ronan, “Jet-Jet Reconstruction in Full Detector Simulations,” presented at Workshop on Physics and Detectors for Future  $e^+e^-$  Linear Colliders, Johns Hopkins University, Baltimore, 19–21 March 2001.
133. A. Juste, “Higgs mass determination from direct reconstruction at a linear  $e^+e^-$  collider,” in *Physics and Experiments with Future Linear  $e^+e^-$  Colliders*, edited by E. Fernández and A. Pacheco (Universitat Autònoma de Barcelona, Bellaterra, Spain, 1999) [hep-ex/9912041].
134. V.D. Barger, M.S. Berger, J.F. Gunion and T. Han, Phys. Rev. Lett. **78**, 3991 (1997) [hep-ph/9612279].
135. P.F. Derwent *et al.*, “Linear Collider Physics,” FERMILAB-FN-701 [hep-ex/0107044].
136. A. Küskinen, M. Battaglia, P. Pöyhönen, “Study of  $e^+e^- \rightarrow H^+H^-$  at a 800 GeV Linear Collider”, in *Physics and experiments with future linear  $e^+e^-$  colliders*, Proceedings of the 5th International Linear Collider Workshop, Batavia, IL, USA, 2000, edited by A. Para and H.E. Fisk (American Institute of Physics, New York, 2001); “Study of  $HA$  Production in  $e^+e^-$  Collisions at  $\sqrt{s} = 800$  GeV, DESY-123-E, p. 417; “Pair production of charged Higgs bosons at future linear  $e^+e^-$  colliders,” in *Proceedings of the APS/DPF/DPB Summer Study on the Future of Particle Physics* (Snowmass 2001), edited by R. Davidson and C. Quigg, SNOWMASS-2001-E3017 [hep-ex/0112015]; A. Andreazza and C. Troncon, “Study of  $HA$  Production in  $e^+e^-$  Collisions at  $\sqrt{s} = 800$  GeV,” DESY-123-E, p. 417.
137. P. Garcia-Abia and W. Lohmann, Eur. Phys. J. direct **C2**, 1 (2000) [hep-ex/9908065].
138. R. Van Kooten, “Separation of the Higgsstrahlung and  $WW$ -fusion process,” presented at Workshop on Physics and Detectors for Future  $e^+e^-$  Linear Colliders, Johns Hopkins University, Baltimore, 19–21 March 2001.
139. C.T. Potter, J.E. Brau and M. Iwasaki, “Standard Model Higgs Boson Branching Ratio Measurements at a Linear Collider,” in *Proceedings of the APS/DPF/DPB Summer Study on the Future of Particle Physics* (Snowmass 2001), edited by R. Davidson and C. Quigg, SNOWMASS-2001-P118.
140. J. Brau, C. Potter, and M. Iwasaki, “Linear Collider Vertex Detector Optimization for Higgs Branching Ratio Measurements,” in *Physics and experiments with future linear  $e^+e^-$  colliders*, Proceedings of the 5th International Linear Collider Workshop, Batavia, IL, USA, 2000, edited by A. Para and H.E. Fisk (American Institute of Physics, New York, 2001).
141. D.J. Jackson, Nucl. Instrum. Meth. **A388**, 247 (1997).
142. C.T. Potter, J.E. Brau and M. Iwasaki, “Standard Model Higgs boson branching ratio measurements at a linear collider,” to appear in the Proceedings of the International Workshop on Linear Colliders, *Workshop on Physics and Experiments with Future Electron-Positron Linear Colliders*, 26–30 August, 2002, Jeju Island, Korea.
143. M.D. Hildreth, T.L. Barklow, and D.L. Burke, Phys. Rev. **D49**, 3441 (1994); K. Kawagoe, in *Proceedings of the 2nd International Workshop on Physics and Experiments with Linear  $e^+e^-$  Colliders*, Volume II, Waikoloa, HI, 26–30 April 1993, edited by F.A. Harris, S.L. Olsen, S. Pakvasa and X. Tata

- (World Scientific, Singapore, 1993) pp. 660–665.
144. G. Borisov and F. Richard, Precise measurement of Higgs decay rate into  $WW^*$  at future  $e^+e^-$  linear colliders and theoretical consequences, in *Physics and Experiments with Future Linear  $e^+e^-$  Colliders*, edited by E. Fernández and A. Pacheco (Universitat Autònoma de Barcelona, Bellaterra, Spain, 1999) [hep-ph/9905413].
  145. M. Battaglia, Nucl. Instrum. Meth. **A473**, 75 (2001) [hep-ex/0012021]; “Measuring Higgs branching ratios and telling the SM from a MSSM Higgs boson at the  $e^+e^-$  linear collider,” in *Physics and Experiments with Future Linear  $e^+e^-$  Colliders*, edited by E. Fernández and A. Pacheco (Universitat Autònoma de Barcelona, Bellaterra, Spain, 1999) [hep-ph/9910271].
  146. M. Battaglia and A. De Roeck, “Determination of the muon Yukawa coupling at high energy  $e^+e^-$  linear colliders,” in *Proceedings of the APS/DPF/DPB Summer Study on the Future of Particle Physics*, (Snowmass 2001), edited by R. Davidson and C. Quigg, SNOWMASS-2001-E3066 [hep-ph/0111307].
  147. J.F. Gunion and P.C. Martin, hep-ph/9610417; J.F. Gunion and P.C. Martin, Phys. Rev. Lett. **78**, 4541 (1997) [hep-ph/9607360].
  148. E. Boos, J.C. Brient, D.W. Reid, H.J. Schreiber and R. Shanidze, Eur. Phys. J. **C19**, 455 (2001) [hep-ph/0011366].
  149. O.J. Eboli and D. Zeppenfeld, Phys. Lett. **B495**, 147 (2000) [hep-ph/0009158].
  150. F. Boudjema, G. Belanger and R.M. Godbole, CERN-TH-2002-141 [hep-ph/0206311]; K. Griest and H.E. Haber, Phys. Rev. **D37**, 719 (1988).
  151. L. F. Li, Y. Liu and L. Wolfenstein, Phys. Lett. **B159**, 45 (1985); S. Bertolini and A. Santamaria, Phys. Lett. **B213**, 487 (1988); A.S. Joshipura and S.D. Rindani, Phys. Rev. Lett. **69**, 3269 (1992); A.S. Joshipura and J.W.F. Valle, Nucl. Phys. **B397**, 105 (1993); M.A. Diaz, M.A. Garcia-Jareno, D.A. Restrepo and J.W.F. Valle, Nucl. Phys. **B527**, 44 (1998) [hep-ph/9803362].
  152. A. Pilaftsis, Z. Phys. **C55**, 275 (1992) [hep-ph/9901206]; V.A. Khoze, hep-ph/0105069; K. Belotsky, D. Fargion, M. Khlopov, R. Konoplich and K. Shibaev, hep-ph/0210153.
  153. G.F. Giudice, R. Rattazzi and J.D. Wells, Nucl. Phys. **B595**, 250 (2001) [hep-ph/0002178]; K.M. Cheung, Phys. Rev. **D63**, 056007 (2001) [hep-ph/0009232]; Phys. Lett. **B524**, 161 (2002) [hep-ph/0110035]; J.L. Hewett and T.G. Rizzo, SLAC-PUB-9132 [hep-ph/0202155].
  154. E.L. Berger, C.W. Chiang, J. Jiang, T.M. Tait and C.E.M. Wagner, Phys. Rev. **D66**, 095001 (2002) [hep-ph/0205342].
  155. R. Van Kooten, “Measurement of the Invisible Branching Ratio of the Higgs,” presented at Chicago LC Workhsop, 7–9 January 2002, Gleacher Center, University of Chicago, Chicago.
  156. D. Atwood and A. Soni, Phys. Rev. **D45**, 2405 (1992); M. Diehl and O. Nachtmann, Z. Phys. **V62**, 397 (1994).
  157. A. Juste and G. Merino, hep-ph/9910301.
  158. F. Boudjema and E. Chopin, Z. Phys. **C73**, 85 (1996) [hep-ph/9507396];

- D.J. Miller and S. Moretti, Eur. Phys. J. **C13**, 459 (2000) [hep-ph/9906395].
159. D.J. Miller and S. Moretti, hep-ph/0001194.
160. C. Castanier, P. Gay, P. Lutz and J. Orloff, hep-ex/0101028.
161. M. Battaglia, E. Boos and W.M. Yao, “Studying the Higgs potential at the  $e^+e^-$  linear collider,” in *Proceedings of the APS/DPF/DPB Summer Study on the Future of Particle Physics* (Snowmass 2001), edited by R. Davidson and C. Quigg, SNOWMASS-2001-E3016 [hep-ph/0111276].
162. A. Djouadi, W. Kilian, M.M. Mühlleitner and P.M. Zerwas, hep-ph/0001169. R. Lafaye, D.J. Miller, M.M. Mühlleitner and S. Moretti, hep-ph/0002238;
163. D. Choudhury, T.M. Tait and C.E.M. Wagner, Phys. Rev. **D65**, 115007 (2002) [hep-ph/0202162].
164. J. Alcaraz and E. Ruiz Morales, Phys. Rev. Lett. **86**, 3726 (2001) [hep-ph/0012109].
165. D. Bardin, P. Christova, M. Jack, L. Kalinovskaya, A. Olchevski, S. Riemann and T. Riemann, Comput. Phys. Commun. **133**, 229 (2001) [hep-ph/9908433].
166. V. Drollinger and A. Sopczak, in *Physics and experiments with future linear  $e^+e^-$  colliders*, Proceedings of the 5th International Linear Collider Workshop, Batavia, IL, USA, 2000, edited by A. Para and H.E. Fisk (American Institute of Physics, New York, 2001) pp. 226–230 [hep-ph/0102342].
167. N. Meyer, “Properties of a 240 GeV SM Higgs,” presented at Chicago LC Workshop, 7-9 January 2002, Gleacher Center, University of Chicago, Chicago.
168. L.D. Landau, Dokl. Akad. Nauk Ser. Fiz. **60**, 207 (1948); C.N. Yang, Phys. Rev. **77**, 242 (1950); J.J. Sakurai, *Invariance Principles and Elementary Particles* (Princeton University Press, 1964).
169. M.T. Dova, P. Garcia-Abia and W. Lohmann, LC Note LC-PHSM-2001-055; and hep-ph/0302113.
170. D.J. Miller, S.Y. Choi, B. Eberle, M.M. Mühlleitner and P.M. Zerwas, Phys. Lett. **B505**, 149 (2001) [hep-ph/0102023].
171. K. Hagiwara and M.L. Stong, Z. Phys. **C62**, 99 (1994) [hep-ph/9309248]; K. Hagiwara, S. Ishihara, J. Kamoshita and B.A. Kniehl, Eur. Phys. J. **C14**, 457 (2000) [hep-ph/0002043].
172. V.D. Barger, K. Cheung, A. Djouadi, B.A. Kniehl and P.M. Zerwas, Phys. Rev. **D49**, 79 (1994) [hep-ph/9306270].
173. T. Han and J. Jiang, Phys. Rev. **D63**, 096007 (2001) [hep-ph/0011271].
174. B. Grzadkowski and J.F. Gunion, Phys. Lett. **B350**, 218 (1995) [hep-ph/9501339].
175. B. Grzadkowski and J.F. Gunion, hep-ph/9503409.
176. M. Krämer, J. Kühn, M.L. Stong and P.M. Zerwas, Z. Phys. **C64**, 21 (1994) [hep-ph/9404280].
177. G.R. Bower, T. Pierzchala, Z. Was and M. Worek, Phys. Lett. **B543**, 227 (2002) [hep-ph/0204292].
178. J.F. Gunion and X.G. He, “Discriminating between Higgs boson models using  $e^+e^- \rightarrow t\bar{t}h$  and  $Zh$  at the NLC,” in *New Directions for High En-*

- ergy Physics*, Proceedings of the 1996 DPF/DPB Summer Study on High Energy Physics, Snowmass '96, edited by D.G. Cassel, L.T. Gennari and R.H. Siemann (Stanford Linear Accelerator Center, Stanford, CA, 1997), pp. 627–631 [hep-ph/9609453].
179. B. Grzadkowski and J.F. Gunion, Phys. Lett. **B294**, 361 (1992) [hep-ph/9206262].
  180. J.F. Gunion and J.G. Kelly, Phys. Lett. **B333**, 110 (1994) [hep-ph/9404343].
  181. C.A. Boe, O.M. Ogreid, P. Osland and J. Zhang, Eur. Phys. J. **C9**, 413 (1999) [hep-ph/9811505].
  182. J.F. Gunion and J. Kelly, “Using Higgs pair production in  $e^+e^-$  or  $\mu^+\mu^-$  collisions to probe GUT-scale boundary conditions in the minimal supersymmetric model,” in *New Directions for High Energy Physics*, Proceedings of the 1996 DPF/DPB Summer Study on High Energy Physics, Snowmass '96, edited by D.G. Cassel, L.T. Gennari and R.H. Siemann (Stanford Linear Accelerator Center, Stanford, CA, 1997), pp. 632–636 [hep-ph/9610421].
  183. J.F. Gunion and J. Kelly, Phys. Rev. **D56**, 1730 (1997) [hep-ph/9610495].
  184. J.L. Feng and T. Moroi, Phys. Rev. **D56**, 5962 (1997) [hep-ph/9612333].
  185. V.D. Barger, T. Han and J. Jiang, Phys. Rev. **D63**, 075002 (2001) [hep-ph/0006223].
  186. J.F. Gunion, T. Han, J. Jiang and A. Sopczak, hep-ph/0212151; J.F. Gunion, T. Han, J. Jiang, S. Mrenna and A. Sopczak, “Determination of  $\tan\beta$  at a future  $e^+e^-$  linear collider,” in *Proceedings of the APS/DPF/DPB Summer Study on the Future of Particle Physics* (Snowmass 2001), edited by R. Davidson and C. Quigg, SNOWMASS-2001-P120 [hep-ph/0112334].
  187. A. Freitas and D. Stöckinger, Phys. Rev. **D66**, 095014 (2002) [hep-ph/0205281].
  188. A. Bartl, H. Eberl, S. Kraml, W. Majerotto, W. Porod, and A. Sopczak, Z. Phys. **C76**, 549 (1997) [hep-ph/9701336]; hep-ph/9909378; M. Berggren, R. Keränen, H. Nowak and A. Sopczak, hep-ph/9911345.
  189. See, e.g., S.Y. Choi, A. Djouadi, M. Guchait, J. Kalinowski and P.M. Zerwas, Eur. Phys. J. **C14**, 535 (2000) [hep-ph/0002033].
  190. ATLAS Collaboration, “Detector and Physics Performance Technical Design Report”, CERN/LHCC/99-15 (1999); CMS Collaboration, Technical Design Reports, CMS TDR 1-5 (1997/98).
  191. P. Chen, G. Horton-Smith, T. Ohgaki, A.W. Weidemann and K. Yokoya, Nucl. Instrum. Meth. **A355**, 107 (1995). See <http://www-acc-theory.kek.jp/members/cain/cain21b.manual/main.html>.
  192. P. Niezurawski, A.F. Zarnecki and M. Krawczyk, Acta Phys. Polon. **B34**, 177 (2003) [hep-ph/0208234].
  193. J.F. Gunion, J.G. Kelly and J. Ohnemus, Phys. Rev. **D51**, 2101 (1995) [hep-ph/9409357].



## INDEX

- collider/detector parameters,
  - luminosities or features, 3, 4, 38, 56–58, 61, 62, 65–67, 78, 80, 81
- coupling constant unification, 5, 11, 42, 51, 83
- CP-violating Higgs sectors, 41, 82
- decoupling limit, 4–6, 8, 25–28,
  - 33–36, 43, 45, 53, 63, 73, 79
  - delayed, 33
  - premature, 65
- effective field theory, 8–11, 23, 42
- electroweak symmetry breaking (EWSB), 6, 7, 42, 45, 83
- extended or exotic Higgs scenarios, 4, 41–46, 48, 51, 77, 82
- Giga- $Z$ , 4–6, 17, 45, 65, 74–76
  - indirect constraints on MSSM particles, 75, 76
- Higgs bosons
  - branching ratios, 12, 13, 18, 21, 22, 33, 34, 54, 57–60, 64–68, 73, 77
  - MSSM results, 34, 39, 60, 73
  - couplings, 12, 21–23, 25, 26, 30–33, 35, 36, 42, 46, 53, 54, 56–58, 63, 65, 67, 68, 73, 74
  - CP properties, 8, 22, 69, 71, 72, 77, 82
  - difficult parameter regimes, 5, 35, 36, 38, 40, 41, 45–49, 52, 73, 79, 80
  - discovery channels, 18, 20–22, 26, 39–41, 46
  - discovery parameter regress, 35, 37–41, 46–48, 50, 52, 79–81
  - experimental limits, 16, 37, 40
  - general two-Higgs-doublet model (2HDM), 5, 22, 23, 25, 34, 41–44, 51, 72, 73, 80
    - special non-decoupling scenarios, 43
  - Majorana couplings, 52
  - mass bounds, 10, 24, 28, 46
  - mass(es), 12, 24, 28–30, 54–56, 68, 83
  - precision measurements, 21, 22, 36, 52–63, 65–74, 79, 82, 83
  - production mechanisms, 13–15, 18, 20, 35, 36, 47, 48, 52, 58, 61, 65, 73
  - self-couplings, 11, 29, 34, 53, 61, 62
  - singlets, 29, 41–43, 46, 47, 51
  - spin and parity, 69, 71
  - theory constraints on masses and parameters, 5, 9, 10, 23–25, 28–30
  - triplets, 5, 29, 46, 51, 52
    - doubly-charged member, 51, 52
  - widths, 21, 68–70, 73, 77
- left-right symmetric models, 52
- naturalness, 9–11
- perturbativity constraints, 9, 23, 24, 29, 42, 43, 46, 77

- photon-photon collider, 3, 5, 6, 13,  
15, 35, 50, 60, 69, 73, 77, 79, 82
- Planck mass ( $M_{\text{PL}}$ ), 8, 9, 29
- precision electroweak constraints, 4,  
6–8, 16, 17, 41, 43, 45, 46, 51, 65,  
74, 76
- pseudo-Nambu-Goldstone bosons, 51,  
53
  
- radiative corrections, 7, 23, 24, 26,  
28–35, 37
  - non-decoupling effects, 31, 32
  - supersymmetric particle loops, 31,  
37, 63
- renormalization group equations, 23,  
28
  
- triviality, 9, 10, 12
  
- unitarity constraints, 23
  
- Yuakwa couplings, 6, 8, 9, 15, 23, 31,  
32, 36, 42, 43, 52, 61, 67, 72, 73